



8-2021

Enhancing Biomechanical Function through Development and Testing of Assistive Devices for Shoulder Impairment and Total Limb Amputation

Patrick Hall

University of Tennessee, Knoxville, phall8@vols.utk.edu

Follow this and additional works at: https://trace.tennessee.edu/utk_graddiss



Part of the [Biomechanics and Biotransport Commons](#), and the [Biomedical Devices and Instrumentation Commons](#)

Recommended Citation

Hall, Patrick, "Enhancing Biomechanical Function through Development and Testing of Assistive Devices for Shoulder Impairment and Total Limb Amputation. " PhD diss., University of Tennessee, 2021.
https://trace.tennessee.edu/utk_graddiss/6562

This Dissertation is brought to you for free and open access by the Graduate School at TRACE: Tennessee Research and Creative Exchange. It has been accepted for inclusion in Doctoral Dissertations by an authorized administrator of TRACE: Tennessee Research and Creative Exchange. For more information, please contact trace@utk.edu.

To the Graduate Council:

I am submitting herewith a dissertation written by Patrick Hall entitled "Enhancing Biomechanical Function through Development and Testing of Assistive Devices for Shoulder Impairment and Total Limb Amputation." I have examined the final electronic copy of this dissertation for form and content and recommend that it be accepted in partial fulfillment of the requirements for the degree of Doctor of Philosophy, with a major in Mechanical Engineering.

Dustin L. Crouch, Major Professor

We have read this dissertation and recommend its acceptance:

David E. Anderson, Jeffery Reinbolt, Joshua Weinhandl, Richard Komistek

Accepted for the Council:

Dixie L. Thompson

Vice Provost and Dean of the Graduate School

(Original signatures are on file with official student records.)

Enhancing Biomechanical Function through Development and Testing of Assistive Devices for Shoulder Impairment and Total Limb Amputation

A Dissertation Presented for the
Doctor of Philosophy
Degree
The University of Tennessee, Knoxville

Patrick Timothy Hall
August 2021

Copyright © 2021 by Patrick Timothy Hall

All rights reserved.

This dissertation is dedicated to my wife, family, friends, research team, and most importantly my Lord and Savior, Jesus Christ.

*“There are some people who live in a dream world, and there are some who face reality;
and then there are those who turn one into the other.”*

– Douglas H. Everett

ACKNOWLEDGMENTS

First and foremost, I would like to thank my advisor, Dr. Dustin Crouch, for his guidance, mentorship, and for giving me the opportunity to pursue higher education at The University of Tennessee. I thank him for taking the risk of hiring me as his first PhD student and am grateful for his dedication to our research and to my academic journey. It takes a truly special advisor to share the load of bi-daily medication and daily bandage changes for 60 days straight as the two of us first started figuring out the physical toll of animal research. I would also like to thank all of my other lab mates throughout my time in the Upper Limb Assist Lab, specifically, Caleb Stubbs, Morteza Asgari, and Katrina Easton. As my roommate, Caleb, and I would not only work together to handle the rabbit care, but also somehow find a way to play a round of disc golf to get outside and keep each other sane.

I would like to thank the team dedicated to our research. Dr. David Anderson not only served as our skilled veterinary orthopedic surgeon, but also somehow balanced our research with his clinical requirements, his own incredible research, and serving on my committee. I learned so much from Dr. Anderson during our many surgeries as he answered my hundreds of questions about animals". Dr. Cheryl Greenacre, our rabbit specialist, taught me so much about rabbits that it would have been impossible to complete my research without her help. Thanks to Dr. Bryce Burton, Dr. Kelsey Finnie, and Chris Carter for their hands-on daily care to ensure the health and wellbeing of all of the rabbits used in our research. Thanks to Dr. Stacy Stephenson for helping me understand things about skin and vasculature that I would be hopelessly lost without. Additionally, I would like to thank the dozens of others throughout OLAC, UTCVM, MABE, and the rest of UTK I do not have room here to acknowledge who were all directly responsible for helping me get to this point in my research.

I would like to thank the faculty and staff at UTK who have taught me over the past 4 years and helped me learn everything needed to prepare me for both my doctoral research and the

future I have ahead of me. I would like to specifically acknowledge the rest of my doctoral committee, Dr. Jeffery Reinbolt and Dr. Joshua Weinhandl, for their support in the completion of this dissertation.

I would like to express my deep gratitude towards my parents, Tim and Laurie, who from an early age encouraged and reinforced all of my dreams. Everything I have would not have been possible if it wasn't for the life they worked hard to provide for me and the prayers they have said for me since the day I was born. I wish to thank my siblings, Kat and Stephen, and their spouses, Larry and Caroline, for building me up and cheering for me every step of the way while simultaneously humbling me and making sure I never forget what's most important. I would like to thank my best friends who are a second family to me: JB, Anthony, Owen, Ty, Erik, Matthew, and Brennan. All of these guys were by my side when I got married and will be by my side on the journey ahead. Through marriage I was able to add to my family with my new in-laws, Johnny, Anita, Brandon and Lauren. They have accepted me and made me feel like family. I am so grateful for their thoughts, prayers, and encouragement during these last 2 years of my dissertation.

And to my new wife Christen, none of this would have been possible were it not for your constant love and encouragement. Whether it was convincing me to relax and take a break from working for a second or encouraging me to keep going and working hard on the days where I felt like I had nothing left to give, I would not have been able to finish this dissertation if it wasn't for you. It is hard to believe that I did not know you when I started writing this dissertation. And sometimes even harder to believe that during that same period we were able to meet, travel, renovate a house, get engaged, survive a global pandemic, plan a wedding, plan 20 honeymoons, and laugh together every step of the way. I love you and cannot wait for the rest of our lives together.

Lastly, this would not have been possible were it not for the grace of our Lord and Savior, Jesus Christ, to whom all glory be given.

Research reported in this dissertation was supported by (1) the Eunice Kennedy Shiver National Institute of Child Health & Human Development of the National Institutes of Health under Award Number K12HD073945, (2) NSF CAREER Award #1944001, (3) a seed grant from the University of Tennessee Office of Research and Engagement, and (4) the University of Tennessee Department of Mechanical, Aerospace and Biomedical Engineering start-up funds.

ABSTRACT

Assistive devices serve as a potential for restoring sensorimotor function to impaired individuals. My research focuses on two assistive devices: a passive shoulder exoskeleton and a muscle-driven endoprosthesis (MDE). Previous passive shoulder exoskeletons have focused on testing during static loading conditions in the shoulder. However, activities of daily living are based on dynamic tasks. My research for passive shoulder exoskeletons analyzes the effect that a continuous passive assistance has on shoulder biomechanics. In my research I showed that passive assistance decreases the muscular activation in muscles responsible for positive shoulder exoskeleton. An MDE has the potential to have accurate and precise control of movement as well as restore a sense of proprioception to the user. Such a transformative and invasive device has never previously been tested. Therefore, my research focused on analyzing fundamental principles of the MDE in an in-vivo rabbit model. The two concepts I tested in my research were the feasibility of implanting an orthopedic device underneath the skin at the distal end of a limb following amputation and the locomotor restorative capabilities of an artificial tendon used for muscle-device connection. In my work I proved the feasibility of implanting fully-footed rigid endoprostheses underneath the skin and isolated the primary factors for a successful surgery and recovery. In addition, my research showed that although artificial tendons have the potential to restore locomotor function, proper in-situ tendon lengths must be achieved for optimal movement. This research informed the design and testing of a fully jointed muscle-driven endoprosthesis prototype.

TABLE OF CONTENTS

Chapter 1. Introduction.....	1
Motivation.....	1
Research Objectives and Approach	2
Chapter Summary	3
Chapter 2. Background Information.....	5
Biomechanics	5
Biomechanics of Movement	5
Focus 1: Shoulder Assistance through a Passive Shoulder Exoskeleton.....	7
Shoulder Anatomy and Movement	8
Shoulder Injury and Prevalence Rates	10
Assistive Devices for the Shoulder	11
Focus 1 of Dissertation	12
Focus 2: Limb Reconstruction through a Muscle Driven Endoprosthesis.....	15
Amputation Prevalence and Risk Factors.....	15
Intervention for Amputation	16
Muscle and Tissue Prosthesis Integration	19
Motivation behind Muscle-Driven Endoprostheses.....	21
Rabbit Hindlimb Anatomy and Biomechanics	24
Focus 2 of Dissertation	26
Summary and Significance of this Research	29
Chapter 3. Effect of Continuous, Mechanically Passive, Anti-Gravity Assistance on Kinematics and Muscle Activity During Dynamic Shoulder Elevation.....	32
Abstract	32
Introduction:	33
Methods:	34
Subjects:	34
Instrumentation and Setup:	35
Procedure:	37
Data Processing and Statistical Analysis:	39
Results	42
Dynamic Phase.....	42
Static Phase.....	42
Discussion:	47

Acknowledgments:	51
Chapter 4. Fully Implanted Prostheses for Musculoskeletal Limb Reconstruction after Amputation: An In Vivo Feasibility Study	52
Abstract	52
Introduction	53
Materials and Methods:	54
Summary:	54
Stem Endoprosthesis:	55
Pre-Surgery Bone Geometry Estimation:	55
Surgical Technique:	57
Post-Surgical Care:	58
Imaging:	58
Weight Bearing Analysis:	58
Results:	58
Bone-Device Interface:	58
Skin Closure:	59
Bandaging and Recovery:	64
Device Design:	64
Discussion:	65
Acknowledgements	69
Chapter 5. Ex-vivo analysis of Skin Tissue Surrounding a Stem Endoprosthesis Implanted in an Amputated Rabbit Hindlimb	70
Abstract	70
Introduction	70
Methods	72
Surgery Outcomes	72
Stem Device	73
Euthanasia, dissection, and fixation	73
CT Processing	74
Histology Analysis	76
Results	78
CT Reconstruction	78
Histology Analysis	78
Discussion	82
Acknowledgements	84

Chapter 6. Biomechanical Analysis of the Rabbit Hindlimb during the Stance Phase of Hopping Gait	85
Abstract	85
Introduction	86
Methods	87
Subjects	87
Instrumentation and Setup	89
Testing Procedure.....	89
Data Processing and Statistical Analysis	89
Results	93
Pressure Analysis	93
Hindlimb Kinematics	97
Discussion	101
Acknowledgments	104
Chapter 7. Analysis of the Effect of Artificial Tendon on Locomotor Function when Implanted in the Rabbit Hindlimb.....	105
Abstract	105
Introduction	105
Methods	107
Summary	107
Artificial Tendon	107
Surgical Procedure	108
Post-Surgical Care	110
Biomechanics Testing	111
Data Processing and Statistical Analysis	112
Results	113
Time-Series Biomechanical Comparison to Healthy Control Group.....	113
Post-surgical Functional Recovery based on Summary Outcome Measures.....	118
Discussion	122
Chapter 8. Conclusion.....	126
Contributions	126
Applications	126
Future Work.....	128
Exoskeleton Testing.....	128
Expanded Endoprosthesis Devices.....	128

Strengthening Residual Muscles after Atrophy.....	129
Skin Expansion and Grafting Techniques.....	130
References	131
Vita	147

LIST OF TABLES

Table 3.1. Static upper extremity postures in which subjects performed maximum voluntary contractions (MVCs).....	38
Table 3.2. Results from Two-Way Repeated Measures ANOVA.	44
Table 5.1. Histology analysis of critical skin locations.....	81

LIST OF FIGURES

Figure 2.1. Overview of Gait Terminology and Phase Breakdown.....	7
Figure 2.2. Shoulder Anatomy Overview.	9
Figure 2.3. Design of an exoskeleton prototype	14
Figure 2.4. Parts of a below-elbow myoelectric prosthesis	18
Figure 2.5. Design of a functioning hindlimb rabbit MDE prototype.	22
Figure 2.6. Mammalian Foot Postures.....	37
Figure 2.7. Synthetic tendon that could serve as a possible solution to muscle-prosthesis connection.	28
Figure 3.1. Subject set up to perform testing in the abduction plane.	36
Figure 3.2. Sample trial elevation angle used to segment trial into dynamic and static phases.	40
Figure 3.3. Maximum muscle activations measured during both dynamic and static elevation from rest to the target elevation angle with (orange) and without (gray) the applied assistive force...43	
Figure 3.4. SPM analysis of shoulder joint kinematics during dynamic straight arm abduction from rest to the target elevation angle both with (orange) and without (gray) the applied assistive force.	45
Figure 3.5. SPM analysis of shoulder joint kinematics during dynamic straight arm scaption from rest to the target elevation angle both with (orange) and without (gray) the applied assistive force.....	46
Figure 3.6. Joint angle kinematics during static elevation at the target elevation angle with (orange) and without (gray) the applied assistive force.	48
Figure 4.1. Stem endoprostheses used during surgery.	56
Figure 4.2. Radiographs of stems in situ.	60
Figure 4.3. A timeline displaying how the skin of the operated limb for each rabbit changed over time.....	61

Figure 4.4. Representation of the change in the incision approach that occurred between R3 and R4.	63
Figure 5.1. CT imaging of the skin from a residual limb of a successful rabbit.	75
Figure 5.2. Location of histology samples.	77
Figure 5.3. 3D skin thickness reconstruction for 3 rabbits.	79
Figure 5.4. Figure 5.4. Residual limbs of each limb normalized against the maximum skin thickness of the contralateral limb.	80
Figure 6.1. Testing setup used to collect motion capture data.	87
Figure 6.2. Example of strike box isolation of the contact foot using the Tekscan Walkway.	88
Figure 6.3. Motion capture analysis of the sagittal plane videos allowed for measurement of the rabbit hindlimb kinematics.	92
Figure 6.4. Vertical Ground Reaction Forces of rabbit hindlimbs throughout Stance Phase.	90
Figure 6.5. Contact Area of the rabbit hindlimb throughout stance phase.	91
Figure 6.6. Pressure of the rabbit hindlimb throughout stance phase.	91
Figure 6.7. Joint Kinematics of the rabbit hindlimb throughout stance phase.	92
Figure 6.8. Normalized joint tracking and kinematic comparison between knee trajectories.	99
Figure 6.9. Euclidian distance between right and left normalized joint positions throughout stance.	93
Figure 7.1. Artificial tendon used to recreate the connection between muscle and bone.	109
Figure 7.2. SPM comparison of pressure mat data throughout stance phase between surgical groups and healthy control at S5.	114
Figure 7.3. SPM comparison of pressure mat data throughout stance phase between surgical groups and healthy control at S5.	115
Figure 7.4. Comparison of normalized hindlimb kinematics between surgical and control groups at S5.	117
Figure 7.5. ROM measured across all testing timepoints.	108

Figure 7.6. Start and end angles measured across all testing timepoints.....	109
Figure 7.7. Pressure mat data measured across all testing timepoints.....	121

LIST OF ABBREVIATIONS

%BW – Percent Body Weight

+SE – Positive Shoulder Elevation

-SE – Negative Shoulder Elevation

AD – anterior deltoid

ADL – Activity of daily living

BLH – biceps brachii long head

CT – Computed Tomography

DOF – Degree of Freedom

EMG – Electromyography

H&E – Hematoxylin and eosin

IACUC – Institutional Animal Care and Usage Committee

IRB – Institutional Review Board

IS – infraspinatus

LD – latissimus dorsi

MD – middle deltoid

MDE – Muscle-Driven Endoprosthesis

MTP – Metatarsophalangeal

MVC – Maximum Voluntary Contractions

NLU – Normalized Length Unit

OLAC – Office of Laboratory Animal Care

PD – posterior deltoid

PM – pectoralis major

PVD – Peripheral Vascular Disease

RMS – Root Mean Square

SPM – Statistical Parametric Mapping

SS – supraspinatus

TLH – triceps brachii long head

vGRF – vertical Ground Reaction Force

UTK – University of Tennessee, Knoxville

UTCVM – University of Tennessee College of Veterinary Medicine

CHAPTER 1. INTRODUCTION

Have you ever experienced an injury or impairment that prevented you from performing basic everyday tasks? If so, you might have recovered your normal functional ability. But what would you do if it were impossible for you to ever return to normal function? Unfortunately, this is the case for millions of people across the world. Their primary hope in ever living a normal life again rests in the use of “assistive devices”. Whether they provide rehabilitation or physical enhancement, assistive devices are artificial devices intended to restore natural movement and sensation to people struggling to perform basic activities of daily living (ADLs). Assistive devices have the potential to help someone with moderate to severe disability live a normal, independent life. Research in the field of assistive devices focuses on improving upon previously existing devices or innovating a new device that can help people like never before. This dissertation addresses both improving upon a previous concept for shoulder assistive devices and developing a state-of-the-art assistive device for limb reconstruction. The work presented in this dissertation marks critical steps towards clinical translation of both assistive devices to eventually restore daily independence to severely disabled populations.

MOTIVATION

The CDC estimates that, in 2020, approximately 26% of Americans suffer from some form of disability or motor impairment [1]. Motor impairments, which disable functional movement, are linked to a variety of conditions, including: injury [2-4], comorbidities from old age [5], stroke [6], and various medical conditions [7, 8], among others. People with motor impairment struggle to perform basic ADLs [9-11]. ADLs are basic activities required to function independently in daily life. There is an ever growing need to develop interventions that can restore functional ability and, in turn, the ability to independently perform ADLs back to affected individuals.

The pursuit of restoring this quality of life to disabled individuals has influenced a focus in biomechanics and engineering towards the development of assistive devices designed to

enhance or restore motor function. Assistive devices are typically designed for specific motor impairments, such as exoskeletons and orthoses for muscle weakness and joint instability [12-15] or prostheses for amputation [16, 17]. My research is focused on two assistive devices for prevalent conditions that lead to a lack of motor function: (1) a passive shoulder exoskeleton to enhance function and aid in rehabilitation following shoulder impairment and (2) an implantable, muscle-driven endoprosthesis (MDE) to reconstruct a limb following amputation.

RESEARCH OBJECTIVES AND APPROACH

The **overall research objective** of this dissertation is to analyze the feasibility and functionality of key characteristics of the two assistive devices, the passive shoulder exoskeleton and the MDE, and their effect on user biomechanics. This research will help inform and optimize the device design and ensure safety and effectiveness to support clinical translation. The research activities are divided into **two research focuses, based on the assistive device, with five total research objectives:**

FOCUS 1: Research Objective 1: Determine the effect of continuous passive anti-gravity assistance on able-bodied muscle activations and shoulder kinematics during dynamic and static phases of shoulder elevation movements. The results will indicate the potential of wearable passive shoulder exoskeletons to lower muscle functional requirements and restore movement.

FOCUS 2: Research Objective 2.1: Determine the feasibility of fully enclosing an unjointed stem endoprosthesis *in vivo* in the hindlimb of a rabbit model of transtibial amputation. We will use an iterative study approach, determining factors in the surgery, device design, and post-surgical care that influence outcomes. **Research Objective 2.2:** Analyze reactionary changes in the skin structure of the rabbit hindlimb *ex vivo* caused by interaction with an unjointed stem endoprosthesis. We will analyze the changes in the skin through histology and microCT imaging of the residual limbs that successfully recover from implanting an unjointed endoprosthesis.

Research Objective 3.1: Measure healthy joint kinematics and vertical ground reaction forces in the rabbit hindlimb during the stance phase of hopping. Our approach will include a novel method for noninvasive rabbit locomotor function testing. **Research Objective 3.2:** Analyze the effect of an artificial, suture-based tendon on joint kinematics and vertical ground reaction forces. The artificial tendons will replace select biological tendons that cross the ankle in the rabbit hindlimb. The results from Research Objectives 2 and 3 will provide new information about fundamental aspects of an MDE prior to *in vivo* testing of MDE prototypes.

CHAPTER SUMMARY

In chapter 2, I overview fundamental concepts critical to understanding the scope of my dissertation. I first give an overview of biomechanics, looking at the experimental methodology, natural human movement, and the subfields within biomechanics. Next, I discuss shoulder anatomy and injury mechanisms, followed by a review of common assistive devices used as interventions for shoulder impairment in the context of informing the research performed in chapter 3. I then discuss different types of amputation alongside various methods for prosthetic intervention. I present the idea that integrating biological tissue into prosthetic design could increase the sensorimotor function of limb replacement. This idea motivates the research performed in chapters 4-7 towards the development of a muscle driven endoprosthesis. Finally, I overview the rabbit model which we use for testing of our prosthesis design concepts and give a summary of the work presented in this dissertation.

In chapter 3, I study the effect of continuous passive overhead assistance on shoulder biomechanics, specifically looking at how continuous assistance affects the muscular activity of muscles crossing the shoulder joint. This study has implications towards the efficacy of using assistive devices for continuous passive assistance to help with activities of daily living. The results indicate the potential of wearable passive shoulder exoskeletons to lower muscle functional requirements and restore movement.

In chapter 4, I analyze the feasibility of implanting a prosthesis completely underneath the skin at the distal end of a residual limb following amputation in a rabbit hindlimb. I show the results from iterative attempts to implant an unjointed stem endoprosthesis in the rabbit hindlimb and discuss the critical factors in the surgery, device design, and post-surgical care that influence outcomes for successful implantation.

In chapter 5, I further analyze the *ex vivo* skin tissue of rabbits with “successful” outcomes from chapter 4. I compare both computed tomography (CT) scans and histology slides of the residual skin covering the endoprosthesis with healthy contralateral control samples to identify potential anatomical changes in the skin in reaction to the endoprosthesis.

In chapter 6, I present a method for noninvasive motion capture for capturing the hindlimb biomechanics of a rabbit. Additionally, I also report data of healthy rabbit hindlimb biomechanics to use as reference or control data in future studies.

In chapter 7, I apply the motion capture technique presented in chapter 6 to rabbits that have undergone surgical artificial tendon replacement on major tendons crossing the hindlimb ankle joint. I present the results suggesting that rabbits with artificial tendon replacement can maintain locomotor function.

Finally, I discuss concluding remarks, limitations, and potential future work for these projects in chapter 8.

CHAPTER 2. BACKGROUND INFORMATION

BIOMECHANICS

Biomechanics of Movement

Biomechanics is the study of the structure, function, and movement of the mechanical aspects of biological tissue. Movement biomechanics encompasses both kinesiology and engineering and focuses on the interaction between bone, muscle, tendon, and ligament that produces movement in a living being. By treating the body as a mechanical system, biomechanics allows for quantification of human movement to better understand musculoskeletal function. Using principle of dynamics, where the bone is treated as a rigid body, muscle is treated as a force applicator, and ligaments and tendons are treated as spring-damper linkages, biomechanists can measure, model, and predict human movement.

Measuring human movement biomechanics can be broken down into measuring the position of bones, the angle of joints (kinematics), and the forces within joints and on bones, through either internal muscle force, joint reaction, or reaction with the outside world (kinetics). In humans, kinematics are traditionally measured through motion capture using reflective markers. Infrared cameras track reflective markers placed on the skin on top of bony landmarks. These markers are digitized into rigid segment representations of bone based on scaling from the 50th percentile person [18]. The relation between bones is tracked and used to calculate joint angles through various functional and experimental activities. Forces acting on or the effect of muscles acting within the body are measured using force sensors and electromyography (EMG), respectively. Force sensors, such as force plates [19, 20] for the lower limb or grip sensors [21] for the upper limb, measure the force that the body puts on an external object such as the ground or a handheld object. EMG electrodes placed across the muscle can measure the neuromuscular activity during tasks. This measured activity can be normalized against a muscle's maximum voluntary contraction (MVC) to estimate what percentage of maximum muscle activation is

occurring during specific movements. The forces of the muscles on the bone can then be calculated using anatomical measures of muscle architecture [22]. Through these various dynamic measuring techniques, biomechanical function can be measured to quantify a person's ability to perform functional tasks. Additionally, these same techniques could also reveal impairments in a person when compared to healthy biomechanical function.

Gait Patterns

Gait is the set or pattern of limb movements that generate a specific form of locomotion [23]. Three common gait patterns in humans are walking, running, and skipping gait that all require different kinematics patterns of movement caused by different muscle coordination patterns [24, 25]. Common measurements used to define human gait include joint and limb kinematics, ground reaction force, stride length, stride width, cadence, and velocity [23, 26-29]. These metrics can all be used to compare gait patterns between different experimental groups to determine the effect of an impairment or intervention.

Humans have a unilateral gait cycle where the right and left leg move in symmetric patterns with offset timing from each other. A full gait cycle refers to the time period between when one foot makes initial contact with the ground twice. Human gait can be subdivided into different phases (Fig. 2.1) [30]. The two primary phases of gait are stance phase and swing phase. Stance phase is the time period between initial contact of the foot ("foot strike" or "heel strike") and when the foot terminates contact with the ground ("toe off"). Each of these phases can be further divided into subphases. Stance phase can primarily be broken down into loading response and forward propulsion, or terminal stance [31]. The division between these two phases happens when the knee movement transitions from flexion to extension. The period where the knee joint is static is sometimes referred to as mid-stance. Similarly, swing phase can be broken down between initial swing and terminal swing, based on either flexion or extension of the knee joint, respectively.

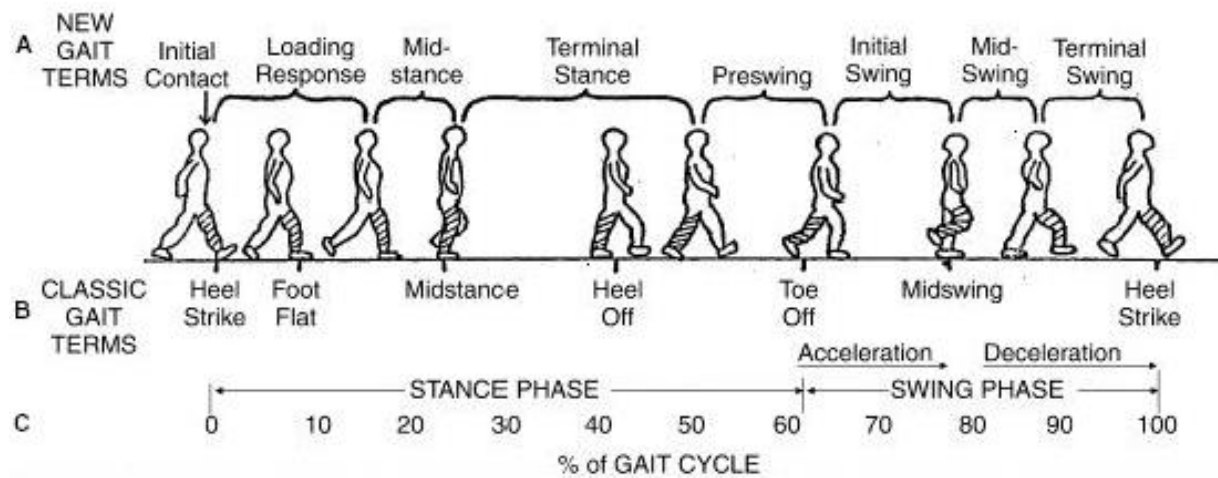


Figure 2.1. Overview of Gait Terminology and Phase Breakdown.

FOCUS 1: SHOULDER ASSISTANCE THROUGH A PASSIVE SHOULDER EXOSKELETON

Shoulder Anatomy and Movement

Anatomically, the shoulder is a joint consisting of a closed kinematic chain comprising the thorax, clavicle, scapula, and humerus as well as the muscles and ligaments that connect these bone [32]. The scapula, or shoulder blade, is a triangular shaped bone on the posterosuperior portion of the thorax. The clavicle, or collarbone, is a long, curved bone on the anterosuperior portion of the thorax. The humerus is a long bone in the arm that branches the shoulder with the elbow and has an ellipsoidal head at the proximal end. The shoulder kinematics mechanism includes three synovial joints, the sternoclavicular joint, the acromioclavicular joint, and the glenohumeral (GH) joint, as well as one non-synovial joint, the scapulothoracic joint. Primary movement in the shoulder joint occurs at the glenohumeral and scapulothoracic joints. The glenohumeral joint, the connection between the glenoid (the concave lateral end of the scapula) and the proximal humeral head, is commonly considered the main shoulder joint. However, movement in the scapulothoracic joint contributes greatly to the high mobility of the shoulder. The scapula rests on the posterior aspect of the thorax and is held to the thorax by muscles that either originate or insert into the scapula. Due to this, during shoulder movement, the scapula slides along the thorax, and its position is determined solely by the muscles attached to it.

There are 11 muscles that cross the shoulder joint (Fig. 2.2) [33]. The four muscles that immediately surround the glenohumeral joint are the supraspinatus, infraspinatus, subscapularis, and teres major, which together comprise the rotator cuff. The rotator cuff muscles originate from the scapula and insert into the proximal humeral head. Because the glenoid fossa does not encapsulate the humeral head, the rotator cuff serves as the primary stability that holds the glenohumeral joint together [34]. Additionally, the rotator cuff muscles are major contributors to shoulder movement. The remaining muscles that cross the glenohumeral joint are the deltoid, teres major, pectoralis major, latissimus dorsi, coracobrachialis, the long head of triceps, and the

Extrinsic Shoulder Muscles

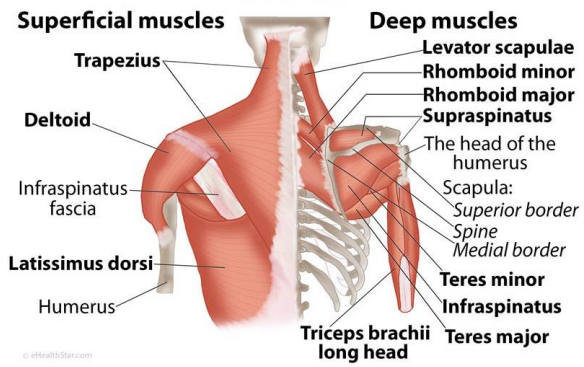


Figure 2.2. Shoulder Anatomy Overview. (Left) Anterior View of the Shoulder. The right arm of the person shows superficial muscles and the left arm shows deep muscles. (Right) Posterior View of the Shoulder. The right arm of the person shows superficial muscles and the left arm shows deep muscles.

long and short heads of biceps. Some of these muscles, such as the deltoid [35] and pectoralis major [36] can be further subdivided into compartments that can be individually activated.

Due to both the minimal contact area between the glenoid and the proximal humeral head and the scapulothoracic articulation, the shoulder boasts the greatest range of motion of any joint in the body. The movement of the scapula relative to the thorax (i.e. scapular kinematics) has become a focal point of research in understanding shoulder mobility and injury mechanisms [37-43]. In 2000, Karduna, *et al.* [39] introduced the concept of how the movement of the scapula altered the Euler angle decomposition of the shoulder. Prior to this, the motion of the scapula was considered planar, only measuring upward rotation, because that was the only rotation that could be assessed clinically. Karduna, *et al.* found that all Euler sequences showed significantly different rotations for at least two different humeral elevation angles when compared to his proposed standard of EUP, proving that it mattered greatly in which order the rotations were performed for the scapula and proposed that for standardization of scapular kinematics, EUP should be used since it is consistent with research and clinical based two-dimensional representations of scapular movements. In 2005, the Standardization and Terminology Committee for the International Society of Biomechanics proposed a 2-1-2 Euler decomposition to describe shoulder joint kinematics, with the positive x-axis being aligned with the direction of the humerus, which is now considered the standard definition for defining movement of the shoulder joint [44].

Shoulder Injury and Prevalence Rates

Upper limb movement disability involving the shoulder is associated with both acute and chronic health conditions. Common acute shoulder injuries include glenohumeral dislocation, rotator cuff tear, and labrum tear. Acute shoulder injuries typically occur through high-impact trauma. Glenohumeral dislocation is the most common joint dislocation, occurring in 24 out of every 100,000 adults [45]. 90% of the time, glenohumeral dislocation occurs through anterior

dislocation caused by abduction, extension, and external rotation on the shoulder [46]. Rotator cuff tear refers to a tear in any of the four muscles of the rotator cuff and is common among elderly populations [47]. Rotator cuff tears are commonly treated through both surgical and nonsurgical intervention, based primarily of the severity of the injury [48]. 5%-40% of all rotator cuff injuries are considered full-thickness in at least one of the four rotator cuff muscles [49]. Common chronic conditions that cause shoulder impairment include peripheral nerve injury [50] and stroke [51]. Both of these conditions commonly lead to neuromuscular impairment in the affected limb, sometimes even leading to total limb paralysis [6, 52].

For all of these various types of impairments, although patients may retain some shoulder strength and function, they are substantially diminished from that of the healthy shoulder [50]. Shoulder impairment may make it more difficult for patients to perform ADLs. For some conditions involving soft tissue injury, such as rotator cuff tear, biomechanical loads during ADLs may lead to high reinjury rates [53]. Assistive devices that can provide continuous mechanical assistance to the shoulder are needed to help augment movement ability and decrease biomechanical loads in soft tissues in patients with shoulder impairment.

Assistive Devices for the Shoulder

There has been an increasing interest in the research, development, and commercialization of exoskeletons that are designed to replace or rehabilitate shoulder joint function [54-57]. Several exoskeletons and orthoses have been designed to support the shoulder. Such devices have promising potential to enhance motor function and prevent injury [58-61]. Exoskeletons are devices that attach externally on the human body and apply forces to assist movement. Exoskeletons typically fall under two different categories based on how the forces are generated: powered and passive.

Powered exoskeletons use motors as actuators, applying forces near the joints to augment movement [12, 62-66]. Many powered exoskeletons are typically intended for cases of

severe impairment that require complete replacement of movement or total neurorehabilitation. However, due to their size, weight, or operation requirements, such powered exoskeletons are usually constrained to clinics and labs, preventing continuous at-home assistance. A powered soft wearable device was recently introduced that is lightweight and portable [52]. However, powered exoskeletons may be relatively expensive to purchase and maintain since they rely on motors, power supply, and computational hardware, which are susceptible to electromechanical malfunction. Powered exoskeletons are also traditionally bulky, which may compromise their comfort and visual appeal.

Compared to powered exoskeletons, mechanically passive exoskeletons may be more practical for home-based movement assistance. Passive exoskeletons incorporate elastic springs to store energy that can be returned to the user to supplement muscle forces for some movements [14, 60, 61, 67-70]. These devices are potentially more reliable, affordable, lightweight, and compact since they do not have electromechanical hardware. Many passive exoskeletons have already been previously developed, including the SpringWear 5-DOF spring actuated exoskeleton [71] and the WREX for children with neuromuscular disabilities [70].

Focus 1 of Dissertation

It is essential to consider how exoskeletons interact with the human limb to ensure that they provide appropriate assistance without impeding motion. This is especially important for passive exoskeletons since their assistance is constrained by mechanical design. Passive shoulder exoskeletons generally apply a continuous (i.e. always present) force to the upper extremity to compensate for gravity. Previous biomechanical studies of continuous anti-gravity shoulder assistance primarily focused on overhead tasks. This is because most commercially available passive shoulder exoskeletons are intended to assist overhead tasks, which are associated with a high prevalence of occupational shoulder injury [72, 73]. During overhead tasks, the shoulder assumes a mostly static posture. Promisingly, anti-gravity assistance reduced

activations of the middle deltoid, anterior deltoid, and biceps brachii muscles by as much as 62%, 80%, and 49%, respectively, while able-bodied subjects performed overhead tasks [59, 61, 74-76]. Continuous anti-gravity assistance may be useful for supporting dynamic shoulder elevation movements, which are more characteristic of activities of daily living [77] and many rehabilitation exercises [11]. A relatively few studies showed that, during dynamic movements, passive shoulder exoskeletons decreased activations of some muscles but increased activations of others [75, 78]. However, these studies averaged results across long time periods, masking the nature and potential mechanisms of activation changes.

We have developed a passive portable exoskeleton that, similar to one reported in a previous study [79], uses a spring-pulley system and a cam wheel to provide gradually increasing mechanical assistance as the shoulder is elevated against gravity. Our previous computer simulations of dynamic shoulder elevation [80], based on a shoulder exoskeleton prototype being developed in our lab (Fig. 2.3), showed that activations of muscles that primarily contribute to positive shoulder elevation (+SE), based on reported muscle moment arms [81], were lower with anti-gravity exoskeleton assistance than without. Conversely, antagonist muscles that primarily contribute to negative shoulder elevation (-SE) had higher activations with assistance to simultaneously decelerate the arm at the endpoint and overcome the assistive force. Our computational study was limited because the simulated kinematics were constrained to be the same with and without an exoskeleton. It is unclear whether human subjects would adapt their kinematics and muscle coordination patterns to avoid increasing activations of -SE muscles with anti-gravity assistance.

The **Research Objective 1** of this dissertation was to determine the effect of continuous passive anti-gravity assistance on able-bodied muscle activations and shoulder kinematics during dynamic and static phases of shoulder elevation movements.

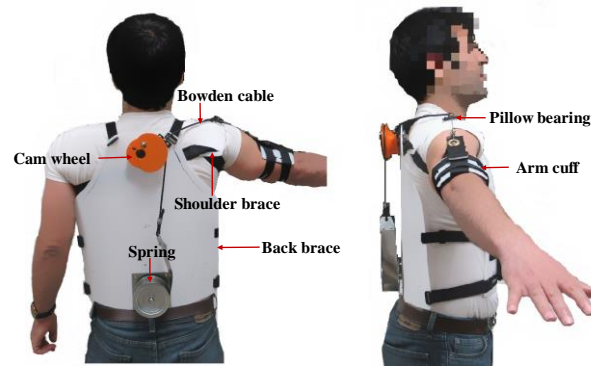


Figure 2.3. Design of an exoskeleton prototype currently under development in our lab. This design uses a cam wheel to gear a passive force to increase the applied force on the shoulder as a function of the elevation angle.

FOCUS 2: LIMB RECONSTRUCTION THROUGH A MUSCLE DRIVEN ENDOPROSTHESIS

Amputation Prevalence and Risk Factors

The number of amputees in the United States is growing. A study by Ziegler-Graham et al. [82] predicted that, if left unchecked, by the year 2050 the number of people living with limb loss will raise to 3.6 million. The two primary causes of amputation are medical-related and trauma-related amputations. According to a breakdown by the Center for Orthotic & Prosthetic Care, approximately 84% of amputations are caused by medical conditions such as dysvascular diseases, diabetes, cancer, and other congenital conditions, while 16% are caused by severe trauma [83]. For the location of amputation, lower body amputations are much more common, comprising 86% of all amputations, as opposed to 14% in the upper body [83].

Approximately 69% of all trauma related amputations occur in upper extremities [83]. Trauma related amputations occur when all the extremity tissue is severed from the rest of the body or damaged beyond repair. The severity of trauma is determined using a scale called the Mangled Extremity Severity (MES) which measures severity by looking at four major tissue systems of the affected extremity: skin, nerve, artery, and bone [84, 85]. Johansen et al. [86] showed that a MES score of 7 out of 10 predicted that trauma repair surgery would end in amputation with 100% accuracy.

In amputation surgery, the two primary goals are to salvage as much of the residual limb as possible and to best prepare the limb for use with a prosthesis. This process looks different for every amputation, with some surgeons choosing to anchor the muscle to the bone, some allowing the muscle to retract into the residual limb, and some choosing to use a bone bridge to allow the muscle to anchor through the bone for a better weight bearing prosthetic interface [85, 87-90]. Every surgery is dependent on several factors ranging from location and severity of injury to patients' desired function after amputation. For example, a trans-osseous bone-bridging

technique is more likely in a transtibial lower limb amputation where the primary concern is weight bearing on a passive prosthetic, while a disarticulation amputation is more likely on an upper limb amputation where the primary concern is maintaining neuromuscular function to interact with a myoelectric prosthetic hand.

Intervention for Amputation

Prostheses are the primary intervention for patients post-amputation and serve to restore movement and mobility. Prostheses generally refer to any device used to replace a missing or damaged body part. The goal of a prosthesis is to replicate the form and/or function of the body part it is replacing. There are many types of prostheses, such as orthopedic implants [91, 92], cosmetic enhancements [93], and sensory prostheses like ocular [94, 95] and cochlear [96, 97] implants). Limb prostheses generally attempt to replicate some combination of the peripheral muscular, skeletal, and nervous tissue of the extremity lost during amputation. Prostheses can be divided into several different groups based on location (upper-limb vs lower-limb) and level (transtibial vs transfemoral) of amputation. However, there are three main types of functional prostheses: passive, powered, and body-powered. Traditionally, all three types are attached to the body using a custom-fit socket that secures to the residual limb. However, they all vary in the methods in which they function.

Passive Limb Prostheses

Passive prostheses can be further subdivided into cosmetic and functional prostheses. Rather than provide a musculoskeletal function, cosmetic prostheses are generally used to disguise injury or impairment [98, 99]. Similar to passive exoskeletons previously mentioned in this chapter, passive prostheses work by storing energy and releasing it to perform movement. Due to the cyclic loading and unloading patterns that occur during a normal gait cycle, passive prostheses are traditionally used for lower limb amputees [100-102]. Common examples of passive lower-limb prostheses include the blade prostheses commonly seen in Paralympic

athletes [103] and more complex feet such as the Ossur Pro-Flex Pivot (Ossur, Reykjavik, Iceland) that provides greater levels of power upon elastic force return and greater ankle range of motion during walking gait compared to other passive devices.

Powered Limb Prostheses

Powered limb prostheses are external devices for musculoskeletal reconstruction that rely on electromechanical systems to recreate functional movement. Traditionally, powered limb prostheses include a robotic manipulating limb, EMG electrodes to measure muscle activation, a socket to affix the device to the residual limb, a battery pack to supply power, and a control unit to move the prosthesis based on measured EMG signals (Fig. 2.4) [104]. These powered prostheses incorporate electromechanical hardware (e.g. motors, microprocessors, sensors, electrodes) [17, 105-118] and control algorithms that decode users' movement intent from electromyograms [119-131]. The algorithms use the decoded EMG signals to predict intended movement and to output movement patterns to the motors in the robotic limb. Control algorithms help determine the complexity of the performed movement and can range from simple 1 degree of freedom control through flexion and extension [132, 133] to complex continuous movement control through modeling user intention through more complex simulations [119]. As opposed to lower limb prostheses that can generate movement through cyclic loading and unloading for locomotion, biomechanical function of upper limb prostheses must rely on unique, idiosyncratic movement. Therefore, powered limb prostheses which allow for volitional control of movement are a common intervention for upper limb amputation.

Body-Powered Limb Prostheses

Body-powered limb prostheses function by using the remaining movement of the residual or contralateral limbs to control and move the distal prosthetic device. This is done by using force across a remaining joint to actuate mechanical components of the prosthesis. A common example of a body-powered prosthesis is the hook hand that is mechanically connected to the residual shoulder or elbow joint [134, 135]. Extension of either of these joints pulls on the bifurcated, jointed

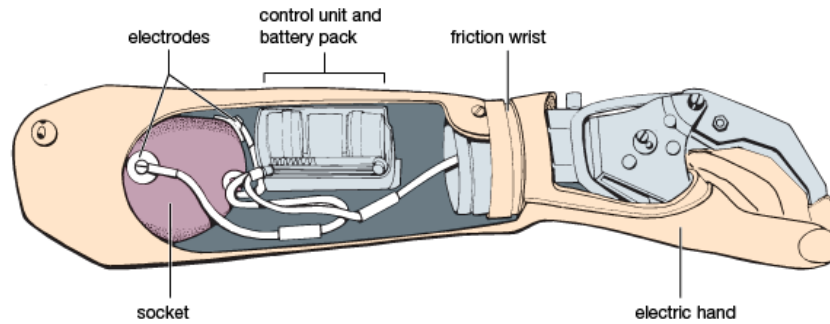


Figure 2.4. Parts of a below-elbow myoelectric prosthesis. A generalized powered prosthesis is comprised of the following parts: 1) A custom-fit socket to attach to the residual limb, 2) An on-board microprocessor that deciphers EMG signals and determines movement, 3) a battery pack that provides power, 4) EMG electrodes that measure neuromuscular activity, and 5) an electromechanical limb that outputs movement.

hook, controlling the opening and closing of the hook [136]. Despite the users having good control of these devices, they have been reported as difficult to use due to the inefficient mechanical leverage of the design of the devices [137, 138].

Muscle and Tissue Prosthesis Integration

Despite the many benefits current prosthetics offer amputees, there is still a high percentage of the amputee population that rejects using a prosthetic for a variety of reasons. In a survey by Biddiss et al. [138], rejection was higher in upper-limb amputees with a more severe level of limb loss. The primary reasons given for rejection were related to prosthetic technology and design, with often-cited reasons being appearance, comfort, function, ease of control, reliability, and cost. Recent prosthetic research has been devoted to addressing these rejection factors.

Considering the anatomical and physiological changes to the residual limb during amputation could help explain the sensorimotor limitations of external prostheses. In a healthy intact limb, muscles produce force across a joint when stimulated by neural signals, creating movement. There are two main types of mechanoreceptors in muscle: (1) muscle spindles, which sense changes in length [139] and (2) Golgi tendon organs, which senses force in the muscle [140]. When these mechanoreceptors sense changes in either the length or force of the muscle, they send afferent signals to the brain. The brain's interpretation of the afferent signals engenders proprioception. The physical link between the muscle and bone causes sensorimotor alignment, which is the experience that the perception of movement matches both the intended and actual motor output. This sensorimotor alignment is critical for accurate motor function in the limb [141]. During amputation, the physical link between the bone and muscle is disconnected, causing sensorimotor misalignment in the residual limb. Therefore, despite external prostheses' attempt to accurately interpret efferent motor commands (i.e. EMG) and simulate afferent proprioception through stimulation, sensorimotor issues of external prostheses persist, likely due to functional

loss caused by sensorimotor misalignment and the prosthetic's physical detachment from biological tissue. (Fig. 2.2)

To solve these sensorimotor issues, recent research has shown that performance of prosthetics can be improved by directly interfacing with and leveraging the functional capabilities of biological tissues. For example, by harnessing the structure integrity of bone [142, 143], transcutaneous osseointegrated sockets provide a more secure and reliable prosthetic attachment than traditional sockets that fit over the residual limb. Osseointegration induces an afferent sensation called osseoperception through mechanoreceptors in the bone and joints that sense vibrations from the ground reaction forces, increasing proprioception [144]. Also, electrodes directly implanted in muscles or nerves provide more precise sensory feedback signals than surface mounted sensors [145].

One potential solution to overcome sensorimotor limitations of external prostheses is to physically attach prostheses to muscles. This is because muscles contribute to both movement generation and sensation, via mechanoreceptors, in the biological limb and, thus, are essential to physiologic sensorimotor function [146]. There is strong evidence that muscles in the residual limb retain their sensorimotor functions after amputation. Reengaging residual muscles in movement has been shown to restore natural proprioceptive pathways through native muscle mechanoreceptors [131], which could enable amputees to experience more realistic sensation of their movements and perform tasks more effectively. One group surgically connected an agonist-antagonist muscle pair in the residual limb, allowing the mechanoreceptors in the residual muscles to experience changes in force and length, which restored a sense of proprioception to the user [147]. Additionally, residual muscles can still produce coordinated contractions to perform functional task, as has been shown in EMG-based control algorithms that allow for continuous control of multiple joints simultaneously [119, 129, 148, 149].

Previously, a surgical technique called cineplasty was used to achieve physical muscle-prosthesis attachment [150-153]. During the cineplasty surgery, the tendon of the residual muscle was passed through a loop created in the skin. The contraction of the skin-tendon loop would pull, via a cable, on an external prosthesis to generate movement. Reports note anecdotally that cineplasty enabled exquisite control and sensation of prosthesis movements [16, 154]. However, cineplasty has several limitations preventing widespread clinical adoption. Primarily, the skin-tendon loop likely did not provide an efficient method for force transmission. The force produced by the muscle would have contracted the skin loop rather than directly move the prosthetic, which would reduce the force actually applied on the external prosthetic. Therefore, the force directed towards movement of the prosthesis would have resulted in only a fraction of what would be required for functional movement. Also, this inefficient force leverage possibly led to fatigue and discomfort over prolonged use. Additionally, the skin loops paired with the external prostheses proved aesthetically displeasing.

Motivation behind Muscle-Driven Endoprostheses

To address the limitations of cineplasty for direct prosthesis control through muscle-prosthesis attachment, we propose a limb replacement approach called a muscle-driven endoprosthesis (MDE) (Fig. 2.5). An MDE is a prosthesis that is implanted completely underneath the skin at the distal end of a residual limb and physically attached to the residual muscles. By being implanted underneath the skin, an MDE allows for direct linear connection between the muscle and prosthesis that could accurately mirror the geometric muscle-tendon orientation of the anatomical limb. Linear connection between the muscle and prosthesis would allow for greater mechanical leverage which would provide more efficient direct force transmission to the prosthesis, which would address the primary limitation of cineplasty. Additionally, by restoring the physical connection between the skeletal and muscular systems, we expect that an MDE would

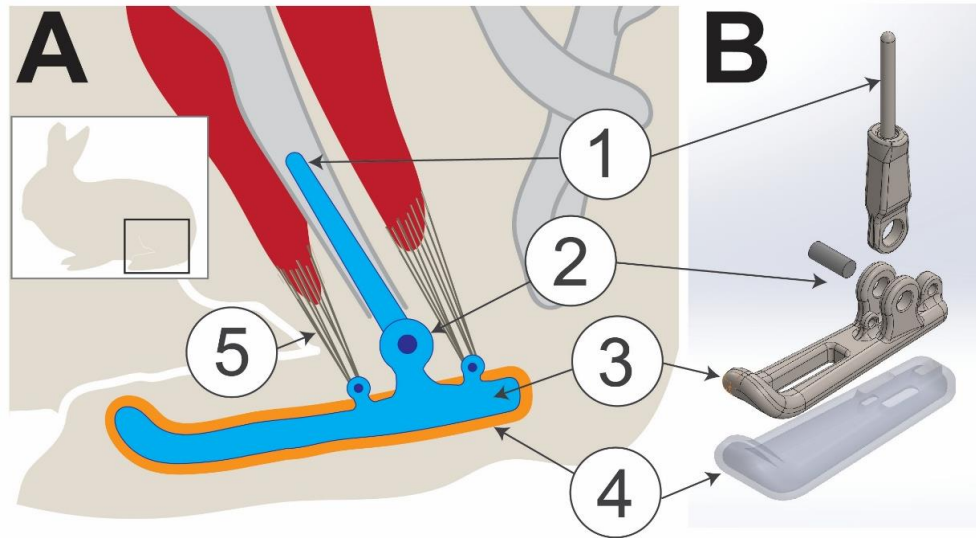


Figure 2.5. Design of a functioning hindlimb rabbit MDE prototype. (1) Tibial bone pin that is implanted into the tibial medullary canal. (2) Joint that allows for 1-DOF rotation to simulate the ankle joint. (3) Rigid foot segment that resembles the structure of the rabbit foot. (4) Silicone coating to help with pressure dispersion and prevent tissue adhesion. (5) Synthetic tendon that is integrated in the muscle and used to apply muscle force across the joint.

substantially increase the quality, control, and dexterity of movements that amputees can achieve over a modern external electromechanical prosthetic limb.

An MDE is a highly invasive device intended to imitate the anatomical musculoskeletal structure of an intact limb. Before testing such an invasive device on humans, we need to develop an animal model and compatible MDE prototype to test the feasibility and functionality of MDEs. Our long-term plan is to test MDE prototypes that replace the hindlimb ankle in the rabbit model due to their (1) prevalence in previous orthopedic and muscle rehabilitation research, (2) high range of motion in the hindlimb, which would allow us to easily detect changes in biomechanical function, and (3) musculoskeletal structure being large enough to test an MDE prototype.

A functioning MDE prototype to replace the rabbit hindlimb ankle would consist of several main components (Fig. 3): (1) Modified bone pins that will be used for osseointegration inside the medullary canal of the long bone. Bone-device integration is a highly studied field in both prosthesis and orthopedics with several techniques being developed for better osseointegration to increase stability of the implant. (2) A moveable joint in the MDE with muscles attached across the joint would allow for controlled movement of the limb segment with muscle activation. In the ankle, a 1-DOF hinge joint would allow for plantar and dorsiflexion. (3) A large rigid segment of a material strong enough to support both muscle forces and ground reaction forces would be used as a moveable foot segment. Eyelets on the foot would allow for connection of the synthetic tendon. (4) The foot segment is over-molded with a biocompatible silicone sleeve intended to increase pressure dispersion along the bottom, weight-bearing surface of the endoprosthesis and prevent tissue adhesion. (5) Finally, an artificial, suture-based tendon would be surgically integrated into the muscle and attached to eyelets on the foot segment to directly translate muscle force to the MDE

Rabbit Hindlimb Anatomy and Biomechanics

The rabbit hindlimb is comprised of 22 bones [155]. The four bones that comprise the leg are the femur, tibia, fibula, and patella. The leg connects to the foot at the tibiotalar joint. The foot can be subdivided into 6 tarsal bones, 4 metatarsal bones, and 8 phalangeal bones. The tarsal bones consist of the calcaneus, talus, distal central tarsal bone, and Os tarsals II-IV. A rabbit has 12 muscles that cross the ankle joint. Though most muscles contribute to more than one movement, they can generally be divided into 2 groups: 7 plantar flexor and 5 dorsiflexor muscles [156]. The plantar flexor muscles are the medial and lateral gastrocnemius, soleus, plantaris, tibialis caudalis, flexor digitorum longus, and the flexor hallucis longus. The primary muscle group that contributes to plantar flexion consists of the medial and lateral gastrocnemius and the soleus. This muscle group is attached to the superiocranial aspect of the calcaneus through the Achilles tendon. The dorsiflexor muscles are the tibialis, extensor digitorum longus, peroneus longus, peroneus brevis, and the peroneus tertius. The primary muscle responsible for dorsiflexion is the tibialis cranialis and it inserts into the medial most tarsal and metatarsal bones through the tibialis cranialis insertion tendon.

The rabbit model is a common model for comparative biomechanics in orthopedic research, and is used to test dental implant osseointegration [157-160], soft tissue analysis [161, 162], and bone degradation and repair [163-166]. Although there are limited studies looking at the biomechanical function of the rabbit hindlimb, the rabbit hindlimb has many similarities to the human foot, making it a good model to study biomechanical changes caused by an intervention. Primarily, as opposed to animals like dogs and cats that are digitigrade [167] or goats and pigs that are unguligrade [168], rabbits and humans are both plantigrade (Fig. 2.6) [169]. This means that rabbits and humans should have more similar kinematic patterns and ground-reaction pressure patterns than a different animal model, such as a cat or dog. Additionally, rabbits qualitatively have a very high range of motion in the ankle joint, allowing high sensitivity in

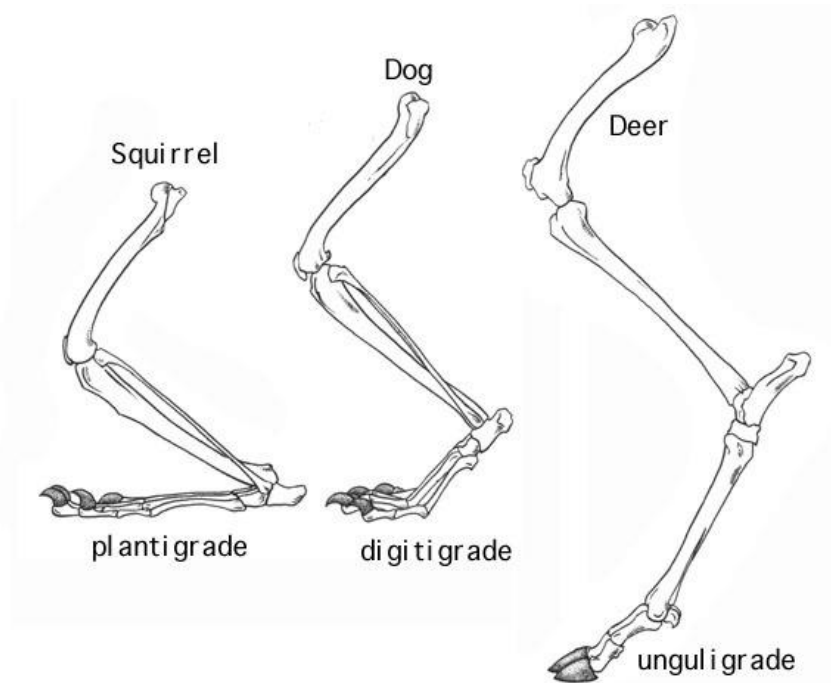


Figure 2.6. Mammalian Foot Postures. Plantigrade mammals, such as humans and rabbits support their weight across the entire foot. Digitigrade mammals, such as cats and dogs support weight on their toes. Unguligrade mammals such as goats and pigs support their weight on a hoof.

detecting kinematic differences between groups. However, the range of motion of the ankle joint has never been reported. This is critical knowledge for designing the function range of motion of an MDE.

Rabbits, like most non-human mammals, are quadrupeds, meaning they walk on four legs. This introduces slight differences between rabbit and human gait. Unlike humans, rabbits have a gait where both hindlimbs perform symmetric movements simultaneously, rather than alternating gait patterns between legs. During quadruped gait, the forelimbs experience approximately 60-65% of body weight and the hindlimbs experience 40-45% of body weight [170, 171]. This means that the rabbit forelimbs are primarily responsible for balance and weight bearing and the hindlimbs are primarily responsible for forward locomotion, while humans perform all three functions on their 2 legs.

Focus 2 of Dissertation

Before testing a full MDE prototype *in vivo*, there was a need to address two key questions to inform MDE prototyping and testing:

Is it feasible to fully enclose a prosthesis in healthy skin at distal end of a residual limb? The proposed endoprosthesis differs from previous percutaneous osseointegrated prostheses, which protrude through skin to provide an anchor point for externally worn limb prostheses. Like other common orthopedic implants such as joint replacements [91, 92], endoprostheses would replace part of the musculoskeletal structure of the missing limb. However, there has never been device implanted at the distal end of a residual limb for such as purpose. The feasibility of this is unknown and needs to be tested with a basic unjointed endoprosthesis before attempting to implant a more complex MDE design.

How does an artificial tendon implant across the ankle in the hindlimb affect a rabbit's locomotor function? In order to directly attach residual muscle to a device, there must

be an interface between the two that mirrors the function of the tendon in the anatomical limb (Fig. 2.7). A durable muscle-tendon interface has been developed and was noted as having secure muscular integration between the fibers of the suture used to make the artificial tendon [172] (Fig. 7, A). This artificial tendinous structure was tested successfully in the quadriceps of the goat model [173] (Fig. 7, B). However, biomechanical analysis was never performed on the animals showing how effectively this artificial tendon restored locomotion. In order to determine the efficacy of this synthetic tendon's ability to restore motor function, we must first test the effect of the artificial tendon on locomotion in our rabbit model.

The objectives of research focus 2 are:

Research Objective 2.1: Determine the feasibility of fully enclosing an unjointed stem endoprosthesis *in vivo* in the hindlimb of a rabbit model of transtibial amputation. We will use an iterative study approach, determining factors in the surgery, device design, and post-surgical care that influence outcomes.

Research Objective 2.2: Analyze reactionary changes in the skin structure of the rabbit hindlimb caused by interaction with an unjointed stem endoprosthesis. We will analyze the changes in the skin through *ex vivo* histology and microCT imaging of the residual limbs that successfully recover from implanting an unjointed endoprosthesis.

Research Objective 3.1: Measure healthy joint kinematics and vertical ground reaction forces in the rabbit hindlimb during the stance phase of hopping. Our approach will include a novel method for noninvasive rabbit locomotor function testing.

Research Objective 3.2: Analyze the effect of an artificial, suture-based tendon on voluntary locomotion. The artificial tendons will replace select biological tendons, either the Achilles or tibialis cranialis insertion tendon, that cross the ankle in the rabbit hindlimb.

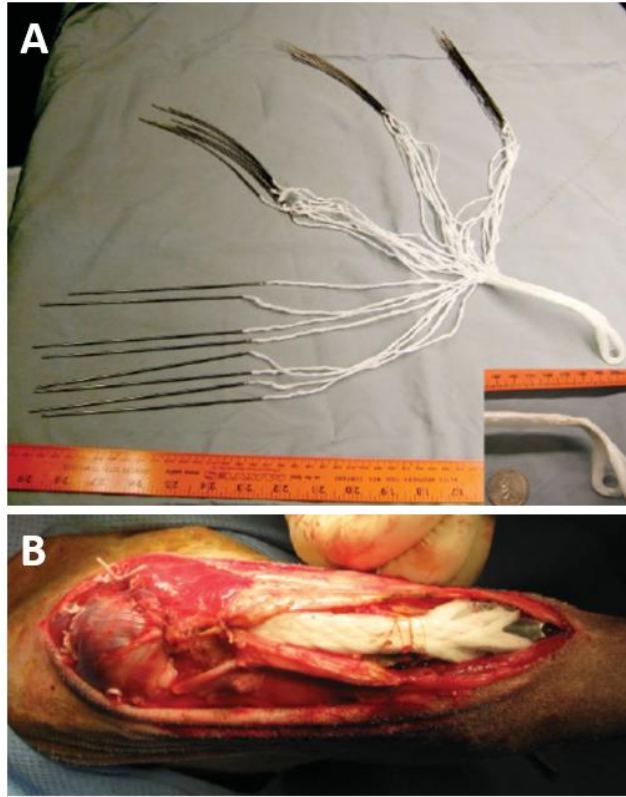


Figure 2.7. Synthetic tendon that could serve as a possible solution to muscle-prosthesis connection. (A) The artificial tendon consists of sutures looped and braided together, then coated in silicone. **(B)** Synthetic tendon implanted in the goat model to reattach the quadriceps to bone.

The results from Research Objectives 2 and 3 will provide new information about fundamental aspects of an MDE prior to *in vivo* testing of MDE prototypes.

SUMMARY AND SIGNIFICANCE OF THIS RESEARCH

My research explores the effect of multiple assistive devices on biomechanics and analyzes functional changes caused by interaction with the assistive devices. I analyzed functional changes throughout shoulder movement in humans with continuous passive assistance and throughout stance phase in rabbits with artificial hindlimb tendons. Additionally, I analyzed the feasibility of implanting an endoprosthesis in the rabbit hindlimb and the device's effect on the surrounding tissue.

Effect of Continuous, Mechanically Passive, Anti-Gravity Assistance on Kinematics and Muscle Activity During Dynamic Shoulder Elevation. In this research I tested the effect an overhead continuous force applicator has on the healthy human shoulder. I evaluated the changes (both decreases and increases) in muscle activation associated with the continuous assistive force about the shoulder and monitored the changes in kinematics in the shoulder joint under the presence of continuous passive assistance. The results indicate the potential of wearable passive shoulder exoskeletons to lower muscle functional requirements and restore movement.

Fully Implanted Prostheses for Musculoskeletal Limb Reconstruction after Amputation: An In Vivo Feasibility Study. In this study I analyzed the feasibility of implanting device intended for musculoskeletal reconstruction completely underneath the skin at the distal end of a rabbit hindlimb. Not only did I show feasibility in three consecutive rabbits, but I also determined key factors of success during surgery and recovery for implanted endoprotheses. This study informs which design, surgery, and recovery practices and techniques should be implemented with future devices as we progress towards a functional “footed” endoprosthesis prototype.

Ex-vivo analysis of Skin Tissue Surrounding a Stem Endoprosthesis Implanted in an Amputated Rabbit Hindlimb. This study analyzed the skin of rabbits who successfully recovered from implantation of a stem endoprosthesis. Virtual reconstruction of the residual rabbit limb through a microCT scan allowed for isolation of thick or thin areas of skin where tissue regrowth could have occurred or not. Additionally, histology of the skin samples allows us to analyze the cellular composition of skin at points of interest, such as along the incision line, to better understand the physiologic response of the cells to the surgery and recovery. The results of this study add quantitative findings to our feasibility analysis and help understand how residual skin reacts when around an endoprosthesis.

Biomechanical Analysis of the Rabbit Hindlimb during the Stance Phase of Hopping Gait. Prior to this study, there was limited research on the hindlimb biomechanics of hopping gait in the rabbit hindlimb. This study not only reports hindlimb kinematics, vertical ground reaction forces, contact area, and pressure in a healthy rabbit hindlimb, but also outlines a method for non-invasive motion capture never reportedly tested on rabbits. The results of this study add valuable information to the limited preexisting reference data for rabbit hindlimb biomechanics. As seen in chapter 7 of this dissertation, the healthy control rabbit reference data can be used to analyze the effect of various orthopedic interventions on locomotor function.

Analysis of the Effect of Artificial Tendon on Locomotor Function when Implanted in the Rabbit Hindlimb. This study showed the effect of artificial tendons implanted in place of either the Achilles or Tibialis Cranialis insertion tendons on rabbit hindlimb biomechanics. Rabbits with Tibialis Cranialis tendon replacement showed near normal levels of locomotor function after 6 weeks post-surgery. Rabbits with Achilles replacement showed lower levels of locomotor function, compared to a healthy control. However, over the course of the 6-week post-surgical period the Achilles rabbits showed significant recovery over initial post-surgical levels of

impairment. This study suggests that artificial tendons could be a viable solution to force transfer between residual muscle and a jointed endoprosthesis prototype.

CHAPTER 3. EFFECT OF CONTINUOUS, MECHANICALLY PASSIVE, ANTI-GRAVITY ASSISTANCE ON KINEMATICS AND MUSCLE ACTIVITY DURING DYNAMIC SHOULDER ELEVATION

This work was published in the Journal of Biomechanics.

Hall P. T. and D. L. Crouch. Effect of continuous, mechanically passive, anti-gravity assistance on kinematics and muscle activity during dynamic shoulder elevation. *Journal of Biomechanics* 103: 109685, 2020.

ABSTRACT

Passive shoulder exoskeletons, which provide continuous anti-gravitational force at the shoulder, could assist with dynamic shoulder elevation movements involved in activities of daily living and rehabilitation exercises. However, prior biomechanical studies of these exoskeletons primarily focused on static overhead tasks. In this study, we evaluated how continuous passive anti-gravity assistance affects able-bodied neuromuscular activity and shoulder kinematics during dynamic and static phases of shoulder elevation movements. Subjects, seated upright, elevated the shoulder from a rest posture (arm relaxed at the side) to a target shoulder elevation angle of 90°. Subjects performed the movement in the frontal (abduction) and scapular (scaption) planes with and without passive anti-gravity assistance. Muscles that contribute to positive shoulder elevation, based on their reported moment arms, had significantly lower muscle activations with assistance during both dynamic and static elevation. Muscles that contribute to negative shoulder elevation, which can decelerate the shoulder during dynamic shoulder elevation, were not significantly different between assistance conditions. This may be partly explained by the trend of subjects to reduce their maximum angular decelerations near the target to offset the positive shoulder elevation moment due to the anti-gravity assistance. Our results suggest that passive anti-gravity assistance could reduce the muscle activations needed to perform dynamic movements. Consequently, the anti-gravity assistance of passive shoulder exoskeletons may

enhance motor function and reduce muscle and joint loads for both able-bodied and disabled users.

INTRODUCTION:

Several exoskeletons and orthoses have been designed to support the shoulder. Such devices have promising potential to enhance motor function [58-61] and prevent injury. Many shoulder exoskeletons generate assistive forces using mechanically passive components such as elastic springs [14, 60, 61, 67-70]. Compared to powered exoskeletons that require electromechanical hardware [12, 62-66], passive exoskeletons may potentially be more cost effective, lighter, more low-profile, and easier to maintain. Passive shoulder exoskeletons generally apply a continuous (i.e. always present) force to the upper extremity to compensate for gravity. To ensure that passive shoulder exoskeletons are safe and effective, there is a need to investigate how continuous anti-gravity shoulder assistance affects biomechanical parameters such as muscle activity and kinematics.

Previous biomechanical studies of continuous anti-gravity shoulder assistance primarily focused on overhead tasks. This is because most commercially available passive shoulder exoskeletons are intended to assist overhead tasks, which are associated with a high prevalence of occupational shoulder injury [72, 73]. During overhead tasks, the shoulder assumes a mostly *static* posture. Promisingly, anti-gravity assistance reduced activations of the middle deltoid, anterior deltoid, and biceps brachii muscles by as much as 62%, 80%, and 49%, respectively, while able-bodied subjects performed overhead tasks [59, 61, 74-76].

Continuous anti-gravity assistance may be useful for supporting *dynamic* shoulder elevation movements, which are more characteristic of activities of daily living [77] and many rehabilitation exercises [11]. A relatively few studies showed that, during dynamic movements, passive shoulder exoskeletons decreased activations of some muscles but increased activations of others [75, 78]. However, these studies averaged results across long time periods, masking

the nature and potential mechanisms of activation changes. In our previous computer simulations of dynamic shoulder elevation [80], activations of muscles that primarily contribute to positive shoulder elevation (+SE), based on reported muscle moment arms [81], were lower with anti-gravity exoskeleton assistance than without. Conversely, antagonist muscles that primarily contribute to negative shoulder elevation (-SE) had higher activations with assistance to simultaneously decelerate the arm at the endpoint and overcome the assistive force. Our computational study was limited because the simulated kinematics were constrained to be the same with and without an exoskeleton. It is unclear whether human subjects would adapt their kinematics and muscle coordination patterns to avoid increasing activations of -SE muscles with anti-gravity assistance.

The objective of our study was to determine the effect of continuous passive anti-gravity assistance on able-bodied muscle activations and shoulder kinematics during dynamic and static phases of shoulder elevation movements. We used a torsion spring and cable to mimic the continuous passive anti-gravity assistance provided by passive shoulder exoskeletons. We hypothesized that activations of +SE muscles would be lower with assistance than without. Additionally, we hypothesized that, unlike our simulations, subjects would adapt their shoulder joint kinematics, specifically by reducing the magnitude of decelerations near the end of dynamic shoulder elevation movements, to prevent increasing activations of -SE muscles.

METHODS:

Subjects:

All subjects gave written informed consent before participating in the study. The University of Tennessee, Knoxville Institutional Review Board approved the testing protocol. Fifteen subjects (10 male, 5 female; age = 21.5 ± 3.5 years, height = 173.4 ± 14.2 cm, mass = 75.4 ± 11.9 kg) volunteered to participate in this study. All subjects were right-handed, and all testing was done on the dominant side. Subjects were excluded from the study if they had any current upper limb

injury, known history of shoulder impairment, or other chronic health conditions, cognitive impairments or other severe movement disability.

Instrumentation and Setup:

The subjects were seated in an upright posture below an elastic torsion spring (Speedaire 5YAP0) mounted overhead. A cable extending from the torsion spring attached to a rigid humeral cuff (Breg Lo Pro) that subjects wore on their dominant arm. The cable attachment occurred at the midpoint between the shoulder and elbow on the lateral aspect of the arm. This setup allowed the spring to apply a continuous passive force against gravity to the subjects' arm (Fig. 3.1). The magnitude of the force applied by the torsion spring through the cable was adjusted for each subject to be approximately 2/3 of the subject's estimated upper extremity weight. This force level was determined during preliminary testing in which four subjects who were not included in this study provided verbal feedback while we adjusted the torsion spring force; the force was adjusted until subjects felt noticeable assistance but were still able to lower their arm by gravity. We estimated each subject's upper extremity weight assuming that its proportion to total body weight was consistent with that of a 50th-percentile male [18]. The applied force, verified before each testing session using a force sensor, ranged from 1.75 - 2.75 kg and averaged 2.08 ± 0.33 kg across subjects.

We placed an acrylic target board behind the subjects' arm to constrain the shoulder elevation movements (described in "Procedure" section below) to the desired elevation plane angles (Fig. 1). Clear acrylic was used to avoid obscuring the motion capture marker clusters. To denote the target shoulder elevation angle of 90°, we placed a foam marker on the board that extended perpendicular to the board towards the subject. We aligned the board approximately with the glenohumeral joint so that the target shoulder elevation angle was consistent across subjects.

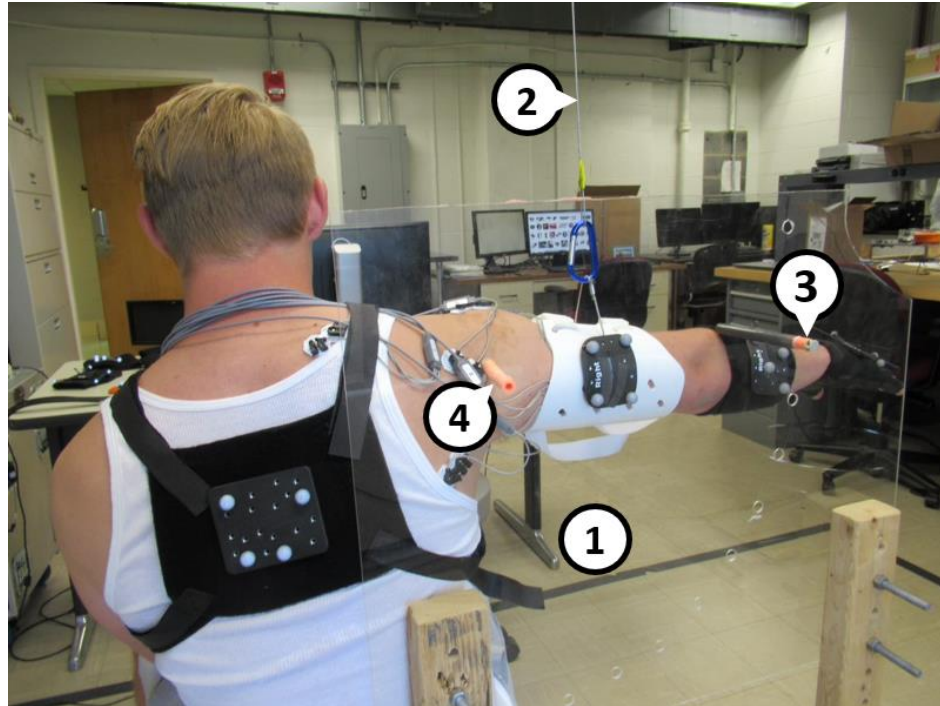


Figure 3.1. Subject set up to perform testing in the abduction plane. (1) Acrylic target board use to constrain elevation plane angle and denote elevation target. (2) Force from torsion spring applied through a cable attached to a rigid humeral cuff. (3) Elevation target marker used to show subjects the maximum trial elevation angle. (4) Marker used to align the board to the approximate glenohumeral joint center.

Muscle activity was determined by measuring raw electromyogram (EMG) signals from surface EMG electrodes (Noraxon TeleMyo 2400T, Scottsdale, AZ) placed over nine muscles and muscle compartments that cross the shoulder joint: anterior deltoid (AD), middle deltoid (MD), posterior deltoid (PD), supraspinatus (SS), infraspinatus (IS), pectoralis major (PM), latissimus dorsi (LD), triceps brachii long head (TLH), and biceps brachii long head (BLH). The EMG signals were recorded at 1500 Hz.

Kinematics for each trial were measured with a seven-camera 6-DOF infrared motion capture system (OptiTrack Prime 13, Corvallis, OR) with rigid body marker clusters placed on the torso and dominant arm, forearm, and hand. Marker cluster motion capture data were collected at 120 Hz and processed in The Motion Monitor software (Innovative Sports Training, Inc., Chicago, IL). We computed the standard Euler decomposition angles of the humerus relative to the thorax (i.e. elevation plane angle, shoulder elevation angle, and shoulder axial rotation) as defined by the International Society of Biomechanics [44]. For processing, we rectified the shoulder elevation angle. The Motion Monitor software also synchronized the kinematic and EMG data.

Procedure:

Before testing, the subjects performed one trial of eight different isometric maximum voluntary contractions (MVC) against resistance (Table 3.1) and one resting trial. We used the EMG collected during the MVC and resting trials to normalize the EMG from testing trials, as described in the “Data Processing and Statistical Analysis” section below. During testing, the subjects were instructed to elevate the shoulder on their dominant side under two assistance conditions, assisted and unassisted. For the assisted and unassisted (control) conditions, the cable connected to the torsion spring was attached or unattached, respectively, to the cuff on the dominant arm. For each assistance condition, subjects performed twenty trials each of two different movements, abduction and scaption (2 assistance conditions x 2 movements x 20 trials

Table 3.1. Static upper extremity postures in which subjects performed maximum voluntary contractions (MVCs).

	Upper Limb Posture	Movement Direction	Muscle Targeted
1	Elbow extended, 0° elevation plane, and 90° shoulder elevation	positive shoulder elevation	MD and SS
2	Elbow extended, 30° elevation plane, and 90° shoulder elevation	positive shoulder elevation	AD
3	Elbow extended, 90° elevation plane, and 0° shoulder elevation	negative elevation plane angle (shoulder extension)	PD
4	90° elbow flexion, 90° elevation plane, and 0° shoulder elevation	external shoulder rotation	IS
5	90° elbow flexion, 90° elevation plane, and 0° shoulder elevation	internal shoulder rotation	PM
6	Elbow extended, 0° elevation plane, and 90° shoulder elevation	negative shoulder elevation	LD
7	90° elbow flexion, 90° elevation plane, and 0° shoulder elevation	elbow flexion	BLH
8	90° elbow flexion, 90° elevation plane, and 0° shoulder elevation	elbow extension	TLH

= 80 trials total). Abduction was defined as shoulder elevation in the frontal plane. Scaption was defined as shoulder elevation in an elevation plane angle of 30° anterior to the frontal plane. We included scaption as a more clinically relevant movement given the prominence of shoulder elevation in anterior plane angles during activities of daily living [77, 174]. Subjects performed all twenty trials of each movement-assistance condition pair consecutively before switching to the next pair. We randomized the order of assistance conditions for each subject and the order of movements within each assistance condition.

In each trial, the subjects performed the movements in two phases. In the *dynamic* first phase, the subjects elevated their shoulder from rest to a target shoulder elevation angle of 90° with the elbow extended over a duration of 2 seconds. In the *static* second phase, after reaching the target shoulder elevation angle, the subjects held their arm in the elevated posture for 2 seconds. Subjects knew when they reached the target elevation angle when their forearm touched the foam target marker on the acrylic board. The speed of movement was constrained by a metronome. Subjects were given a 10-second rest between trials as well as a two-minute rest between movement-condition pairs to minimize fatigue.

Data Processing and Statistical Analysis:

We performed all data processing in MATLAB (MathWorks, Inc., Natick, MA). We defined the beginning timepoint for each trial as the point where average elevation angular velocity of 5 consecutive timepoints increased over 2 degrees per second. The following 4 seconds of data defined each individual trial. For each trial, we divided the dynamic and static phases by manually identifying the first peak in shoulder elevation angle once the subject reached the target angle (Fig. 3.2). Both trial phases were normalized by the duration of each respective phase.

The raw EMG data was filtered using a high-pass 4th-order Butterworth filter at a cut-off frequency of 40 Hz, rectified, and finally filtered using a low-pass 4th-order Butterworth filter at a cut-off frequency of 10 Hz. We processed the EMG from both resting and MVC trials by computing

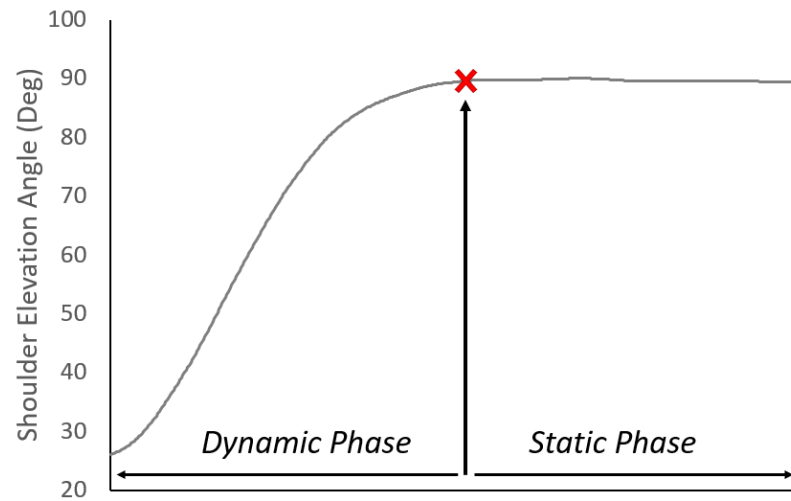


Figure 3.2. Sample trial elevation angle used to segment trial into dynamic and static phases. The red “x” symbol denotes where we manually divided the trial at the first peak of shoulder elevation angle.

the root mean square (RMS) with a window size of 225. We normalized the filtered EMG data collected during trials by the peak values of the processed EMG collected during MVCs to calculate muscle activations. The average activation calculated from the resting trial was used to set a minimum value for muscle activations. Muscle activations ranged from 0 (inactive) to 1 (maximally active).

Before performing a statistical analysis of muscle activations, we first divided muscles into two groups, +SE and -SE. We then calculated the maximum muscle activations during the dynamic phase and the average muscle activations during the static phase for every trial.

We analyzed the shoulder elevation angle over time as a function of the percent of the dynamic phase duration. For the static phase kinematics, we quantified postural stability, which we defined as the ability to hold the arm at the target shoulder elevation angle. To quantify postural stability, we computed (1) the average shoulder elevation angle across the static phase, (2) the shoulder elevation range of movement, which was the difference between the maximum and minimum shoulder elevation angles during the static phase, and (3) the average angular velocity of shoulder elevation across the static phase.

We performed a two-way repeated measures ANOVA ($\alpha = 0.05$) in SPSS (IBM, Armonk, NY) to compare muscle activations (both phases) and postural stability (static phase) between assistance conditions. The ANOVA considered factors “assistance condition” (assisted, unassisted) and “movement” (abduction, scaption). We ran a separate ANOVA for each muscle and postural stability measure. We performed Statistical Parametric Mapping (SPM) in MATLAB to compare shoulder elevation angles between assistance conditions throughout the dynamic phase of the movements [175].

RESULTS

Dynamic Phase

The maximum muscle activations occurred between 70-90% of movement (Fig. 3.3). Table 2 outlines the ANOVA results. Maximum activations of all five +SE muscles were significantly lower with assistance than without (Fig. 3.4). The two +SE muscles with the largest activation difference between assistance conditions were the anterior deltoid (31%, $p < 0.001$) and supraspinatus (28%, $p < 0.001$). Activations of -SE muscles were not significantly higher with assistance. In fact, the activation of one -SE muscle, latissimus dorsi, was 22% ($p = 0.041$) lower with assistance.

Shoulder elevation angles were significantly different between assistance conditions only during the first 59% of abduction (Fig. 3.4) and the first 39% of scaption (Fig. 3.5). Specifically, elevation angles were higher with assistance than without because the anti-gravity assistance pulled the shoulder into a higher resting shoulder elevation angle at the beginning of the assisted trials. Shoulder elevation angular decelerations were lower with assistance than without by up to 22% ($p = 0.006$) and 17% ($p = 0.01$) during abduction and scaption, respectively. The differences in maximum angular deceleration occurred near the point of maximum deceleration at approximately 60% of the dynamic phase.

Static Phase

Average muscle activations were significantly lower with assistance than without in all muscles except the triceps long head and biceps long head, for which there was no significant difference between assistance conditions (Fig. 3.5). The activations of all +SE muscles were significantly lower with assistance. Differences in activations were largest for three +SE muscles: anterior deltoid (35%, $p < 0.001$), supraspinatus (30%, $p < 0.001$), and infraspinatus (29%, $p = 0.001$). Activations of -SE muscles were not significantly higher with assistance. In fact,

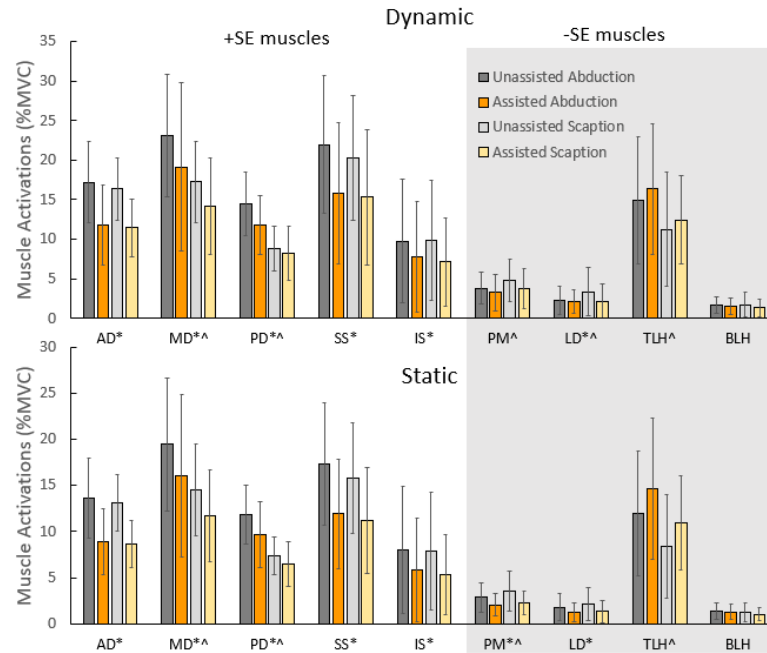


Figure 3.3. Maximum muscle activations measured during both dynamic and static elevation from rest to the target elevation angle with (orange) and without (gray) the applied assistive force. The darker and lighter bars correspond to abduction and scaption movements, respectively. Muscles in the shaded area are -SE muscles. Statistical significance ($p < .05$) is marked with an asterisk (*) for assistance and a carrot (^) for movement plane.

Table 3.2. Results from Two-Way Repeated Measures ANOVA

Dynamic Phase									
Muscle	AD	MD	PD	SS	IS	PM	LD	BLH	TLH
Assistance	54.825 (<.001)	6.489 (.023)	8.267 (.012)	21.914 (<.001)	17.806 (.001)	3.732 (.074)	5.068 (.041)	.661 (.430)	1.24 (.284)
Plane	.672 (.426)	13.375 (.003)	73.032 (<.001)	2.452 (.140)	.274 (.609)	11.715 (.004)	2.284 (.153)	13.025 (.003)	.291 (.598)
Assistance x Plane	.293 (.597)	.434 (.521)	3.385 (.087)	.810 (.383)	1.909 (.189)	2.572 (.131)	2.990 (.106)	.049 (.828)	2.332 (.149)
Static Phase									
Muscle	AD	MD	PD	SS	IS	PM	LD	BLH	TLH
Assistance	69.385 (<.001)	11.483 (.004)	9.559 (.008)	28.719 (<.001)	18.873 (.001)	16.56 (.001)	16.399 (.001)	3.331 (.089)	.981 (.339)
Plane	0.566 (.464)	14.918 (.002)	64.718 (<.001)	3.348 (.089)	.843 (.374)	12.611 (.003)	2.269 (.154)	13.575 (.002)	4.237 (.059)
Assistance x Plane	0.141 (.713)	0.397 (.539)	3.209 (.095)	2.152 (.164)	3.219 (.094)	2.626 (.127)	9.565 (.008)	.011 (.917)	.086 (.292)
Measurement	End Angle			Velocity			Range of Motion		
Assistance	.717 (.411)			.040 (.845)			.378 (.549)		
Plane	.220 (.647)			.206 (.657)			13.71 (.002)		
Assistance x Plane	.001 (.979)			.198 (.663)			.494 (.494)		

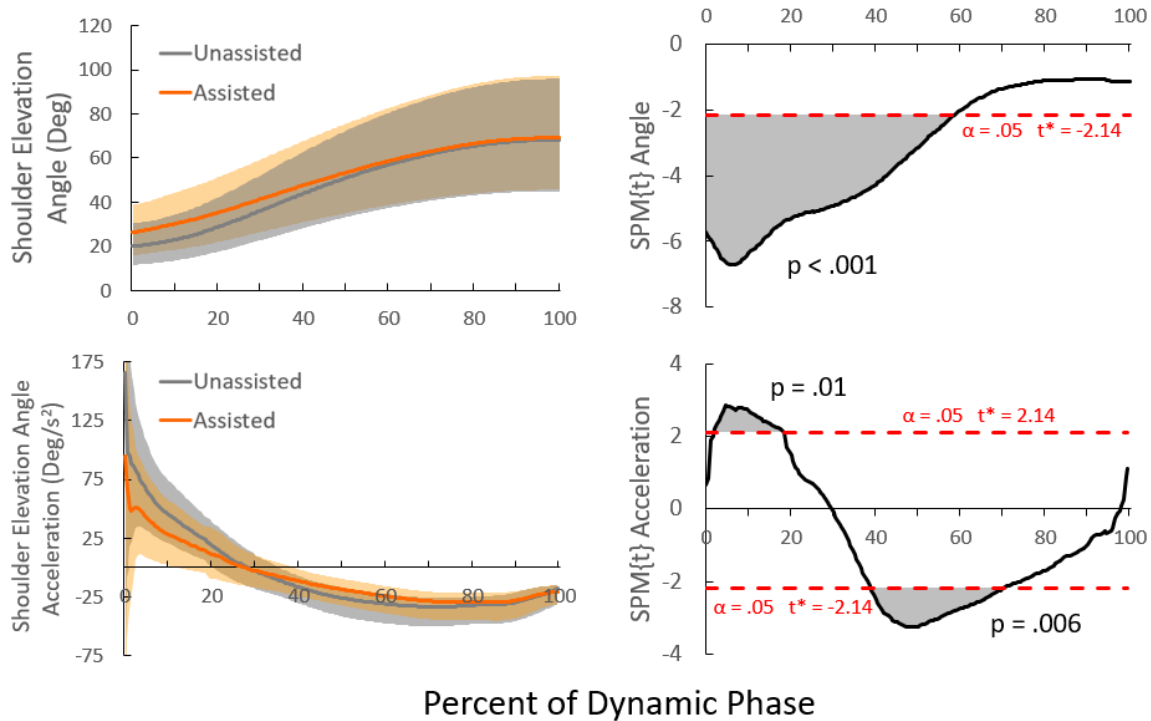


Figure 3.4. SPM analysis of shoulder joint kinematics during dynamic straight arm abduction from rest to the target elevation angle both with (orange) and without (gray) the applied assistive force. (Top) Analysis of the joint elevation angle throughout shoulder elevation. (Bottom) Analysis of the joint elevation angular acceleration throughout shoulder elevation. Statistical significance ($p < .05$) is marked through shaded area on the right graphs.

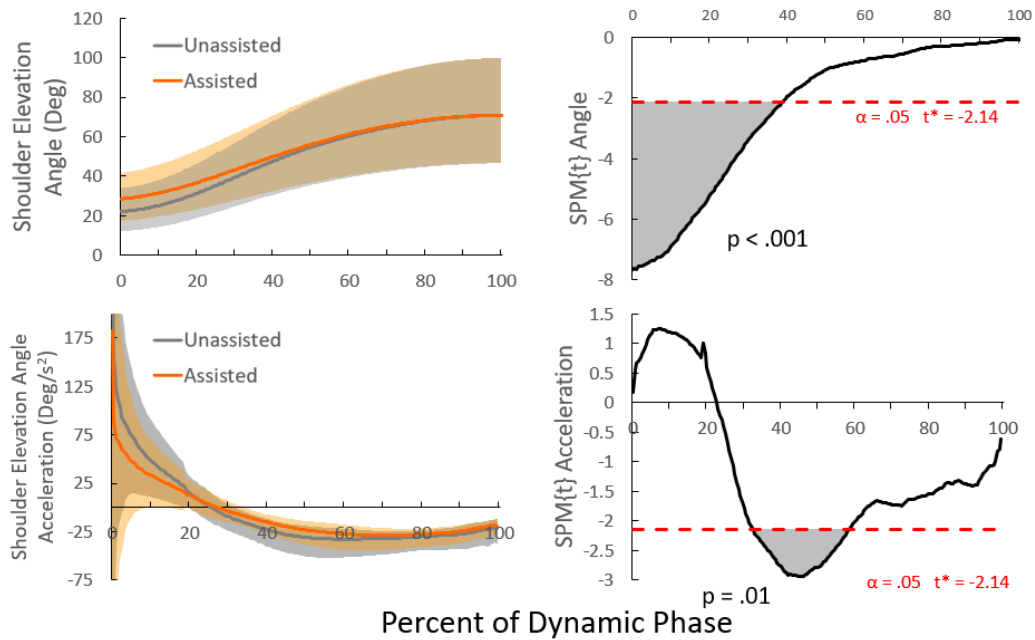


Figure 3.5. SPM analysis of shoulder joint kinematics during dynamic straight arm scaption from rest to the target elevation angle both with (orange) and without (gray) the applied assistive force. (Top) Analysis of the joint elevation angle throughout shoulder elevation. (Bottom) Analysis of the joint elevation angular acceleration throughout shoulder elevation. Statistical significance ($p < .05$) is marked through shaded area on the right graphs.

activations of pectoralis major and latissimus dorsi, both -SE muscles, were significantly lower with assistance than without.

For both assistance conditions, subjects had similar postural stability based on average shoulder elevation angles ($p = 0.411$), average shoulder elevation angular velocities ($p = 0.845$), and ranges of movement ($p = 0.549$) (Fig. 3.6).

DISCUSSION:

Activations of +SE muscles were lower with passive anti-gravity assistance than without, corroborating data reported for other passive shoulder exoskeletons [75, 78]. This is not surprising since the anti-gravity assistance and +SE muscles both acted about the shoulder to generate +SE joint moments. Thus, anti-gravity assistance reduces the joint moments that muscles need to generate to elevate the shoulder.

Contrary to our previous simulation results [80], the activations of -SE muscles were not different between assistance conditions. Near the end of simulated abduction, the activations of -SE muscles were higher with assistance than without to (1) decelerate the shoulder when approaching the target shoulder elevation angle of 90° and (2) overcome the +SE moment generated by the exoskeleton. However, the simulated abduction movement was from experimental data of an unassisted able-bodied subject and was the same for simulations with and without assistance. Conversely, during our experiments, human subjects adapted their kinematics by having lower decelerations with assistance as they approached the target 90° shoulder elevation angle. Lower decelerations may explain why -SE muscle activations were not higher with assistance.

Subjects' adaptation to the anti-gravity assistance mirrors that observed in previous motor control studies. For example, Novakovic and Sanguineti showed that when reaching toward a target, subjects who were given a relatively high level of assistance initially moved slowly and actively resisted the assistance to avoid overshooting the target[176]. Over time, subjects

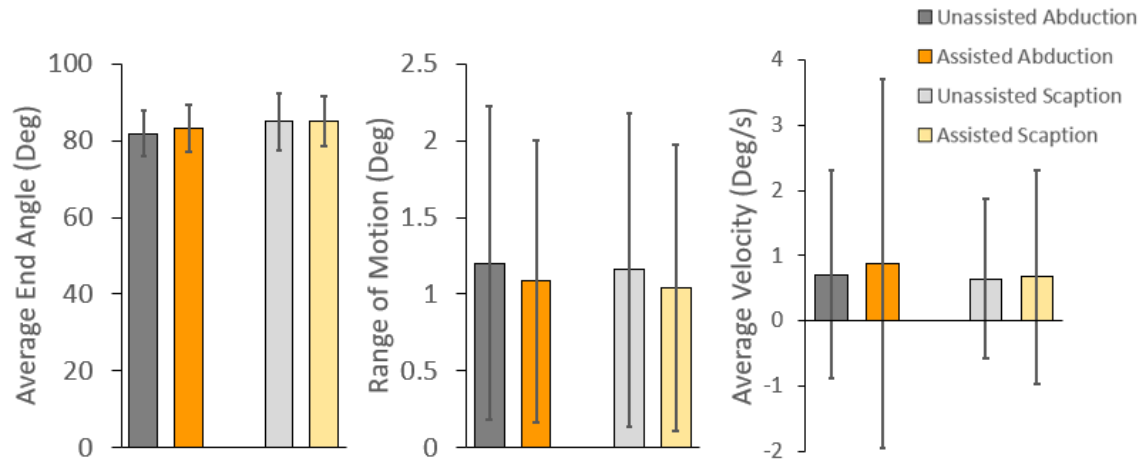


Figure 3.6. Joint angle kinematics during static elevation at the target elevation angle with (orange) and without (gray) the applied assistive force. The darker and lighter bars correspond to abduction and scaption movements, respectively. **(Left)** Average shoulder elevation angle during a static hold. **(Middle)** The range of shoulder elevation joint angle for each trial during a static hold. **(Right)** The average elevation angular velocity during a static hold. No significant changes are present.

eventually moved faster and resisted less until their kinematics with assistance to match those of unassisted movements. Though subjects in our study adapted to the assistance in a positive way, this may not necessarily be true for all devices and subjects, especially those with impairment. Maladaptation could have many negative practical consequences, including more inefficient movement, poor task performance, and injury. Therefore, it is critical to characterize adaptation to movement assistance for the intended user population.

A limitation of our experiment set-up was that the assistive force increased the resting shoulder elevation angle, reducing the angular “distance” subjects had to cover during the dynamic phase. This limitation potentially confounded the results during the dynamic phase. However, after about 60% of the dynamic phase, the kinematic differences between assistance conditions were not statistically significant. Coincidentally, peak muscle activations primarily occurred after 70% of the dynamic phase. Therefore, differences in peak activations between assistance conditions were likely caused by the assistance rather than differences in kinematics.

That the anti-gravity assistance increased the resting shoulder elevation angle highlights the importance of tuning the magnitude of anti-gravity assistance. If anti-gravity assistance exceeds the shoulder elevation moment due to gravity at any point, then the assistance alone will produce unintentional movements or posture changes unless the user actively resists. Various mechanisms can be applied to prevent over-assistance at lower shoulder elevation angles. For example, the exoskeleton in our musculoskeletal model [80] and another reported by Perry et al. [79] used a cam wheel gearing mechanism to tune the anti-gravity assistance. We are currently developing a physical prototype of a tunable cam-based wearable passive shoulder exoskeleton and plan to test it on human subjects in future studies.

Postural stability, which is the ability to maintain a target posture, is an important criterion for performing functional tasks effectively. We expect that anti-gravity assistance makes shoulder posture more sensitive to small changes in muscle force or to external perturbations, potentially

reducing postural stability. On the other hand, anti-gravity assistance may improve postural stability by delaying the onset of fatigue [61, 74, 75]. We observed no difference in the postural stability of shoulder elevation angle between assisted and unassisted conditions. However, future studies are needed to explore the effect of anti-gravity assistance on the resiliency of postural stability against other factors, such as fatigue and perturbations, that may occur during daily activities.

Anti-gravity assistance could also affect glenohumeral joint stability and alignment. Our results indicated that the force balance due to muscle forces shifted in the -SE direction, since muscle activations of +SE muscles were lower. This could change how the humeral head aligns with the scapular glenoid. Disrupting glenohumeral alignment could lead to or exacerbate existing shoulder pathology (e.g., subacromial impingement) or glenohumeral instability. Therefore, future studies should investigate the effect of anti-gravity assistance on glenohumeral stability and alignment.

Anti-gravity assistance could enhance function and prevent injury for both healthy and disabled individuals. For example, the reduced muscle activations we observed may allow users to perform repetitive tasks with less effort, prolong time to fatigue and task failure [177], and reduce muscle loads and the associated risk of strain-based injury [4]. For patients with musculoskeletal disorders such as rotator cuff tear, continuous anti-gravity assistance could (1) promote muscle recovery by reducing loads in damaged or repaired tissues or (2) prevent secondary injuries caused by overactivation of compensatory muscles [11, 41, 178]. Additionally, anti-gravity assistance could effectively enhance the user's strength or range of motion, which would be especially useful for patients with acute or chronic disability, potentially allowing them to perform more functional tasks.

Our study had some additional limitations. First, the cable of the tool retractor was not completely vertical, introducing a small horizontal force component. We expect that this had a

minor effect on muscle contributions and the pattern of differences between assistance conditions. Additionally, we tested only two movements that are simplified compared to movements during activities of daily living; future research should include more functional tasks. We also only tested one level of assistance. A variety of assistance levels should be studied, since others have shown that assistance level affects how users adapt their muscle activations and kinematics [75, 176, 179]. Finally, the surface electrodes used to measure EMG from the triceps and biceps long head muscles were located underneath the humeral cuff; the cable force was applied to the cuff only during the assisted trials, which could have confounded EMG differences between assistance conditions.

In conclusion, our results suggest that passive anti-gravity assistance can lower muscle activations during dynamic shoulder elevation movements, which has several potential benefits as described above. Subjects were able to adapt their kinematics slightly in a way that potentially avoided increasing activations of -SE muscles. Our study contributes critical knowledge about the effect of passive anti-gravity assistance on motor function during dynamic tasks. However, more research is needed before devices that provide continuous anti-gravity assistance, such as passive shoulder exoskeletons, can be broadly applied to different user populations, especially those with impairment and disability.

ACKNOWLEDGMENTS:

This work was supported by start-up funds from the University of Tennessee, Knoxville. The authors thank Eric Wade, PhD, and Jeffrey T. Fairbrother, PhD, for helpful discussions regarding the study design.

CHAPTER 4. FULLY IMPLANTED PROSTHESES FOR

MUSCULOSKELETAL LIMB RECONSTRUCTION AFTER

AMPUTATION: AN IN VIVO FEASIBILITY STUDY

This work was published in the Annals of Biomedical Engineering.

Hall P. T., S. Z. Bratcher, C. Stubbs, R. E. Rifkin, R. M. Grzeskowiak, B. J. Burton, C. B.

Greenacre, S. M. Stephenson, D. E. Anderson and D. L. Crouch. Fully Implanted Prostheses for Musculoskeletal Limb Reconstruction After Amputation: An In Vivo Feasibility Study. *Annals of biomedical engineering* 2020.

ABSTRACT

Previous prostheses for replacing a missing limb following amputation must be worn externally on the body. This limits the extent to which prostheses could physically interface with biological tissues, such as muscles, to enhance functional recovery. The objectives of our study were to (1) test the feasibility of implanting a limb prosthesis, or endoprosthesis, entirely within living skin at the distal end of a residual limb, and (2) identify effective surgical and post-surgical care approaches for implanting endoprostheses in a rabbit model of hindlimb amputation. We iteratively designed, fabricated, and implanted unjointed endoprosthesis prototypes in six New Zealand White rabbits following amputation. In the first three rabbits, the skin failed to heal due to dehiscence along the sutured incision. The skin of the final three subsequent rabbits successfully healed over the endoprostheses. Factors that contributed to successful outcomes included modifying the surgical incision to preserve vasculature; increasing the radii size on the endoprostheses to reduce skin stress; collecting radiographs pre-surgery to match the bone pin size to the medullary canal size; and ensuring post-operative bandage integrity. These results will support future work to test jointed endoprostheses that can be attached to muscles.

INTRODUCTION

A major goal of limb prostheses is to return intuitive control and realistic sensation of movements associated with the lost limb following amputation. Such sensorimotor function is especially important for upper[154, 180, 181] limb amputees since it enables the closed-loop motor control needed to perform manual, dexterous tasks. This goal has hitherto been pursued using external (i.e. worn outside of the body) prostheses. Most external prostheses incorporate electromechanical hardware (e.g. motors, microprocessors, sensors, electrodes)[117, 118] and algorithms that decode users' movement intent from electromyograms[119, 120] and stimulate nerves to provide sensory feedback. Electromechanical systems do not yet accurately replicate sensorimotor physiology and, thus, likely introduce errors in decoding intended movement patterns, generating prosthesis movements, and delivering proper sensory feedback that directly correlates with the movements. The sensorimotor limitations of external myoelectric prostheses are a major reason why many are eventually abandoned[138].

One potential solution to overcome sensorimotor limitations of external prostheses is to physically attach prostheses to muscles. This is because muscles contribute to both movement generation and sensation, via mechanoreceptors, in the biological limb. There is strong evidence that muscles in the residual limb retain their sensorimotor functions after amputation[119, 147, 148, 182]. Since all current prostheses are worn externally, the previous attachment approach required transferring muscle forces through skin using a procedure called cineplasty[150, 154]. Reports note anecdotally that cineplasty enabled exquisite control and sensation of prosthesis movements[16, 154]. However, cineplasty has several limitations in function, comfort, and appearance that are directly related to the need to transfer muscle forces through skin. Given these limitations, cineplasty has not been widely adopted.

Our proposed novel approach to better facilitate physical muscle-prosthesis attachment is to implant prostheses completely within skin. With an implanted prosthesis, or *endoprosthesis*,

the residual muscles could be attached in a more cosmetic and anatomically realistic way that would overcome the limitations of cineplasty. Like other common orthopedic implants such as joint replacements[91, 92], endoprostheses would replace part of the musculoskeletal structure of the missing limb. The proposed endoprosthesis differs from previous percutaneous osseointegrated prostheses, which protrude through skin to provide an anchor point for externally worn limb prostheses.

The objectives of our proof-of-concept study were to (1) test the feasibility of implanting a limb prosthesis, or endoprosthesis, entirely within living skin at the distal end of a residual limb, and (2) identify effective surgical and post-surgical care approaches for implanting endoprosthesis prototypes in a rabbit model of hindlimb amputation. We iteratively implanted an unjointed endoprosthesis prototype *in vivo* in six New Zealand White rabbits with transtibial (i.e. below-knee) amputation. We refined the surgery, post-operative care, and endoprosthesis design between surgery iterations. Our criteria for a successful proof of concept was that at least two rabbits with the endoprosthesis could recover enough post-surgery to forego bandages and medications.

MATERIALS AND METHODS:

Summary:

This study was approved by the University of Tennessee, Knoxville Institutional Animal Care and Use Committee. We used six male New Zealand White rabbits (R1-R6; average pre-surgery weight = 2.92 kg, average age = 18 weeks), since the rabbit is a common orthopedic model and large enough for testing physical endoprosthesis prototypes compared to other smaller mammals. We used an iterative study design; in the same survival surgery and in one rabbit at a time (from R1 to R6), we amputated the hind limb below the knee and implanted the stem endoprosthesis. We monitored the rabbits during post-surgical recovery, qualitatively noting any adverse events that negatively affected the surgical outcome. We reviewed the observations as

a team and adapted our surgery or device as necessary to address the problems in the subsequent iterations. Rabbits were euthanized either at a humane endpoint or after post-surgical recovery (at around 60 days post-surgery), whichever was sooner. The rabbits were housed with at least one companion rabbit in adjacent cages. Enrichment and positive human interaction were given to the rabbits daily.

Stem Endoprosthesis:

The stem endoprosthesis was comprised of three parts: a metal segment, a modified intramedullary bone pin, and an over-molded silicone sleeve (Fig. 4.1). The metal segment was designed in Solidworks (Dassault Systemes, France) and 3D-printed in 316 stainless steel. We drilled and tapped a hole on the flat proximal surface of the stem with a reverse thread for later integration with the bone pin. Four of the stems (R3-R6) had sites for muscle attachment to stabilize the stem in the bone and mimic future muscle attachment to a muscle-driven endoprosthesis; the muscle attachment sites were added at will and not in response to an adverse surgical outcome. Commercially available intramedullary bone pins (IMEX Veterinary, Inc.), which we used to anchor the stems to the tibia bone, were cut to a shorter length and tapped with additional threads to screw into the metal segment. A range of pin sizes were available (Table 1). The metal segment was over-molded with an approximately 2-mm-thick coating of biocompatible silicone of hardness 40 shore A (BIO LSR M140, Elkem Silicones) using a custom, 3D-printed 316 stainless steel mold. Once the three parts were assembled, the stems were sterilized using ethylene oxide gas.

Pre-Surgery Bone Geometry Estimation:

We amputated the hindlimb approximately 4 cm from the distal end of the tibia. This allowed us to screw the bone pin into the approximate mid-diaphyseal area of the tibia where the medullary canal is narrowest. We approximated the canal diameter from either micro-computed

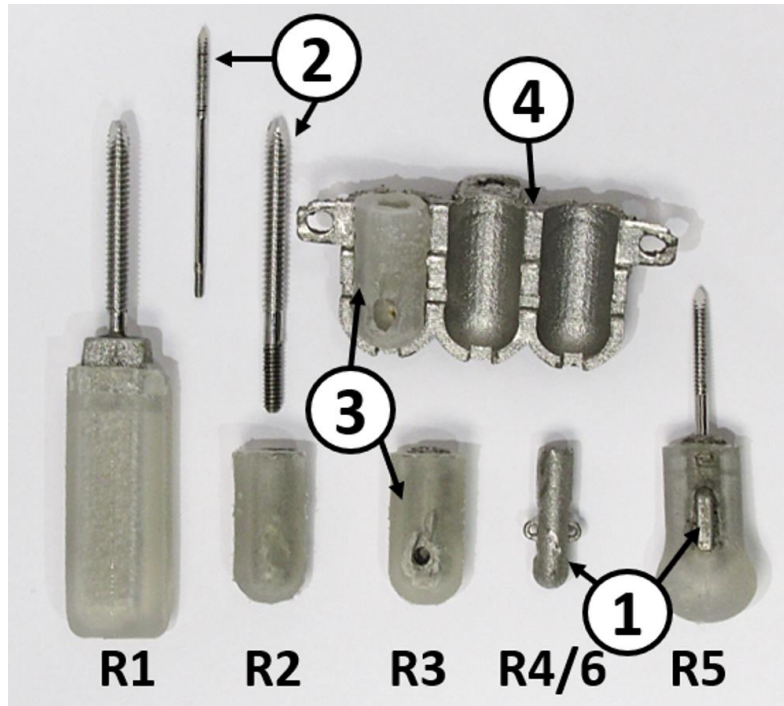


Figure 4.1. Stem endoprotheses used during surgery. Corresponding animal number noted below each device. (1) 3-D printed 316L stainless-steel stem. (2) modified threaded intramedullary bone pin. (3) biocompatible, over-molded silicone sleeve. (4) 3-D printed stainless-steel mold used to over-mold silicone onto stem.

tomography images from another rabbit of similar size (R1) or pre-surgery radiography images of the operated rabbits (R2-R6).

Surgical Technique:

The general surgical procedure for each rabbit was as follows, although we modified some steps in each surgery iteration (see Results) based on the surgical outcomes of preceding iterations. The rabbits were given a pre-emptive analgesic, either buprenorphine (0.03-0.05 mg/kg) or hydromorphone (0.2 mg/kg), and induced into general anesthesia with either a solution of ketamine (30-40 mg/kg) and xylazine (3-7 mg/kg) or midazolam (0.75-1 mg/kg). Anesthesia was maintained with 3-5% isoflurane gas. We removed the hair from the operated limb with electric clippers and depilatory cream (Nair Hair Remover Cream, Church & Dwight Co., Ewing Township, NJ). We positioned the rabbit in right lateral recumbency with the left leg suspended, and aseptically prepared the limb with chlorohexidine, betadine, and 70% isopropyl alcohol. The surgeons (Anderson, Rifkin, and Grzeskowiak) made an incision on the hindlimb preserving enough skin and soft tissue to create a skin flap to cover the implanted stem. The surgeons then used an osteotomy saw blade to cut the bone in the distal tibial diaphysis. The bone pin of the stem was then screwed into the exposed tibial medullary canal. For the stems for R3-R6, which had sites for muscle attachments, the surgeons used a 5-0 synthetic absorbable monofilament suture (PDS) to anchor the gastrocnemius tendon and the tibialis cranialis insertion tendon to the stem with a locking loop. The skin flap created during the incision was wrapped across the distal end of the stem and sutured closed in a continuous subcuticular pattern using a 4-0 synthetic absorbable monofilament suture. In R2-R6, the closure was reinforced with a 2-0 synthetic absorbable monofilament applied in an interrupted cruciate pattern. Liquid topical tissue adhesive (3M Vetbond Tissue Adhesive) was placed over the external surface of the incision line.

Post-Surgical Care:

Silver sulfadiazine topical cream was applied over the incision to prevent infection, but immediately post-operatively and at every bandage change. The limb was bandaged using, from inner to outer layers, non-adherent dressing, undercast padding, elastic bandage wrap, and elastic tape (ELASTIKON, Johnson & Johnson) to protect the incision site. We changed the bandage at least once every three days and monitored skin integrity and incision healing. We administered an analgesic (buprenorphine 0.03 mg/kg) subcutaneously every 6 hours for at least 72 hours post-surgery, as well as antibiotics every 12 hours for at least 7 days (enrofloxacin 5 mg/kg diluted) and an anti-inflammatory drug every 24 hours for at least 7 days (meloxicam; 0.6 mg/kg) subcutaneously for at least 7 days post-surgery.

Imaging:

We acquired radiographs of the operated limb postoperatively and approximately every two weeks post-surgery to monitor the bone pin alignment, stem position, and bone.

Weight Bearing Analysis:

After the skin healed and fully enclosed the endoprosthesis in R4 and R6, we removed the bandage. To determine the extent to which the rabbit was willing to apply pressure to the endoprosthesis limb, we conducted a testing session to measure ground-limb pressures. The rabbit was guided onto a pressure mat (Tekscan Very HR Walkway 4) and we measured the pressure of both the operated and intact contralateral limbs simultaneously over an 8-second period while the rabbit was standing still. We compared, between limbs, the magnitude of both vertical pressure and total vertical force applied by each limb.

RESULTS:

Bone-Device Interface:

When inserting the bone pin in the tibia of R1, the dorsal tibial cortex fractured, requiring a more proximal amputation to remove the fractured bone. Since the amputation was performed

more proximally than intended, the threads of the bone pin were aligned with the wider area of the tibia medullary canal, creating a loose fit between the bone and bone pin (Fig. 4.2). Therefore, bone cement (polymethyl methacrylate) was placed into the medullary canal to secure the bone pin. The tibia fractured in R1 because the bone pin diameter, estimated from micro-computed tomography images from another rabbit of comparable size, was too large. We also had only one bone pin size available for R1, which prevented the surgeons from switching pins during surgery in case of a size mismatch. Therefore, for the next five surgeries (R2-R6), the tibial medullary canal measurements were determined from *in vivo* radiographs of each rabbit taken 1-2 weeks prior to surgery. We selected the diameter of the bone pin to be the same as or slightly less than the medullary canal diameter so that the pin would fit snugly in the canal without fracturing the tibia. Additionally, three different bone pin size options were available if determined to be needed intraoperatively: the pin with a thread diameter nearest the smallest medullary canal diameter measured from radiographs, the next larger pin, and the next smaller pin. Table 1 outlines the available pin sizes from which we selected. Using this approach, for R2-R6, we experienced no complications with the bone pin fit and achieved a snug fit without need for bone cement. The endoprosthesis or bone pin did not appear to move based on the post-surgical radiographs (Fig. 2). Post-surgical radiographs indicated proliferative bone ongrowth over the cranial aspect of the device as early as 12 days after surgery in all rabbits (Fig. 4.2). However, this bone growth was visibly smaller in R4-R6, which had the muscle attachments.

Skin Closure:

For R1, we used a cranial circumferential incision to create a caudal skin flap and cranial suture line. This preserved the calcaneal fat pad to absorb the pressure applied to the skin when the rabbit bore weight on the residual limb. At 3 days post-surgery, the skin surrounding part of the implant was dark, indicative of ischemia (Fig. 4.3). A portion of the incision line dehiscd by

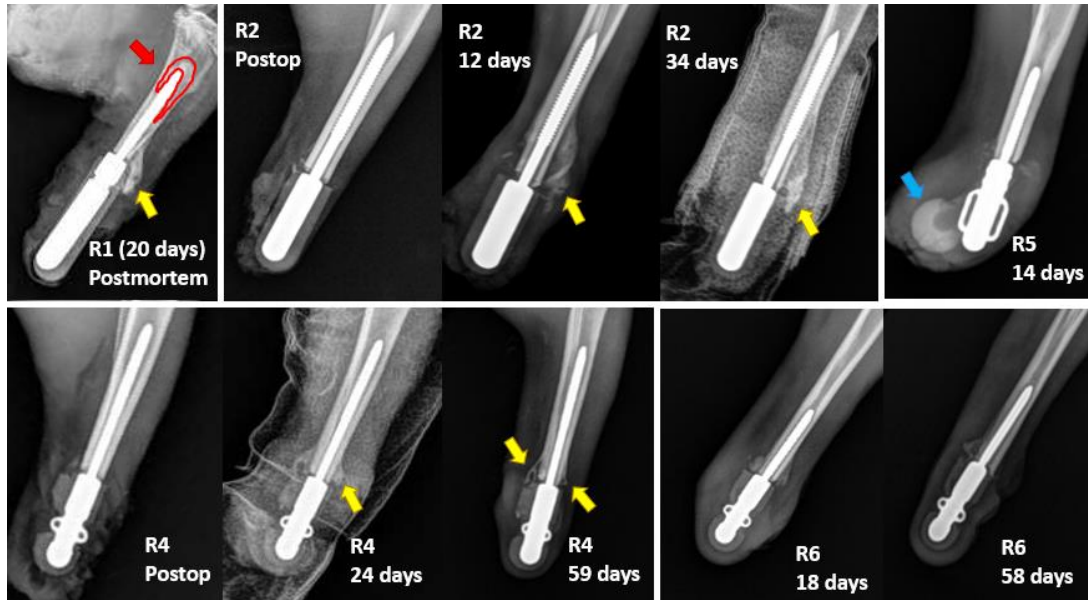


Figure 4.2. Radiographs of stems in situ. **Top Left:** R1 postmortem 3-weeks post-surgery showing bone cement (red outline and arrow) and proliferative bone ongrowth indicated by yellow arrow. **Top Middle:** Progression of R2 over 5 weeks showing development of bone ongrowth (yellow arrow). **Bottom Left:** Progression of stem in R4 showing development of bone ongrowth (yellow arrow). **Top Right:** X-ray of R5 two weeks post-surgery showing where the silicone slipped off the end.

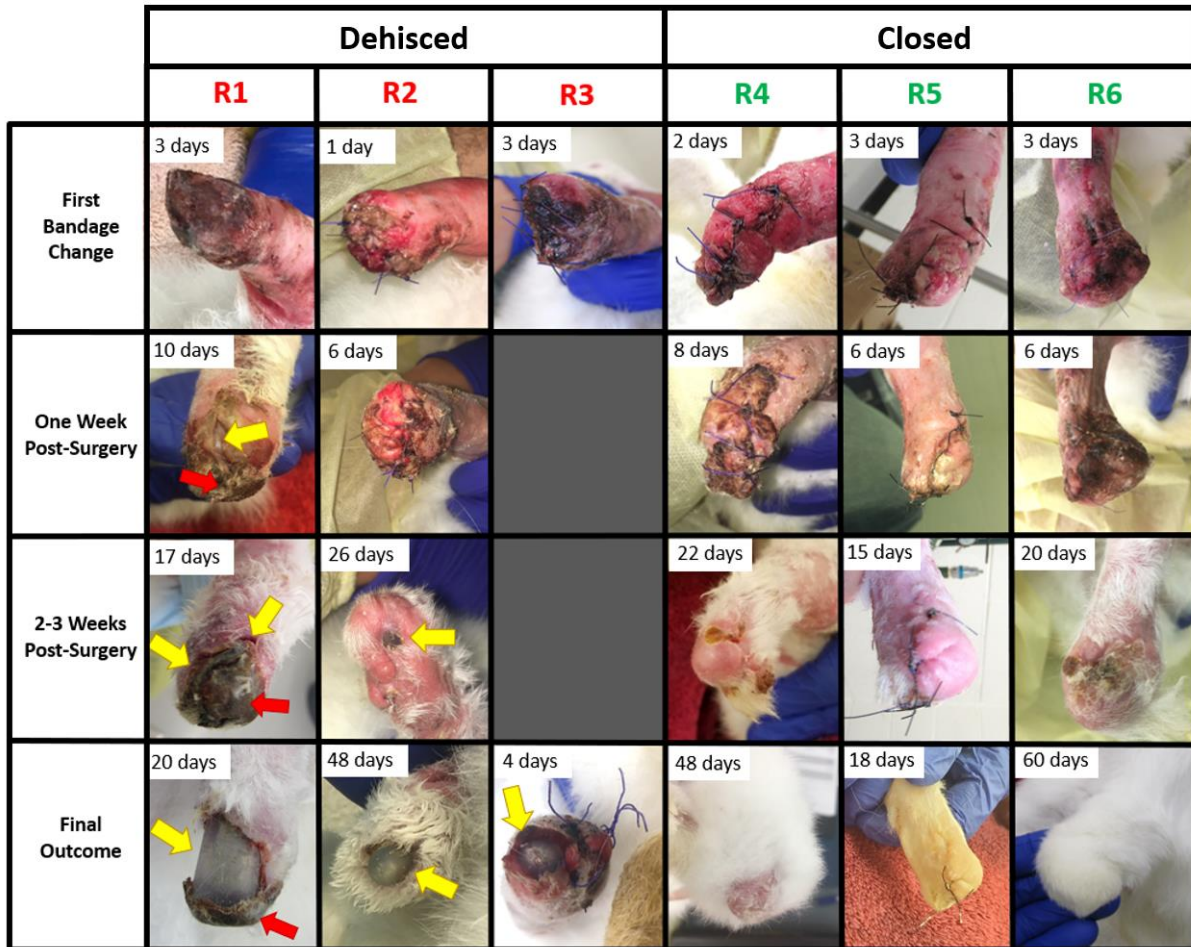


Figure 4.3. A timeline displaying how the skin of the operated limb for each rabbit changed over time. Pictures were taken at every bandage change, and progress noted at various timepoints. The number of days after surgery the picture was taken is in the top left corner of each cell. Yellow arrows indicate dehiscence in the skin. Red arrows indicate ischemic skin locations. The animal numbers indicate the order of surgeries (i.e. R1 was performed first, then R2, etc.).

10 days. At 3 weeks, the skin at the distal end of the residual limb broke off at the edge of the ischemic area, exposing the stem and requiring euthanasia of the rabbit. The skin complications in R1 were potentially due to the stem geometry and incision technique. The stem for R1 was relatively long and had corners with relatively small radii, which could have created areas of high mechanical stress in the skin. In subsequent surgeries, we made the stem shorter and increased the radius of the distal end of the stem. Additionally, for R2 and R3, we reversed the incision to create a caudal skin closure to prevent weight bearing and loading on the incision line.

R2 showed no sign of ischemia (Fig. 16). However, at 3 weeks post-surgery, the skin had failed to completely heal and a small dehiscence (~2 mm diameter) had formed along the incision line. The dehiscence enlarged by about 7 weeks, exposing the stem and requiring euthanasia of the rabbit. At 4 days post-surgery, R3 had removed the bandage and appeared to have chewed on the sutures and stem, causing the incision line to dehisce. Attempts to close the incision failed, so the rabbit was euthanized.

Although we had only observed ischemia in R1, we were concerned that the circumferential incision traditionally used during amputation could disrupt the microvasculature arising from the femoral artery that runs caudally along the hindlimb[183]. Therefore, starting with R4, we altered the surgical approach to a cranial linear incision to preserve the vasculature (Fig. 4.4). This technique is similar to one used in human knee arthroplasty [184]. By as late as 22 days post-surgery in R4-R6, the skin was healthy and the incision line healed (Fig. 4.3). After determining successful healing of the residual limb, we permanently removed the bandage. In R4 there were some areas of skin over the distal end of the stem that appeared bruised, presumably from impacts against the ground or cage bottom, but the skin remained closed over the stem. Pressure analysis of R4 and R6 showed that the residual limb experiences pressures of up to 0.92 kg/cm^2 , which was 3.28 times that of the maximum intact contralateral limb under general weight bearing (Table 2). On average, the residual limb experienced about 2.6 times greater

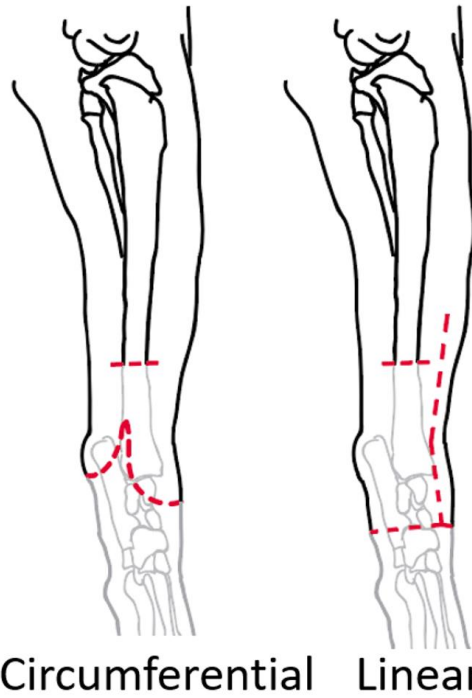


Figure 4.4. Representation of the change in the incision approach that occurred between R3 and R4. We switched to a linear incision to preserve the vasculature of the skin flap provided through the femoral artery. The tibia was amputated at approximately the same location for both incision approaches.

pressure than the intact contralateral limb over an 8 second timeframe. This is due to the smaller surface contact area in the residual limb. Despite high pressure, the rabbits were willing to place the equivalent of about 25% body weight on the endoprosthesis.

Bandaging and Recovery:

Rabbits R1-R3 were able to remove the bandages on their own, potentially exposing the operated limb to trauma and infection. The bandage removal may have contributed to dehiscence in R1 and R2. There were clear indications that R3 chewed on the stem, suggesting that the rabbit may have also caused the dehiscence after removing the bandage. We took several steps to try to prevent the rabbits from removing the bandages. We monitored the bandages more closely, at least twice per day, for two weeks post-surgery. If we noticed that the bandage was damaged or beginning to slip off, we applied additional elastic tape to reinforce the bandage. For R4-R6, we preemptively applied an extra bandage layer, which drastically reduced the number of times that the rabbits were able to remove the bandage.

Device Design:

As noted above, we modified the implant design after R1 by making the endoprosthesis shorter (20mm vs 40mm) and with larger radii to improve the chance of successful skin closure and reduce stress concentrations on the skin. To further decrease pressure on the skin in R5, we increased the radius of the silicone sleeve tip from 4.5mm to 10mm by increasing the thickness of the silicone cover without changing the design of the metal segment. We performed the same surgical technique as R4 to implant the stem in R5. However, radiographs of R5 at 14 days post-surgery revealed that the larger silicone sleeve had slipped off the tip of the metal segment (Fig. 2). We were able to realign the silicone temporarily, but it would not stay in place. Therefore, given the potential high risk of skin trauma against the exposed metal segment, we euthanized R5 once the bandaged skin incision had healed and fully closed (18 days post-surgery).

DISCUSSION:

In this first-of-its-kind study, we demonstrated convincingly in an *in vivo* model that it is feasible to fully enclose an endoprosthesis in living skin at the distal end of a residual limb. That all three final surgeries resulted in a successful shows the repeatability of our approach. Closing living skin over an endoprosthesis is a major challenge. This is partly because the skin at the distal end of the rabbit hindlimb is very thin, making it difficult to achieve suitable apposition of the wound edges along the suture line to promote wound healing. Additionally the suture line closing the wound lies directly over the synthetic endoprosthesis, which could interfere with wound healing [185]. As with all wounds, the suture itself can damage tissue and, if tied too tight, crush cells or occlude blood flow to the wound [186]. Despite these challenges, our approach was sufficient to achieve wound closure by about 3 weeks post-surgery.

Preserving the blood supply to the skin is critical for wound healing and for maintaining long-term skin health. Along the length of an intact limb, branches from deep, central vessels extend superficially into the skin's vascular network. In rabbits, the terminal arterial supply is extremely fragile and susceptible to disruption. Additionally, the skin covering the endoprosthesis cannot receive blood flow from such deep branches and, thus, must rely only its own vascular network. The central vessels in the rabbit hindlimb, the femoral and saphenous arteries, run along the caudal aspect of the hindlimb. During the first three surgeries, we used a circumferential incision with proximal reflection because it is the more traditional approach for limb amputation and closure of the skin around the residual limb. However, the circumferential incision, especially in R1, may have severed branches derived from the femoral or saphenous arteries and decreased the blood flow to the incision site. Thus, for rabbits R4-R6, we changed to a linear incision, an approach used in other orthopedic procedures [184]. Though the wound closed in all three rabbits after changing the incision, additional studies would be needed to confirm whether the change in surgical approach was the reason for improved outcomes.

Endoprostheses may place relatively high stress on the suture line and overlying skin since, unlike traditional orthopedic implants, they directly contact the skin. It has been shown in both pig [187] and rabbit [188] models that some mechanical loading along the skin surface and directly across a wound encourages healing. However, the skin over an endoprosthesis would also experience pressure on the suture line due to ground contact forces, which could damage the suture line and cause dehiscence. We took two steps to reduce the risk of skin trauma with the endoprosthesis. First, we applied the padded bandage over the limb for about 3 weeks after surgery, which reduce the pressure applied to the suture line as it healed. Second, we covered the endoprostheses with a compliant material (silicone), which would reduce skin pressure when external loads are applied. Additional studies are needed to determine the resilience of the skin covering the endoprosthesis to trauma under typical and severe biomechanical loading conditions.

Silicone, the material selected as the compliant coating for our endoprosthesis prototypes, has been used in some orthopedic devices to, for example, prevent soft tissue adhesions that would interfere with the implant's function[173]. Silicone is also common in other subdermal implants used in cosmetic surgery[189]. A potential drawback of coating the metal segment in silicone is that it could increase the risk of infection. Advanced multi-step sterilization procedures or incorporation of anti-bacterial coatings may be needed to prevent infection with long-term use of silicone-coated devices. Alternatively, biomaterials could be used to provide mechanical compliance and other benefits. For example, integration of a collagen layer over a tracheal prostheses improved the rate of epithelization over the prosthesis [190]. Biomaterial coatings over an endoprosthesis could promote wound healing and make the skin over the endoprosthesis more resilient to trauma.

Like many other orthopedic implants, such as joint replacements, our endoprosthesis was osseointegrated in the medullary canal of a long bone. Osseointegration is also becoming more

widely used to attach external limb prostheses to a residual limb [191, 192] since it overcomes problems of external prosthesis sockets such as skin breakdown and discomfort. In our proof-of-concept study, for convenience, we attached the endoprostheses to bone using off-the-shelf stainless-steel bone pins with machined threads. This osseointegration approach is not as sophisticated and effective as the clinical and state-of-the-art devices that incorporate, for example, porous metal frameworks [193] and osseointegrative coatings [194]. Such features encourage bone cells to adhere to or grow within the device so that it is more structurally stable relative to the bone [195, 196]. Of course, in future studies, our endoprosthesis could leverage state-of-the-art design features to achieve more effective long-term osseointegration.

We are unaware of previous reports that show similar bone ongrowth over the exterior of an osseointegrated implant as we observed in the post-surgery radiographs (Fig. 14). The bone ongrowth is likely a biological response by the bone to achieve better mechanical fixation and may have been further stimulated by external loading from ground-limb contact. Since the bone growth occurs cranially and caudally, it could potentially interfere with muscles attached to the endoprosthesis by protruding into the muscle's path. However, when we attached muscles to the endoprosthesis in R3-R6, we qualitatively observed less proliferative bone ongrowth, supporting the notion that the muscle attachment improved mechanical stability and fixation of the endoprosthesis in the bone. We plan to conduct histology to better understand the structure of the bone ongrowth tissue. Quantifying the extent of bone ongrowth and evaluating its effect on the performance of muscle-driven endoprostheses will also be part of our future research.

The unjointed endoprosthesis presented in this study is a first step toward our larger goal to develop jointed endoprostheses that are physically attached to muscles. Muscle-driven endoprostheses could potentially restore realistic movement control and proprioception in people with amputation far beyond the level enabled by current external prostheses that remain physically detached from muscles. Additional benefits of endoprostheses include a more natural

cosmetic appearance; fewer skin problems associated with external prostheses; lower prosthesis weight compared to electromechanical prostheses that require motors and batteries; and more convenience without the need to recharge or replace batteries. The potential benefits of endoprostheses would radically improve function and quality of life of people with limb amputation and other major musculoskeletal defects.

Our study had several limitations. First, we used the native skin of a healthy rabbit to enclose the endoprosthesis. When implanting an endoprosthesis in a person who has already undergone amputation, enough native skin to cover the implant would not be present. Thus, future research should investigate approaches, such as tissue expansion or skin grafting, to increase the amount of skin available to cover an endoprosthesis. Second, we had a small sample size ($n=6$), which was sufficient for our proof-of-concept study, though larger sample sizes will be needed to evaluate endoprostheses while accounting for inter-specimen variation. Third, the duration of study was relatively short. The rabbits with successful outcomes were kept alive for up to 60 days, which was enough to achieve our study objective but too short to determine long-term effects on tissues. Fourth, the endoprosthesis did not incorporate many state-of-the-art features for osseointegration, as described above, or materials that are common in orthopedic implants. For example, we used 316L stainless steel rather than titanium, which is traditionally used in orthopedic implants, because of our ability to 3-D print stainless steel in-house to quickly and affordably iterate on our endoprosthesis design. However, state-of-the-art materials and features could easily be incorporated, which we expect would only enhance the biocompatibility and performance of endoprostheses.

In conclusion, we showed that it is feasible to fully enclose an endoprosthesis in living skin at the distal end of a residual limb. We identified several critical factors that need to be considered when implanting an end-of-limb endoprosthesis, such as preserving vascularization, protecting the limb, and limiting the pressure applied to the skin. Our next steps include (1) comprehensively

evaluating the interfacing bone and skin tissues using imaging and histology, and (2) testing progressively larger implants, with the ultimate goal of implanting a jointed, muscle-driven endoprosthesis prototype to replace the foot and ankle of the rabbit hindlimb. Our repeatable success in implanting unjointed endoprostheses is a promising early step toward realizing our revolutionary and transformational muscle-driven endoprosthesis concept.

ACKNOWLEDGEMENTS

The authors thank Elizabeth Croy for her assistance with surgeries and radiography; Dr. Lori Cole and Chris Carter for veterinary care provided for the rabbits in this study; the Office of Laboratory Animal Care and Animal Housing Facility staffs at the University of Tennessee, Knoxville for animal care assistance; Dr. William Hamel for use of the stainless-steel 3-D printer; Dr. Brett Compton for providing silicone preparation equipment; and Danny Graham for his assistance in machining parts for the endoprostheses. Research reported in this publication was supported by (1) the Eunice Kennedy Shiver National Institute of Child Health & Human Development of the National Institutes of Health under Award Number K12HD073945, (2) a seed grant from the University of Tennessee Office of Research and Engagement, and (3) the University of Tennessee Department of Mechanical, Aerospace and Biomedical Engineering start-up funds.

CHAPTER 5. EX-VIVO ANALYSIS OF SKIN TISSUE SURROUNDING A STEM ENDOPROTHESIS IMPLANTED IN AN AMPUTATED RABBIT HINDLIMB

ABSTRACT

In a previous study we showed that it is feasible to implant a stem endoprosthesis underneath living skin at the distal end of a residual limb following transtibial amputation in the rabbit model. However, we did not analyze the effect of the endoprosthesis on the overlying skin, an important consideration since skin serves many key biological roles (e.g., germ barrier, temperature and moisture regulator). In this study we analyzed the thickness and cellular structure of the skin in the distal hind limb of three rabbits following successful implantation of stem endoprostheses. Reconstruction of the CT scan using thickness mapping revealed that the residual limbs developed the thickest area at the distal tip of the limb. The skin around the stem endoprostheses seemed to adapt to the additional mechanical loading experienced from the implant. Despite full healing along the incision line in the residual limbs, histology for all rabbits showed deep dermal fibrosis from the procedure. The results from this study show that healthy skin in a residual limb successfully heals and adapts when enclosed around a foreign endoprosthesis device. Results from this study will help inform the design and surgery of future larger endoprosthesis devices.

INTRODUCTION

In the previous chapter [197] we showed that it is feasible to implant a novel endoprostheses used for musculoskeletal reconstruction completely underneath the skin at the distal end of a residual hindlimb in rabbits following amputation. We suspect that the difference between successful and unsuccessful outcomes was due to factors such as maintaining adequate blood flow to the skin covering the endoprosthesis in order to promote healing and prevent ischemia. Switching from a circumferential incision to a linear incision likely helped maintain blood flow from the femoral artery and resulted in successful outcomes in three consecutive rabbits.

Despite the success of these surgeries, little is known about the effect of the subdermal implant on the surrounding tissue. Analyzing the effect of our endoprostheses on the surrounding tissue would elucidate, for example, how the skin successfully adapted to the device, which would help us predict long-term outcomes.

Studying the effect of a medical device with interfacing tissue is critical for predicting long-term biological acceptance or rejection of the device. For example, osseointegration, commonly used in total knee and hip arthroplasty [193, 198, 199] and lower limb replacement [142, 143], involves intimate device-bone interaction. Osseointegrated implants may change the mechanical loads experienced by the interfacing bone. It is well known that bone structure and mechanical properties are responsive to mechanical loading conditions [200, 201]. Therefore, it is critical to analyze how the bone structure adapts to the new loading conditions to ensure that bone health and the mechanical strength of the bone-implant linkage are preserved. For artificial tendon replacement, discussed later in Chapter 8, previous studies focused on the adaptation of muscle on a cellular level to the intertwining suture [173]. This gave a better understanding as to why the tendons maintained structural integrity during stress testing. Similarly for the skin covering an endoprosthesis, it is critical to analyze mechanical structure, thickness, and cellular composition to understand if the device is causing an adverse reaction that might lead to future rejection of the device.

Most previous literature on the effect of implanted devices on skin focused on analyzing compatibility with transcutaneous or percutaneous osseointegrated prostheses [202, 203]. However, traditional osseointegrated prostheses differ from an endoprosthesis because it is implanted completely underneath the skin and, therefore, the skin is subjected to external forces (e.g., ground reaction force). Previous studies suggest that, under increased levels of stress and pressure, skin adapts by increasing its mechanical strength [188, 204] and thickness [205]. The stem endoprosthesis is fully covered in skin, which exhibits increased pressure across the skin

during weight bearing. Additionally, the skin is completely surrounding a foreign body which has the potential to interfere with the skin's basic physiological functions and cause infection[206] or irreparable cellular damage [203, 207]. To ensure that the endoprosthesis does not degrade the structural integrity of the skin, there is a need to evaluate the structural changes of the skin in the residual limb caused by interaction with the device.

In this study, I analyzed the thickness of the skin in the distal hind limb of three rabbits with successful outcomes after implanting stem endoprostheses. The goal of this study was to analyze how the skin thickness changes in reaction to the endoprostheses by creating a three-dimensional map of hindlimb skin thickness and comparing it between the operated limb and intact contralateral limb. I hypothesized (1) that the rabbits who survive 60 days after surgery and used their residual limbs for weight-bearing would have the thickest skin at the distal end of the residual limb, and (2) that the skin thickness of the distal tip of the residual limb, which experiences higher ground reaction pressures, would be thicker than skin at the same approximate location on the contralateral limb.

METHODS

Surgery Outcomes

This study was approved by the University of Tennessee, Knoxville (UTK) Institutional Animal Care and Use Committee. We used New Zealand White rabbits since they are a common orthopedic model and large enough for testing physical endoprosthesis prototypes compared to other smaller mammals. The six (rabbits in our previous study (R1-R6) were approximately 18 weeks old and had an average pre-surgery weight of 2.92 kg. [197]. For each rabbit, we surgically implanted an unjointed stem endoprosthesis underneath the skin of the distal rabbit hindlimb immediately following transtibial amputation. We monitored each rabbit post-surgery with gross skin analysis, biweekly radiography, and pressure mat analysis.

Of the six rabbits who received an endoprosthesis, the final three consecutive rabbits (R4-6) healed from surgery enough to forego bandaging. The skin surrounding the endoprostheses had healed as early as 18 days post-surgery and the hair surrounding the limb had regrown around the entire limb as early as one-month post-surgery (Fig. 4.3). R4 and R6 showed no signs of adverse reaction to the device during a 60-day post-surgical period, so we performed euthanasia at the two-month timepoint. For R5, we had added a silicone “bulb” to the end of the endoprosthesis to increase pressure dispersion (see next paragraph for details). However, the bulb slipped off of the metal implant and we were unable to correct the issue (Fig. 4.2). Due to this, we euthanized the rabbit 18 days post-surgery, when the skin was qualitatively deemed by a veterinarian (Burton) to have healed.

Stem Device

The endoprosthesis stems discussed in this study can be further outlined in chapter 4 [197]. The stems used in this study consisted of three parts: 1) a 316L stainless steel tibial segment, 2) an intramedullary bone pin with custom reverse threading to screw into the steel segment, and 3) a biocompatible silicone over-molded sleeve made of a hardness 40 shore A silicone (BIO LSR M340, Elkem Silicones). These endoprostheses were designed to replace the part of the tibia bone that was removed during transtibial amputation. We found in chapter 4 that R4 and R6 had maximum pressures in the endoprosthetic limb of up to 3.28 times the healthy contralateral limb. We suspect that higher pressures caused the rabbits to develop slight pressure necrosis and a callus. Because of this, I designed the endoprosthesis prototype for R5 with a silicone bulb at the distal tip to increase pressure dispersion (Figure 4.1).

Euthanasia, dissection, and fixation

Prior to euthanasia, the rabbits were induced into general anesthesia with midazolam (0.75-1 mg/kg). Anesthesia was maintained with 3-5% isoflurane gas. While under anesthesia, we euthanized the rabbits through barbiturate overdose (1 cc/10 lb) via an intravenous ear

catheter. After euthanasia, I shaved both hindlimbs and prepared the limbs for dissection. I removed both hindlimbs of each rabbit through disarticulation at the hip joint. After disarticulation, the entire hindlimb was left intact and submerged in 10% neutral buffered Formalin for at least 7 days. The rabbit hindlimb was then transferred into 70% ethanol until time for further dissection.

To image the skin via CT, I first dissected the skin from both hindlimbs after at least one week in ethanol. I started by making a circumferential incision just above the knee and severing the fascia from proximal to distal, leaving the skin intact in a “sleeve” that resembled the skin’s orientation on the residual limb (Fig. 5.1). I performed this dissection on the residual limbs for R4-6 and the healthy contralateral limb for R6. The skin around the contralateral ankle was tightly adhered to the underlying tissue, so, in order to dissect off the entire “sleeve”, I made a linear incision down the caudal aspect of the limb. This allowed me to get leverage when dissecting around the ankle but resulted in a skin segment that was not fully intact.

We used a micro-computed tomography (microCT) method described in a previous study to obtain high-resolution, 3-D images of individual layers of the skin [208]. Before microCT imaging, I submerged the skin in Lugol’s Solution (15% I2KI / 85% diluted water) for 48 hours. After 48 hours, I flushed the skin with diluted water and submerged the skin in distilled water for at least 24 hours. This staining technique helped differentiate the dermal and epidermal tissue from the subcutaneous tissue. Next, I collected microCT images with the assistance of a radiographer (Alan Stuckey). Voxel dimensions were 0.052 x 0.052 x 0.052mm and slices were taken transverse to the tibial axis of the shank.

CT Processing

I wrote a custom MATLAB script to process the CT images and measure the thickness of the skin (Appendix A). This code processed the DICOM file frame-by-frame, analyzing the transverse cross-sections of the skin. First, I manually applied a threshold to the DICOM to exclude all tissue that was not part of the stained dermal or epidermal layers (Figure 5.1). Next, I

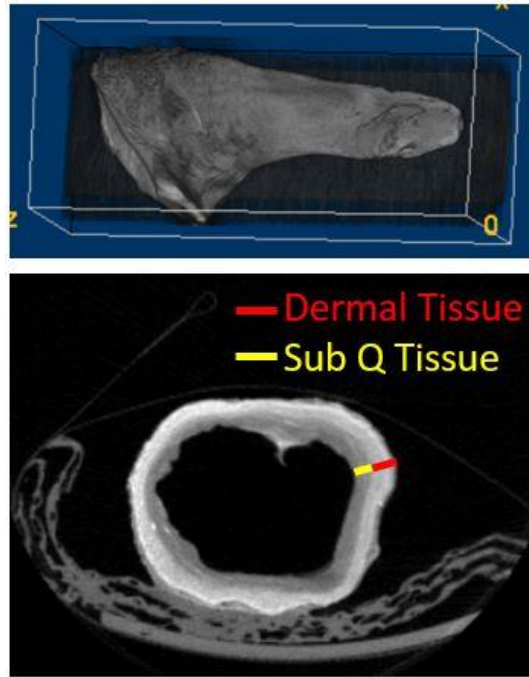


Figure 5.1. CT imaging of the skin from a residual limb of a successful rabbit. (Top) 3D reconstruction of the dissected skin. The skin was left intact to image skin thickness at different area of the leg. **(Bottom)** Cross-sectional analysis at a CT image of the skin. Staining shows distinction between the epidermis and dermis.

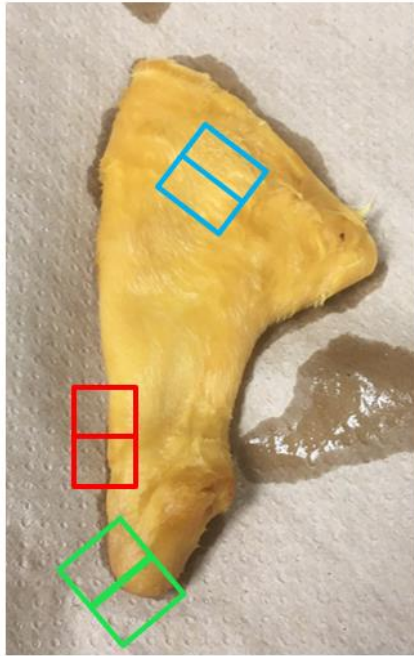
binarized each pixel into false or true based on whether or not it contained dermal and epidermal tissue. I then binarized each transverse frame and found the outside border of the skin, and the area centroid bounded by that outside border. For every pixel on the outside border, I calculated a line from the pixel to the centroid and counted the number of “true” cells in the image matrix. When scaled by the length of one pixel, the number of “true” cells between the centroid and the edge of the skin was determined as the skin thickness at that point.

Once the MATLAB code calculated the thickness of every external voxel on the outside of the skin, I created a 3D mapping of skin thickness across the entire residual limb for all three rabbits and for the shank of the healthy contralateral limb of R6. First, to determine the color scaling for the map of each limb, I normalized the skin thickness of each voxel by the maximum skin thickness measured across the entire limb. I reconstructed a 3D map of the limb to visualize skin thickness across the entire residual limb and locate areas of thicker and thinner skin. During surgery, the skin at the craniodistal part of the shank of the healthy intact limb was used as the new weight bearing tissue over the distal end of the endoprosthesis. Therefore, for the comparison mapping I normalized the thickness of each voxel in the residual limbs by the maximum thickness of the distalmost centimeter (48 frames) of the residual shank. This allowed for analysis in the change of skin thickness in the distal skin.

Histology Analysis

Following CT imaging, the dissected skin segments were submerged in distilled water for at least 2 weeks to remove the Lugol’s stain. Next, from each skin segment from the residual limbs, obtained samples from the following locations for histology: the shank proximal to the endoprosthesis, across the incision line, at the distal end of the endoprosthesis, and the caudal aspect of the limb over the endoprosthesis (Fig. 5.2). Additionally, on the contralateral intact limb, I obtained samples from the cranial aspect of the shank (for comparison to the incision site on the

Residual Implant Limb



Contralateral Limb

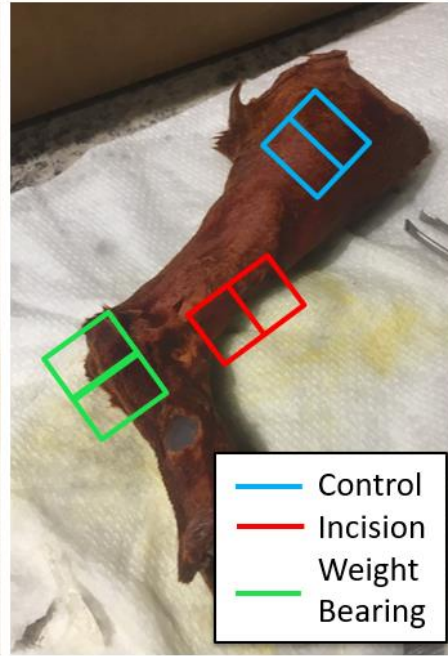


Figure 5.2. Location of histology samples. Boxes indicate the approximate location of where the sample was taken from. The line dividing each box represents the direction of the cross-sectional slice used for histology analysis

residual limb) and the bottom of the foot (for comparison to the weight-bearing distal tip of the residual limb).

The histology samples were obtained by slicing the skin into thin segments perpendicular to the area of interest. The histology samples were encased in histology cassettes and given to the UTCVM histopathology lab for slide generation. Each sample was stained with Hematoxylin and eosin (H&E) stain and sliced into thin segments to place on the slides. The histology slides were examined by a histopathologist (Lisa D. Duncan, M.D.).

RESULTS

CT Reconstruction

Rabbits who lasted 60 days post-surgery had a maximum skin thickness of 5.7 mm (R4) and 7.9 mm (R6). In both of these rabbits the maximum thickness was at the distal end of the hindlimb (Fig. 5.3). There were no noticeable signs of skin thinning along the cranial incision line. The maximum skin thickness of the rabbit who was euthanized 18 days post-surgery (R5) was 7.5 mm, but it occurred at the caudoproximal aspect of the residual limb. The thickest portion of skin in the distalmost centimeter of R5's limb was 4.6 mm.

The rabbits with the endoprosthesis had thicker skin in the distalmost centimeter of skin compared to the intact contralateral shank of R6 (Fig. 5.4). The maximum skin thickness within the distalmost centimeter of skin in the contralateral hindlimb was only 3.9 mm. The average skin thickness at the distalmost centimeter of the shank in the contralateral intact hindlimb of R6 was 1.9 mm, compared to 4.3 mm in the residual limb of R6. This is an increase of 126.3% average thickness between the residual and contralateral limb.

Histology Analysis

Histology revealed mild to deep fibrosis along the incision location in all three residual limbs (Table 5.1). Additionally, there were foreign body giant cells (FBGC) located in the distal tip

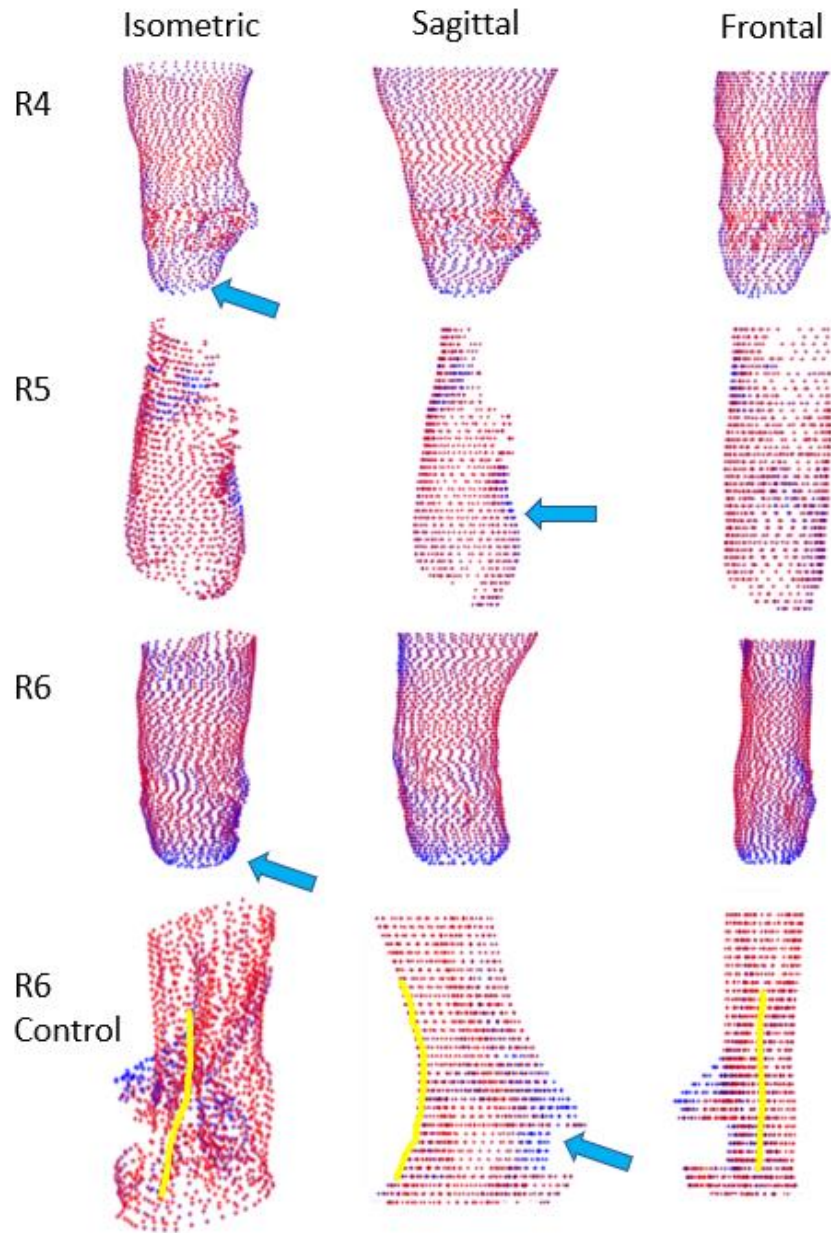


Figure 5.3. 3D skin thickness reconstruction for 3 rabbits. The thickest skin was at the distal weight-bearing aspect of the residual limb (blue = thick, red = thin). In the contralateral limb, there is relatively uniform skin thickness across the approximate incision location (yellow line represents approximate location of incision used in surgery on residual limb) compared to other area within the limb. The blue arrow indicated the thickest area of skin on each rabbit.

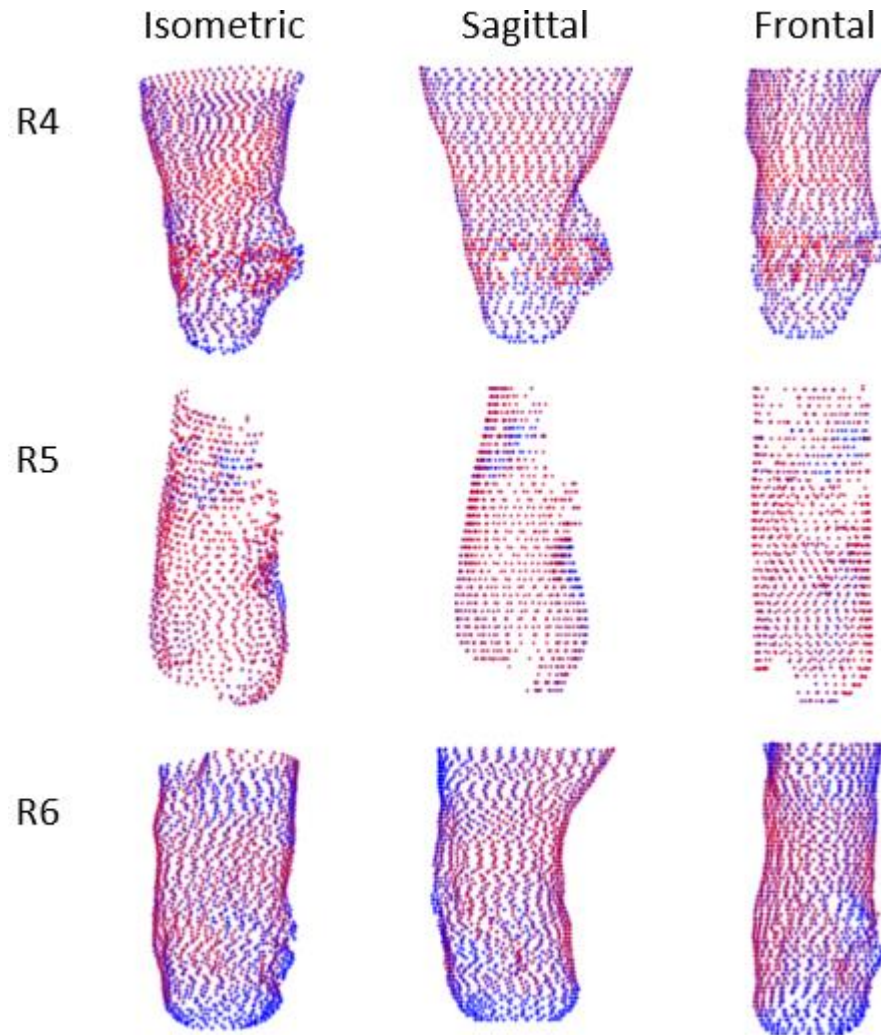


Figure 5.4. Residual limbs of each limb normalized against the maximum skin thickness of the contralateral limb. The virtual map of R4 and R6 showed that the thickest area of the skin of the contralateral limb was thinner than the thickest skin in the residual limb

Table 5.1. Histology analysis of critical skin locations.

	R4 Residual	R5 Residual	R6 Residual	R6 Contralateral
Control	Normal	Normal	Normal	Normal
Incision	Deep dermal fibrosis	Mid and deep dermal fibrosis	Deep dermal fibrosis, FBGC reaction	Normal
Weight Bearing	Extensive mid to deep dermal fibrosis, FBGC reaction	Mid and deep dermal fibrosis, FBGC reaction	Deep dermal fibrosis, FBGC reaction	Superficial and mid dermal fibrosis

of all three residual limbs. FBGCs were not located in the comparable weight bearing surface at the bottom of the contralateral foot. They are likely a response to either the implant or the surgical procedure.

DISCUSSION

The results from the study confirmed my hypothesis that skin on the weight-bearing distal end of a residual limb with a stem endoprosthesis implant would be thicker than a similar skin location on the contralateral limb. As reported in the previous study, rabbits with the endoprosthesis experienced up to 3.28 times more pressure on the residual limb than on the healthy contralateral limb. This increased pressure likely led to the formation of a callous in response. Skin has been shown to develop hard, dense calluses under higher pressures, specifically under weight-bearing circumstances [209]. This is a common problem in amputees with improperly fit prosthetic sockets [210, 211]; increased pressure from either weight bearing on the residual tibia or femur can cause calluses as well as pain and discomfort in the residual limb of an amputee. Despite the formation of the callus at the residual limb of the rabbits used in this study, the rabbits showed no signs of pain or discomfort.

We first normalized skin thickness in each residual limb to find areas of thick or thin skin. However, comparison to the contralateral limb is important to estimate how the skin may have adapted from its normal thickness after surgery. Therefore, we normalized the skin thickness in the residual limb against the maximum skin thickness measured in the contralateral limb to quantify relative adaptation. The skin in the distal residual limb was thicker than comparable skin locations in the contralateral limb. Therefore, the thicker skin in the residual limb was likely due to an increase in skin thickness rather than thinning of the more proximal skin in reaction to the endoprosthesis.

In all three rabbits, the skin incision successfully healed over our endoprosthesis prototypes that were made with bioinert materials. However, we might need more advanced

techniques to promote skin healing as we progress into surgeries with larger endoprotheses with mobile feet. For example, tracheal implants use a collagen-infused exterior to promote skin healing and reepithelization over the incision line [212]. We are investigating ways to implement this technology into future endoprosthesis designs. Additionally, in our histological analysis, we noticed fibrosis occurring along the incision line. Integration of stem cell therapies has been shown to decrease fibrosis across an incision line and promote skin healing [213].

Though gross skin analysis can provide valuable, qualitative assessment of the outside of the skin, various imaging modalities have been adapted to better analyze issues within the skin. In our study, we used microCT to assess the 3D distribution of thickness of the skin samples. However, microCT is not as well suited as other imaging modalities for imaging soft tissues. Magnetic resonance imaging (MRI) can image the skin to allow physicians to analyze the different layers for concern or irregularity [214]. Tran et al. used MRI to image skin under orthogonal loading in order to determine the mechanical properties of the skin in the human arm [215]. However, MRI is more expensive and cannot achieve as high resolution as the microCT used in this study.

This study had several limitations. First, we made several assumptions in our method to calculate the skin thickness from the CT images. We computed the thickness on a straight line from the edge of the skin to the centroid of the area bounded by the outer perimeter of the skin. Another approach would be to measure skin thickness along the line perpendicular to the outside or inside edge of the skin. However, the outside border of the skin was not smooth, so the calculation based on the area centroid was deemed more reliable. A second limitation was that we had a small sample size, so our results may not generalize to a larger population. However, the results were similar in both rabbits who survived the entire 60-day period. We are also building a larger database of samples as we test larger endoprosthesis prototypes in our ongoing projects.

In conclusion, we used a virtual skin reconstruction technique to quantitatively analyze the thickness of the skin surrounding we confirmed our hypothesis that there would be greater skin thickness at the residual tip than comparable skin locations in the contralateral limb. The higher skin thickness at the tip was likely caused by the high weight-bearing pressure compared to the intact contralateral limb [197]. We plan to apply the same skin analysis technique to rabbits with larger endoprostheses as we progress toward a mobile, jointed device.

ACKNOWLEDGEMENTS

I would like to thank Dr. Jonathan Wall for allowing us to use the microCT scanner, Alan Stuckey for acquiring the images used in this study, and Dr. Lisa Duncan for analyzing the histology samples. Research reported in this publication was supported by (1) the Eunice Kennedy Shiver National Institute of Child Health & Human Development of the National Institutes of Health under Award Number K12HD073945, (2) NSF CAREER Award #1944001, (3) a seed grant from the University of Tennessee Office of Research and Engagement, and (4) the University of Tennessee Department of Mechanical, Aerospace and Biomedical Engineering start-up funds.

CHAPTER 6. BIOMECHANICAL ANALYSIS OF THE RABBIT HINDLIMB DURING THE STANCE PHASE OF HOPPING GAIT

This work is currently in review with the Journal of Biomechanics.

Hall P. T., C. Stubbs, D. E. Anderson, C. B. Greenacre and D. L. Crouch. Biomechanical Analysis of the Rabbit Hindlimb during the Stance Phase of Hopping Gait. *Journal of Biomechanics* In Review: 2021.

ABSTRACT

Despite the wide use of the rabbit model for orthopedic research, there is a very limited existing data set throughout literature that describes healthy rabbit biomechanics. The objective of this study was to quantify the normative hindlimb ankle and foot biomechanics of New Zealand White rabbits during the stance phase of hopping gait. Specifically, we measured bilateral hindlimb kinematics, vertical ground reaction force, and ground-foot contact area and pressure during the stance phase of both hindlimbs of six healthy New Zealand White rabbits. In addition to reporting normal values for the rabbit hindlimb, data were compared between hindlimbs to determine any bilateral differences in our sample population. We measured biomechanics by synchronously recording sagittal plane motion and ground-paw pressure using a video camera and pressure mat, respectively. The range of motion of the foot-ground angle and ankle angle during stance phase was 108.9 degrees and 78.1 degrees, respectively; there was no bilateral difference for either joint angle throughout stance. The maximum vertical ground reaction force and contact area, both averaged across rabbits, were 46.6%BW and 8.1cm², respectively. There were statistically significant bilateral differences in (1) vertical ground reaction force from 48-50% of stance and (2) the temporal positions of the ankle and knee joint center in the sagittal plane for most of stance. Future studies can reference our data to quantify the extent to which orthopedic interventions affect rabbit biomechanics.

INTRODUCTION

Animal models are essential tools for conducting biomedical research. The rabbit is a common animal model in orthopedic research to study, for example, mechanical instability [163, 165, 216-226], knee joint load distribution [227-229], muscle atrophy and control [22, 230-232], osteoarthritis [162, 163, 165, 218, 228, 233, 234], and postural control [235]. Additionally, the rabbit model is used to test implantable medical devices and tissue-device interactions, such as for osseointegrated implants [157-159, 236] and fracture healing [166, 237]. Recently, we have adopted a rabbit model to test the feasibility of a new functional limb replacement approach for people with amputation [197]. Our *in vivo* orthopedic studies will involve replacing the rabbit hindlimb ankle and foot with functional, implanted endoprosthesis prototypes that intimately integrate with bone, skin, and muscle.

For many orthopedic interventions, their effect on motor function with respect to that of the intact biological limb must be determined to support clinical translation. Since our endoprosthesis prototypes will replace the hindlimb ankle and foot, we need to quantify the motor function these biological joints to benchmark the motor function enabled by the prototypes. Motor function may be assessed by measuring biomechanical variables, such as kinematics and ground reaction forces, using motion capture techniques. One previous motion capture study in rabbits reported knee joint kinetics and, for one rabbit, vertical ground reaction forces [170]. To our knowledge, multi-sample ground reaction forces and kinematics of the ankle and foot have not been reported for the rabbit hindlimb.

Several techniques have been developed to measure limb kinematics and ground reaction forces. The previous rabbit biomechanics study [170] attached reflective motion capture markers to transdermal bone pins. This invasive method can track bone motion accurately but is relatively difficult to implement and may interfere with movement either mechanically or by causing discomfort. Alternatively, non-invasive motion capture methods are more straightforward to

implement and could elicit more natural movement by avoiding mechanical interference and discomfort. Non-invasive motion capture methods that have been used for small animals include reflective marker-based infrared motion capture [170], marker-less motion capture from videos [238], and bi-plane fluoroscopy [239, 240]. The two primary tools for measuring ground reaction forces are force plates and pressure mats. Force plates measure the *resultant* forces along 6 degrees of freedom, which requires that only one limb contacts the plate at a time to distinguish forces among limbs [170, 241]. Pressure mats, which measure vertical pressure and contact area, are more convenient to use with quadrupedal animals since individual limbs can be distinguished even if multiple limbs contact the mat simultaneously [242-244]. The pressure mat data can be used to calculate vertical ground reaction force (vGRF).

The goal of our study was to quantify intact biological hindlimb ankle and foot kinematics and ground reaction forces during the stance phase of hopping gait in rabbits. A secondary goal was to analyze the extent of bilateral symmetry of the measured biomechanics variables during the stance phase. We measured hindlimb kinematics and ground-foot kinetics from sagittal-plane video recordings and a pressure mat, respectively. We hypothesized that there would be no difference between hind limbs for measured kinematics and forces.

METHODS

Subjects

All procedures were approved by the University of Tennessee, Knoxville Institutional Animal Care and Use Committee. For this study we used six 14-week-old New Zealand White (NZW) Rabbits (weight = 2.7 ± 0.33 kgs). During the two-week acclimation period prior to testing, rabbits were trained to hop through an acrylic tunnel when given negative reinforcement (i.e. prodding). Rabbits were housed in pairs and given daily enrichment and positive human interaction.

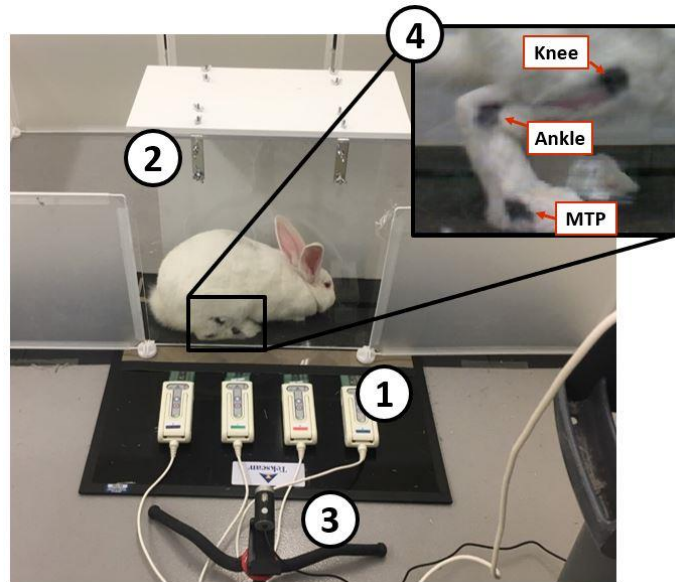


Figure 6.1. Testing setup used to collect motion capture data. (1) Tekscan Very HR Walkway 4 to collect pressure data. (2) Acrylic tunnel used to guide and constrain rabbit movement. (3) 60 Hz Camera recorded sagittal plane kinematics. (4) Black ink markers on the sagittal plane joints based on bony landmarks.

Instrumentation and Setup

The setup for our locomotor measurement system included several components (Fig. 1, 1-3). A pressure mat (Tekscan, Very HR Walkway 4; South Boston, MA) was used to record pressure data at 60 Hz. We taped 320-grit sandpaper to the top of the smooth pressure-sensing area to prevent the rabbits from slipping. We placed a 3-kg weight on the sandpaper-covered mat and calibrated the mat through the Tekscan software calibration program. The mat was placed inside a clear acrylic tunnel to guide the rabbits across the pressure mat. The mat width (11.2 cm) permitted only unilateral pressure measurements; therefore, to record data for both hindlimbs, we laterally offset the mat in the tunnel and had the rabbit hop across the mat in both directions (see Testing Procedure below). A camera (1080P HD Webcam, SVPRO), placed three feet away from the clear acrylic panel, captured video at 60 Hz. Video and pressure mat data were synchronized using the Tekscan Walkway software (Tekscan, South Boston, MA).

Testing Procedure

Before testing, we shaved both hindlimbs and marked the metatarsophalangeal (MTP), ankle, and knee joint centers on the lateral side of each hindlimb with black ink (Fig. 6.1, 4). The marks were made so that we could identify the joint locations during the kinematics analysis described below. After marking, we placed the rabbit into a pen with the acrylic tunnel and pressure mat. Each trial began when the rabbit entered the tunnel. A trial was deemed successful if the rabbit continued the hopping motion through the entire length of the tunnel without stopping. The rabbits completed 10 trials of hopping through the tunnel in each direction while we synchronously recorded pressure and video data for each trial.

Data Processing and Statistical Analysis

For each trial, we extracted the pressure, contact area, and vertical ground reaction force (vGRF) of the hind foot from the pressure recordings in the Tekscan Walkway software. The hind foot was isolated by drawing a strike box around the foot contact location, as indicated by pressure

data (Fig. 6.2). The contact area was calculated as the total geometric area within the strike box for which the pressure was greater than zero. The vGRF was calculated as the product of foot contact area and the average pressure across the contact area. We also computed the total contact area over the entire stance phase and the average pressure of the foot inside the strike box as a function of time. The stance phase of a given limb was designated as the portion of the gait cycle for which pressure was detected for that limb.

We calculated joint angles from the video frames corresponding to stance phase. We processed the video frames with a custom motion analysis program written in MATLAB (Mathworks, Natick, MA). The program used a bottom-hat morphology filter to distinguish the black ink marks from the white fur and calculate the centroid of each marker position (Fig. 6.3). Then, frame-by-frame, we visually verified the marker centroids and, if the centroid location appeared inaccurate, corrected the location by manually approximating the centroid from the still frame. This method assumed that the sagittal plane orientation of the foot and shank was aligned with the line segments connecting the centroids; this was a reasonable approximation given the arrangement of the camera with respect to the acrylic tunnel. Finally, we calculated the angle between the foot segment and ground (i.e. foot angle) and between the foot and shank segments (i.e. ankle angle) throughout stance (Fig. 6.3). Since the camera was approximately level with the ground, we defined the ground as the horizontal line that intersected the MTP joint.

In each trial, the timepoints were normalized by the duration of stance phase, permitting comparison among trials of different stance durations. We averaged time-series joint angles, vGRFs, contact areas, and contact pressures across all rabbits for each hindlimb (right and left) and normalized the vGRF by body weight (%BW). We compared the averaged time-series data between the right and left limbs using statistical parametric mapping (SPM), with $\alpha=0.05$ [175]. We used a paired Student's t-test to compare stance duration between the right and left hindlimb.

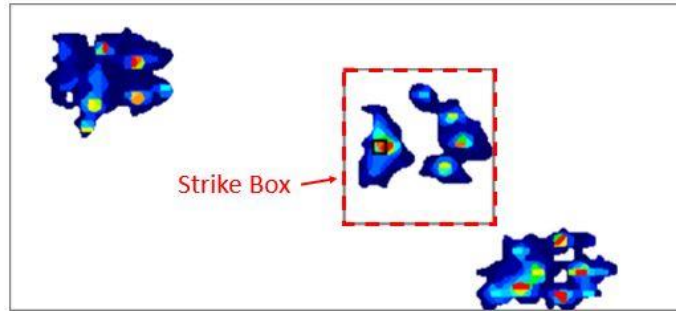


Figure 6.2. Example of strike box isolation of the contact foot using the Tekscan Walkway. Through the Tekscan software we isolated the force and contact area of a specific hindlimb foot strike.



Figure 6.3. Motion capture analysis of the sagittal plane videos allowed for measurement of the rabbit hindlimb kinematics.

Frame-by-frame top hat morphology allowed for detection of joint markers. Joint segments (orange) were drawn between the centroids of the joint segments. From these joint angles we calculated the ankle angle (yellow) and the angle between the foot and ground (blue) through the dot product of unit vectors of the joint and ground segments. The ground (dashed blue) was determined as the horizontal line segment that intersects the MTP joint.

Evaluating joint angles separately for each joint provides an incomplete picture of rabbit hindlimb kinematics. This is because the hindlimb is a kinematic chain, so the positions and orientations of proximal limb segments depend on those of distal limb segments. Therefore, we implemented a technique to calculate the knee and ankle joint center positions in the sagittal plane. To permit comparison among rabbits of different sizes, we applied the joint angles to a geometrically normalized model of the rabbit hindlimb. The foot and shank segments of the model were 2 and 3 normalized length units (NLUs), respectively, to approximate the length proportions between the two segments. For each rabbit, we computed the time-series “trajectory” of the joint positions throughout stance for each trial; averaged trajectories across trials separately for the right and left hindlimb; and calculated the Euclidean distance between the averaged right and left hindlimb trajectories at every one percent of stance. We used SPM ($\alpha=0.05$) to identify portions of stance for which the Euclidean difference was significantly different from zero, which would indicate a significant difference in joint position between hindlimbs.

RESULTS

Pressure Analysis

The vertical ground reaction force (vGRF) was 4.9-5.9 %BW larger ($p = 0.048$) for the right leg ($36.4\% \pm 7.9$ %BW) than the left leg (31.4 ± 8.5 %BW) for a small portion (48-50%) of stance (Fig. 6.4). This portion of gait corresponded approximately to the beginning of the propulsion phase. There was no significant bilateral difference in contact area during stance (Fig. 6.5). The vGRF and contact area showed similar bimodal trends during stance with the first peak occurring at approximately 25% of stance and the second occurring at approximately 75% of stance. The vGRF and contact area curves were strongly correlated, with a Pearson’s correlation coefficient of 0.986 and 0.984 for the left and right hindlimbs, respectively. There was no significant bilateral difference in contact pressure during stance phase. Both hindlimbs maintain a nearly constant average pressure of approximately 0.15 kg/cm^2 through the middle 80% of stance (Fig. 6.6),

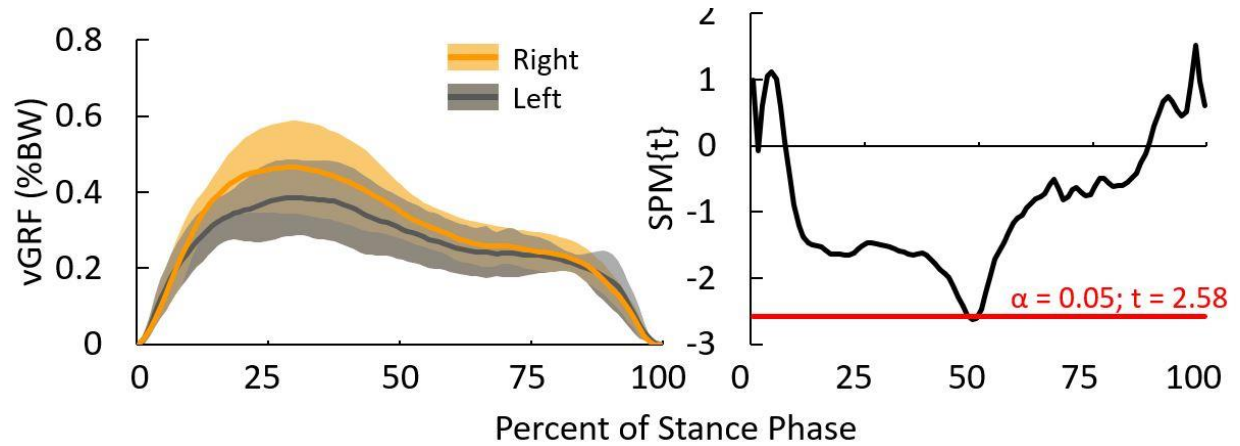


Figure 6.4. Vertical Ground Reaction Forces of rabbit hindlimbs throughout Stance Phase. The left graph shows the comparison of the total vGRF between the right and left hindlimb throughout stance phase. The right graph shows the SPM comparison between hindlimbs of the vGRF. There was a slight significant difference between the right and left hindlimbs between 48-50% of stance.

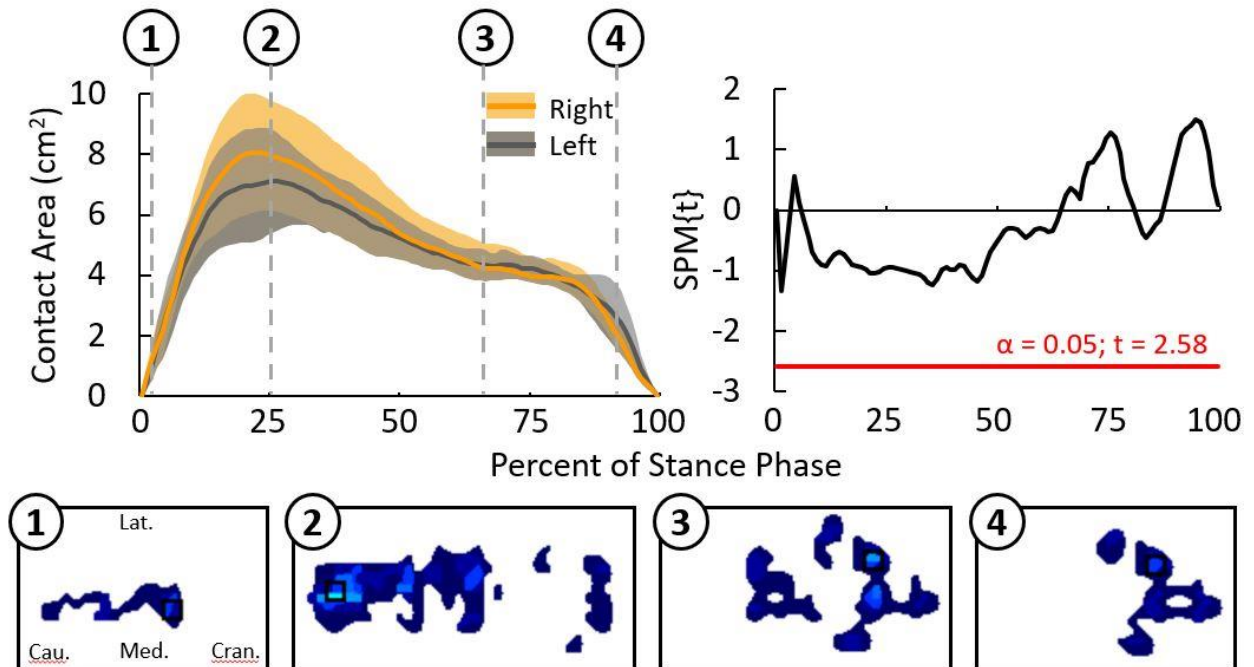


Figure 6.5. Contact Area of the rabbit hindlimb throughout stance phase. The left graph shows the comparison of the contact area between the right and left hindlimb throughout stance phase. The numbered timepoints correspond to contact area screenshots from a representative trial of a left rabbit stance. The right graph shows the SPM comparison between hindlimbs of the contact area. There was no statistical difference between hindlimbs throughout stance.

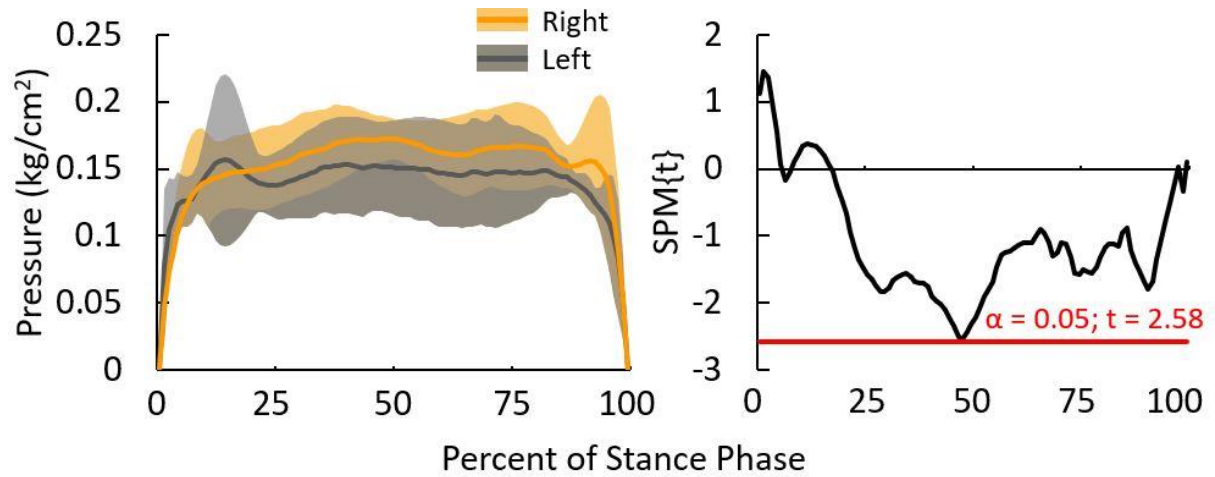


Figure 6.6. Pressure of the rabbit hindlimb throughout stance phase. The left graph shows the comparison of the pressure between the right and left hindlimb throughout stance phase. The right graph shows the SPM comparison between hindlimbs of the pressure. There was no statistical difference between hindlimbs throughout stance.

unlike vGRF and contact area, whose time-series curves were bimodal. Stance duration was not significantly different ($p=0.38$) between the right (0.46 ± 0.16 s) and the left (0.54 ± 0.16 s) hindlimbs.

Hindlimb Kinematics

There were no significant kinematic differences in joint angles between the right and left hindlimb (Fig. 6.7). Averaged across rabbits and sides, the foot angle ranged from 15-123.9 degrees and the ankle angle ranged from 67.6-135.7 degrees. The ankle angle started with a negative slope and switched to a positive slope at approximately 40% of stance; this point of peak dorsiflexion (i.e. lowest) ankle angle divided the stance phase into loading response and forward propulsion sub-phases, as with human stance [245]. The average standard deviations of the foot angle are 7.05 and 7.53 degrees for the right and left hindlimb, respectively. The average standard deviations of the ankle angle are 11.25 and 14.27 degrees for the right and left hindlimbs, respectively.

During stance, the knee joint center traveled approximately 1.5 NLUs downward and 5.5 NLUs forward (Fig. 6.8). Because the normalized foot segment was of a fixed length and rotated about a fixed point, the normalized ankle joint centers from all trials were restricted to an arc. The average standard deviation in normalized knee position across rabbits was approximate 1 NLU. Additionally, average difference in joint positions between hindlimbs, calculated as the Euclidean difference between hindlimbs, ranged from 0.16 - 0.33 NLUs for the ankle and 0.39 - 0.78NLUs for the knee throughout stance (Fig. 6.9). The knee position difference was significantly different from zero throughout stance, with the largest differences occurring during the first 25% of stance phase. The ankle position difference was statistically significant from zero throughout most of stance.

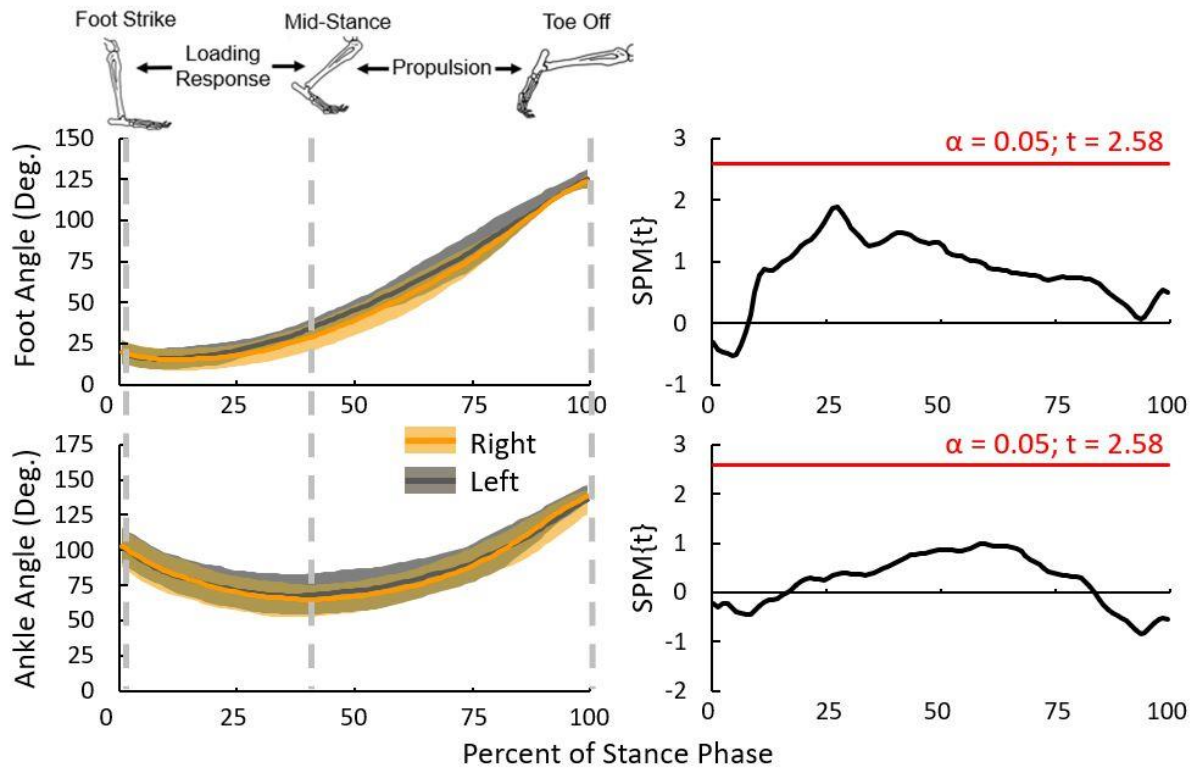


Figure 6.7. Joint Kinematics of the rabbit hindlimb throughout stance phase. (Left) Foot and ankle angles throughout stance phase. Rabbit stance can be broken down into two phases, loading response and propulsion, based on the timepoint of the minimum ankle angle. **(Right)** SPM analysis of the joint angles. There was no statistically significant differences for either joint angle.

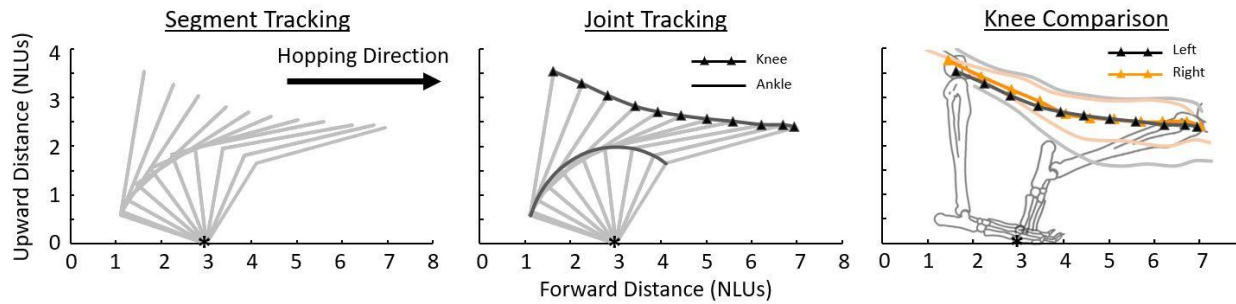


Figure 6.8. Normalized joint tracking and kinematic comparison between knee trajectories. (Left) Recreation of rabbit stance using normalized limb segments. Each hindlimb location represents hindlimb kinematics at each 10% of stance. **(Middle)** Using the normalized hindlimb kinematics, we recreated the kinematics and trajectories of both the ankle and knee joint throughout stance. **(Right)** Comparing the knee joint trajectories throughout stance allows for visual comparison between hindlimbs. There was minimal noticeable difference between the right and left knee trajectories measured in this study.

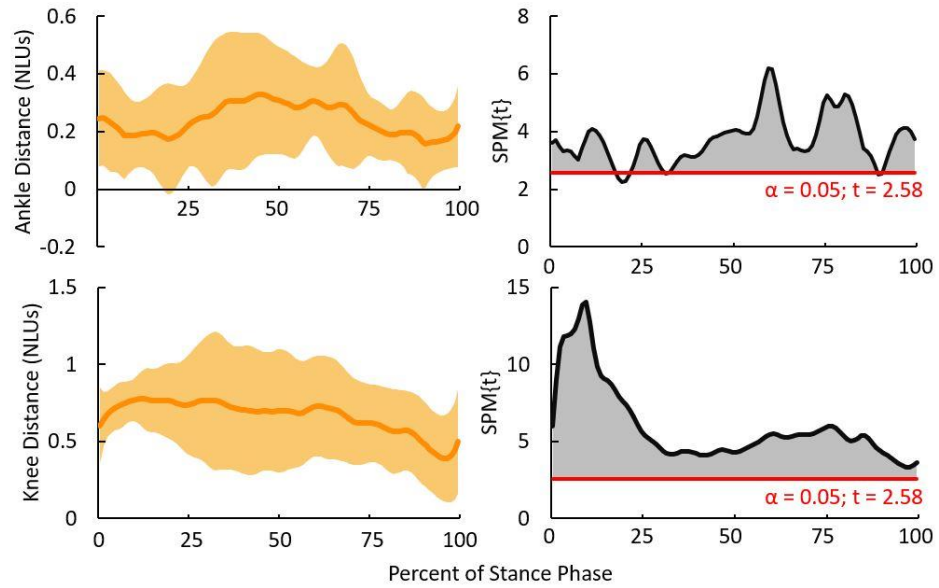


Figure 6.9. Euclidean distance between right and left normalized joint positions throughout stance. (Left) Euclidean distance between the right and left normalized ankle position (top) and knee position (bottom) throughout stance. **(Right)** One-sample SPM analysis of the Euclidean distance between hindlimb joint positions. The knee position showed statistically significant difference throughout the entirety of stance and the ankle showed statistically significant distance between hindlimbs for the majority of stance.

DISCUSSION

In this study we achieved our main goal of measuring select biomechanics variables from the intact biological hindlimb of rabbits. The data serve as reference data to benchmark how future orthopedic interventions, such as our endoprosthesis, affect hindlimb biomechanics. The two sub-phases of stance, loading response and forward propulsion, mirror stance patterns seen in humans. However, during foot strike, the rabbits landed with a positive foot angle with respect to the ground, whereas humans generally land with a negative foot angle during walking gait [31]. Despite this difference in foot angle, rabbits and humans are both considered plantigrade [246]; as opposed to other common research animal models that are digitigrade (e.g. cats, dogs) [167], or unguligrade (e.g. pigs and goats) [168]. Therefore, the similar stance patterns and plantigrade nature of both rabbits and humans support using the rabbit as a comparative biomechanical model of human gait.

We computed the sagittal-plane position of the ankle and knee joint centers, which reflect whole-limb kinematics better than joint angles since they are a function of one or more joint angles and limb segment lengths; in our study, the knee joint center was a function of the foot and ankle angles and the foot and shank segment lengths. Thus, joint center position data provide an essential complement to individual joint angle data, which mask differences in whole-limb kinematics. For example, a previous study found that rats with peripheral nerve injury recover whole-limb kinematics even as individual joint kinematics remained altered [247].

The time-series vGRF data exhibited a bimodal pattern that is consistent with the trial reported in the previous rabbit biomechanics study [170] and the vGRFs during human walking [248]. We expect that, as with humans, the maximum vGRF that occurs at approximately 25% of stance corresponds to the loading response triggered by the need to support the rabbit's body weight during landing [29]. As with the second mode of stance vGRF in humans [31], the leveling off of the curve of the vGRF at approximately 75% of stance presumably corresponds to forward

propulsion, though we could not confirm this since the pressure mat cannot record the horizontal ground reaction forces needed to assess forward propulsion. Despite this limitation, pressure mat data are useful for comparing among experimental groups because they reveal how kinetics are changing over both space and time [26].

Contact area was strongly correlated with vGRF magnitude, with correlation coefficients of 0.984 and 0.986 for the right and left hindlimbs, respectively. The correlation partly explains why the average pressure was nearly constant throughout stance phase. Maintaining a constant ground-paw pressure may be a locomotor strategy employed by the rabbit's sensorimotor system. As seen in our prior study [249], orthopedic interventions can alter the pressure between the hindlimb and ground. When testing our endoprosthesis in the future, it will be interesting to see if rabbits adapt their hindlimb movement to preserve ground-foot pressure throughout stance phase.

Per our secondary goal, we observed some bilateral biomechanical differences. For one, there was a statistically significant bilateral difference in vGRF over a very small (2%) portion of stance. More notably, the bilateral difference in the position of the ankle and knee joint centers was statistically significant over most of the stance phase. The difference could have been due to the way we calculated joint center positions by applying measured joint angles to a generic hindlimb model; though this approach allowed us to control for the effect of limb length, it also magnified any potential bias in our joint angle measurements by projecting joint angles over a long distance (i.e. to the end of the limb segments). The formula used to calculate knee joint center position also compounded errors or bias across two joints (ankle and foot joint). A potential explanation for all bilateral differences is that the data for each hindlimb side were recorded in separate trials, a limitation noted below. Finally, the observed bilateral differences may have been due to limb preference, though this is difficult to determine given our setup limitations and small sample size.

Our study was limited in several ways. Pressure mats measure pressure/force only in the vertical direction. A force plate could be used in place of our pressure mat to measure 6-DOF force vectors. Our video-camera-based motion capture setup and custom MATLAB software allowed analysis of 2-D motion in the sagittal plane only. We could more comprehensively characterize hindlimb kinematics with 3-D data obtained either with a multi-camera motion capture system or more advanced software. One such software, DeepLabCut, uses machine learning to track anatomical features without joint markers and can calculate 3-D kinematics from a 2-D video [250, 251]. We tracked marked joint locations on the skin, which are more convenient than bone pins used in the previous rabbit biomechanics study [170] but can move relative to underlying bony landmarks. Because our pressure mat was relatively narrow (11.2 cm), we could only measure pressure under one hindlimb at a time. As previously mentioned, this possibly attributed to the small bilateral differences in the vGRF we observed in our study. The length of our motion capture setup only allowed us to capture stance phase. In future studies we plan to use a wider pressure mat and longer tunnel with two cameras (one on each side) to capture bilateral gait data over an entire gait cycle.

In conclusion, we have reported select ground-paw pressure and kinematic data from the intact biological hindlimbs of healthy New Zealand white rabbits. Our results showed that, although rabbits have a plantigrade gait pattern, they make initial contact with the ground either flat-footed or on their toes. The rabbit vGRF and contact area have similar curves throughout stance, resulting in a relatively flat pressure curve. The most prominent bilateral difference was observed for joint center positions; more investigation is needed to determine if the difference was real or due to a weakness in our calculation method. Our results add significantly to the limited existing data on rabbit hindlimb biomechanics. In future research we intend to use the data reported in this study as an experimental control or reference to quantify the extent to which orthopedic interventions affect rabbit biomechanics. Additionally, knowledge of rabbit hindlimb

biomechanics can inform the design and development of orthopedic interventions, such as our endoprosthesis, to improve functional outcomes of patients.

ACKNOWLEDGMENTS

The authors thank Dr. Bryce Burton, Dr. Kelsey Finnie, Dr. Lori Cole, and Chris Carter for veterinary care provided for the rabbits in this study, and the Office of Laboratory Animal Care and Animal Housing Facility staffs at the University of Tennessee, Knoxville for animal care assistance. Thanks to Dr. Katrina Easton for providing constructive feedback on the manuscript. Research reported in this publication was supported by (1) the Eunice Kennedy Shiver National Institute of Child Health & Human Development of the National Institutes of Health under Award Number K12HD073945, (2) NSF CAREER Award #1944001, (3) a seed grant from the University of Tennessee Office of Research and Engagement, and (4) the University of Tennessee Department of Mechanical, Aerospace and Biomedical Engineering start-up funds.

CHAPTER 7. ANALYSIS OF THE EFFECT OF ARTIFICIAL TENDON ON LOCOMOTOR FUNCTION WHEN IMPLANTED IN THE RABBIT HINDLIMB.

ABSTRACT

Surgical reconstruction of the muscle-tendon unit might not be possible after several clinical conditions such as acute tendon rupture, tendinosis, and limb amputation. Artificial tendon has been developed as a replacement for irreparable damaged tendon. Although previous studies have shown the mechanical capabilities of this artificial tendon, they did not analyze the effect of the tendon on locomotor function. The objective of this study was to analyze how replacing ankle tendons affects locomotor function in the rabbit hindlimb. We individually replaced either the Achilles or Tibialis Cranialis tendon in 2 New Zealand White rabbits each. Over the next 6 weeks we measured biomechanics by synchronously recording sagittal plane motion and ground-paw pressure using a video camera and pressure mat, respectively. We analyzed 1) how end point biomechanics of the hindlimb compared to a healthy control group and 2) how the biomechanics changed throughout the post-surgical testing. Rabbits with Tibialis Cranialis replacement recovered to within both pre-surgical and healthy control levels of function. Rabbits with Achilles replacement started to recover towards pre-surgical levels of function. However, the ankle angle, and vertical ground reaction force never fully recovered. That locomotor function improved over time in rabbits having artificial tendon replacement in the biological hind limb supports the idea that such tendons could enable function when attached to an endoprosthesis. Artificial tendons could be used to restore function for other orthopedic conditions, such as tendon rupture, degeneration, and necrosis.

INTRODUCTION

Biological tendon, the anatomical link between muscle and bone, contributes to sensorimotor function in many ways. Mechanically, tendons transmit forces and store and release energy through its elastic strain, while using inherent mechanoreceptors to sense force and length

changes across the musculotendon unit. There are several clinical conditions that result in irreparable damage to the tendon or the junctions between the tendon and other tissues. Acute tendon rupture is one of the most common tendon injuries [252], occurring frequently in the Achilles tendon [252-254], Patellar tendon [255], and quadriceps tendon [256]. Tendon rupture incidence is commonly associated with age and underlying medical conditions [252], and repair can only typically be achieved through prompt diagnosis and surgical intervention. The breakdown of collagen tissue within a tendon stemming from chronic overuse of the tendon is called Tendinosis [257]. Tendinosis is common in the elbow [258, 259], shoulder [260, 261], and ankle [262] joint, and can cause severe impairment and disability. Secondary injuries such as UCL tear and rotator cuff tear [263] can be caused by Tendinosis.

Artificial tendons have been developed to repair or replace damaged or missing biological tendons. Compounds that mirror tendon mechanical properties allow for tendon healing and regrowth for severe tendon injury [264-267], similar to a bone or nerve scaffold. Studies have shown that, by maintaining a gliding external surface that prevents tissue adhesion could allow for a permanent artificial tendon replacement [268, 269]. Melvin, *et. al* developed a permanent artificial tendon replacement with a durable muscle interface that serves as a promising technology for direct muscle-prosthesis connection [172]. Suture based tendon gives the advantage of an inert material for the growing muscle to grow through and develop strong mechanical linkages [270]. This muscle-suture junction has been shown to withstand stronger mechanical loads than a natural myotendinous unit [271].

The effect of tendon replacement devices on motor function is poorly understood. The previous studies performed by Melvin *et al.* in a goat model have shown stiffness and failure loads similar to biological tendons [173]. However, the effect of permanent artificial tendon on motor function, which has strong implications for the effectiveness of both tendon repair after injury and replacement following amputation, remains unclear. Motor function, specifically in cyclic loading

and unloading patterns such as gait, relies heavily on the functional elasticity of tendon [272]. Tendon injuries and affect this functional range, limiting movement and inhibiting gait pattern [273, 274]. Motor function relies not only on strength and stability, but also on other key factors such as muscle coordination and viscoelasticity to produce coordinated movement. Despite, the strong mechanical properties of suture-based tendon, it is important to measure how the device affects locomotor function in order to determine its efficacy towards eventual clinical tendon replacement.

The goal of this study was to determine the effect of replacing biological tendon with suture-based artificial tendon on locomotor function in a rabbit model. We hypothesized that locomotor function would decrease immediately following surgery but subsequently recover toward pre-surgical levels.

METHODS

Summary

This study was approved by the University of Tennessee, Knoxville Institutional Animal Care and Use Committee. Four rabbits had either the Achilles tendon (A1&2) or Tibialis Cranialis tendon (T1&2) replaced, while all other tendons remained intact. The rabbits were 16 weeks old and 3.40 ± 0.26 kg at the time of surgery. We used the rabbit model because they are a small mammal large enough to test physical device prototypes and the large range of motion about the angle allows increased sensitivity to detect changes in kinematics. For each surgery we resected the tendon of interest; integrated one end of the artificial tendon with the distal end of the muscle; and attached the other end of the artificial tendon across the ankle to the foot using a suture anchor. We performed biomechanical testing on the rabbits once pre-surgery and at five weekly timepoints starting at 2 weeks post-surgery.

Artificial Tendon

The artificial tendons used in this study were based on the prostheses developed by Melvin, *et al.* [172, 173]. To manufacture the artificial tendons, we used customized USP size 0

polyester braid suture cut to 12" length and double-armed with swaged 3/8-circle taper point needles (0.028" wire diameter) (RK Manufacturing Corp, Danbury, CT, USA). These sutures were grouped into bundles of 2 strands for the TC tendon and 3 strands for the Achilles tendon. The suture bundles were folded in half and braided, creating a loop at the distal end and either 4 or 6 suture needles at the proximal end (Fig. 7.1). The artificial tendons were coated in biocompatible silicone (BIO LSR M140, Elkem Silicones, Lyon, FR) over the braided section to prevent adhesion to surrounding biological tissues. After fabricating the artificial tendons, we cleaned them in an ultrasonic bath to remove any foreign debris and particulates. Finally, the artificial tendons were sterilized using ethylene oxide gas.

Surgical Procedure

The rabbits were given a pre-emptive analgesic of hydromorphone (0.2 mg/kg) and induced into general anesthesia with midazolam (0.75-1mg/kg). The rabbit was intubated, and anesthesia was maintained with 3-5% isoflurane gas vaporized into 100% O₂. We removed the hair from the operated limb with electric clippers and depilatory cream (Nair Hair Remover Cream, Church & Dwight Co., Ewing Township, NJ). We positioned the rabbit into dorsal recumbency with the operated leg suspended, and aseptically prepared the limb with chlorohexidine, betadine, and 70% isopropyl alcohol. The rabbit was placed on a fluid drip with a constant rate infusion (CRI) of Lidocaine (2 mg/kg) diluted in 25 ml Ringer's Solution. During surgery, anesthesia was reinforced with intraoperative doses of a 10:1 saline-xylazine (3 mg/kg) dilution if the rabbits heart rate increased above 240 bpm.

To begin the procedure, the attending surgeon (Anderson) made a lateral longitudinal skin incision over the either the Achilles or Tibialis Cranialis insertion tendon, extending approximately from the point of the calcaneus or talus bone to the mid-belly of the gastrocnemius or tibialis cranialis muscle, respectively. The surgeons retracted the skin to expose the biological insertion tendon. The biological tendon was excised by cutting it at its insertion on the bone and at the

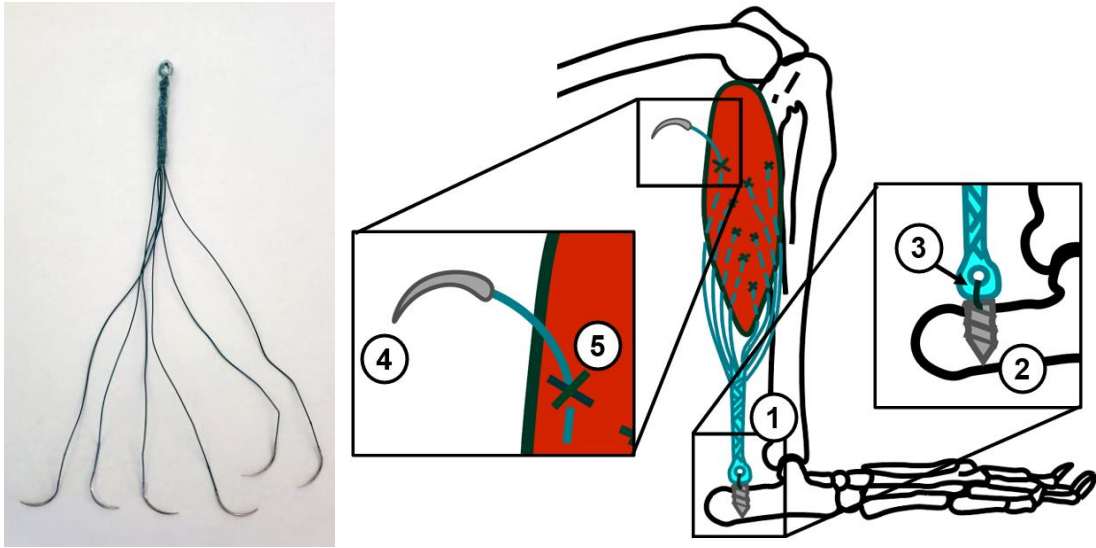


Figure 7.1. Artificial tendon used to recreate the connection between muscle and bone. (Left) The tendon is comprised of 4 Fiberwire suture looped together and braided into a 16 - 18 mm length unit with curved needles on each end for muscle attachment. The tendon is coated in silicon to prevent tissue adhesion. **(Right)** Illustration outlining the synthetic tendon implantation surgery in the gastrocnemius. (1) Synthetic tendon comprised of modified Fiberwire suture. (2) Arthrex tendon anchor. (3) Fiberwire suture connecting the synthetic tendon to the tendon anchor. (4) Suture needles attached to the end and woven through muscles. (5) Once woven through the muscle, the suture is tied off and cut at the suture extrusion site.

myotendinous junction. The suture needle ends of the artificial tendon prosthesis were inserted individually through the distal end of the muscle (Fig 7.1). The sutures were sewn through the muscle, exiting from the side of the muscle about 1 cm proximal to the suture insertion. The adjacent suture strings were tied together using square knots, and the surgeons cut and removed excess suture material.

To attach the artificial tendon to the bone, a hole was first pre-drilled into either the superior aspect of the calcaneus (A1&2) or the lateral aspect of the talus (T1&2). The surgeons screwed a tendon anchor into the drilled hole. The surgeons tied down the looped distal end of the artificial tendon to the implanted tendon anchor using FiberWire suture (Arthrex, Naples, FL, USA). The skin was closed with 4-0 synthetic absorbable monofilament suture in an interrupted cruciate pattern and reinforced with 3-0 synthetic absorbable monofilament skin suture in a simple interrupted pattern.

Post-Surgical Care

We applied silver sulfadiazine topical cream over the incision site, both immediately post-surgery and at every bandage change, to help prevent infection and promote healing. We bandaged the limb using, from deepest to most superficial, non-adherent dressing, undercast padding, elastic self-adherent bandage wrap, and elastic tape (ELASTIKON, Johnson & Johnson, New Brunswick, NJ, USA) to protect the incision site during recovery. Additionally, the bandage helped fix the hindlimb at a desired natural ankle flexion posture to prevent overloading the muscles and artificial tendons during the early integration period. We changed the bandage every three days to monitor the incision site and the overall hindlimb skin integrity. We administered an analgesic of hydromorphone (0.2 mg/kg) intramuscularly every six hours for at least 72 hours post-surgery. Additionally, we administered antibiotics (enrofloxacin; 0.05 mg/kg) orally every 12 hours and anti-inflammatory medication (meloxicam; 0.6 mg/kg) orally every 24 hours for 7 days post-surgery. To monitor *in-vivo* integrity of the artificial tendon prosthesis, we performed bi-

weekly radiography of the operated limb, starting on the day of surgery. When analyzing the radiographs, we looked at three locations to inspect for potential mechanical failure: 1) the suture connecting the artificial tendon and suture anchor, 2) the suture anchor relative to the bone, and 3) the muscle-tendon interface. The rabbits were given pen time as part of an informal rehabilitation program. The rabbits were housed with at least one companion rabbit in adjacent cages. Enrichment and positive human interaction were given to the rabbits daily.

Biomechanics Testing

For noninvasive rabbit gait testing, we used a method that we reported previously for healthy rabbits [275]. The motion capture setup used a pressure mat (Tekscan, Very HR Walkway 4; South Boston, MA) located inside an acrylic tunnel. The pressure mat was synchronized with 60 Hz webcam (1080P HD Webcam, SVPRO) through Tekscan Walkway software (Tekscan, South Boston, MA). The webcam was placed approximately 3 feet from the acrylic tunnel to record sagittal plane kinematics. Before testing, we shaved both hindlimbs of each rabbit and marked the approximate joint centers of the knee, ankle, and metatarsophalangeal (MTP) joint with black ink, based on bony landmarks.

For each trial, the rabbits were prodded to hop over the pressure mat through the acrylic tunnel. The width of our pressure mat (11.2cm) permitted only unilateral pressure recording. Therefore, each rabbit completed about 10 trials of hopping in each direction through the tunnel while we recorded biomechanics data for the leg facing the camera. Each trial began when the rabbit entered the tunnel, and a trial was deemed successful if the rabbit continued the hopping motion through the entire length of the tunnel without stopping. Each rabbit underwent 6 biomechanics testing sessions (S0-S5) over the course of the study. We conducted the first testing session during the week before surgery (S0). After surgery, we waited 2 weeks for the rabbits to recover before starting weekly post-surgical testing for five weeks (S1-S5).

Data Processing and Statistical Analysis

Additional details about the data processing were reported in [275]. All data analyses were performed only with data from the stance phase of hopping gait, when the hindlimb experiences the most biomechanical loading.

To extract pressure data from the Tekscan Walkway software, we first isolated the contact foot of the hindlimb of interest by drawing a strike box around the area of contact. We then extracted pressure, contact area, and vertical ground reaction force (vGRF) data for each contact foot. vGRF was expressed as a percentage of body weight (%BW). The hindlimb stance phase was defined as the time window over which the total pressure under the foot was greater than zero. We calculated the hindlimb kinematics from the frames of the synchronized video corresponding to stance phase. Frame-by-frame, a custom MATLAB (Mathworks, Natick, MA) program (1) identified the centroids of joint centers marked with black ink, (2) defined foot and shank limb segments as lines connecting adjacent joint centers, and (3) calculated the foot and ankle joint angles (Fig. 6.3).

We evaluated the extent of post-surgery recovery in the context of healthy rabbit gait. Specifically, we compared time-series biomechanical data (foot and ankle angle, vGRF, contact area, and pressure) throughout stance between the study rabbits ($n=2$ per experiment group) at the week-6 post-surgery timepoint (S5) and healthy “control” rabbits ($n=12$) reported in a previous study [275]. To permit comparison among trials of different stance durations, we normalized the timepoints of the stance phase data by the duration of stance phase. The normalized time-series data were averaged across rabbits in each group and compared between experiment and control groups using statistical parametric mapping (SPM), with $\alpha=0.05$ [175].

Analyzing joint angles individually masks changes that occur in the whole kinematic chain of the hindlimb. Therefore, we computed the positions of the ankle and knee joint centers throughout stance using the joint angles and a generic kinematic model of the rabbit hindlimb

[275]. The foot and shank segments of the kinematic model were 2 and 3 normalized length units (NLU), respectively, based on the approximate anatomical length proportions measured between the two segments. We qualitatively analyzed this normalized model between experimental (S5) and control groups to compare changes in holistic hindlimb kinematics.

We compared summary outcome measures across the 6 testing timepoints to characterize functional changes (1) between pre- and post-surgery and (2) across post-surgery timepoints. The summary outcome measures, computed from the time-series data for each trial, were: (1) range of motion (difference between maximum and minimum joint angle) for each joint, (2) the minimum and maximum joint angles, (3) the joint angles at foot strike and toe off, and (4) the average vGRF, contact area, and pressure across stance phase. For each testing timepoint, the outcome measures were averaged across trials for each rabbit, then averaged across rabbits within each experiment group. Due to our small sample size, we analyzed summary outcome measures and data trends to compare within experimental groups over different timepoints, rather than performing an ANOVA for comparison.

RESULTS

Time-Series Biomechanical Comparison to Healthy Control Group

Tibialis Cranialis (TC) Group

At S5, rabbits that underwent TC replacement had significantly similar foot angles to the healthy controls after the first 35% of stance and similar ankle angles throughout the entirety of stance. Fig. 7.2). The minimum ankle angle, which corresponds to the end of loading response and beginning of propulsion, occurred at 40% of stance phase for both TC and control groups. Additionally, the pressure was significantly different between TC and control groups during 18-89% of stance phase. Both vGRF and contact area were not significantly different between TC and control groups throughout most of stance (Fig. 7.3).

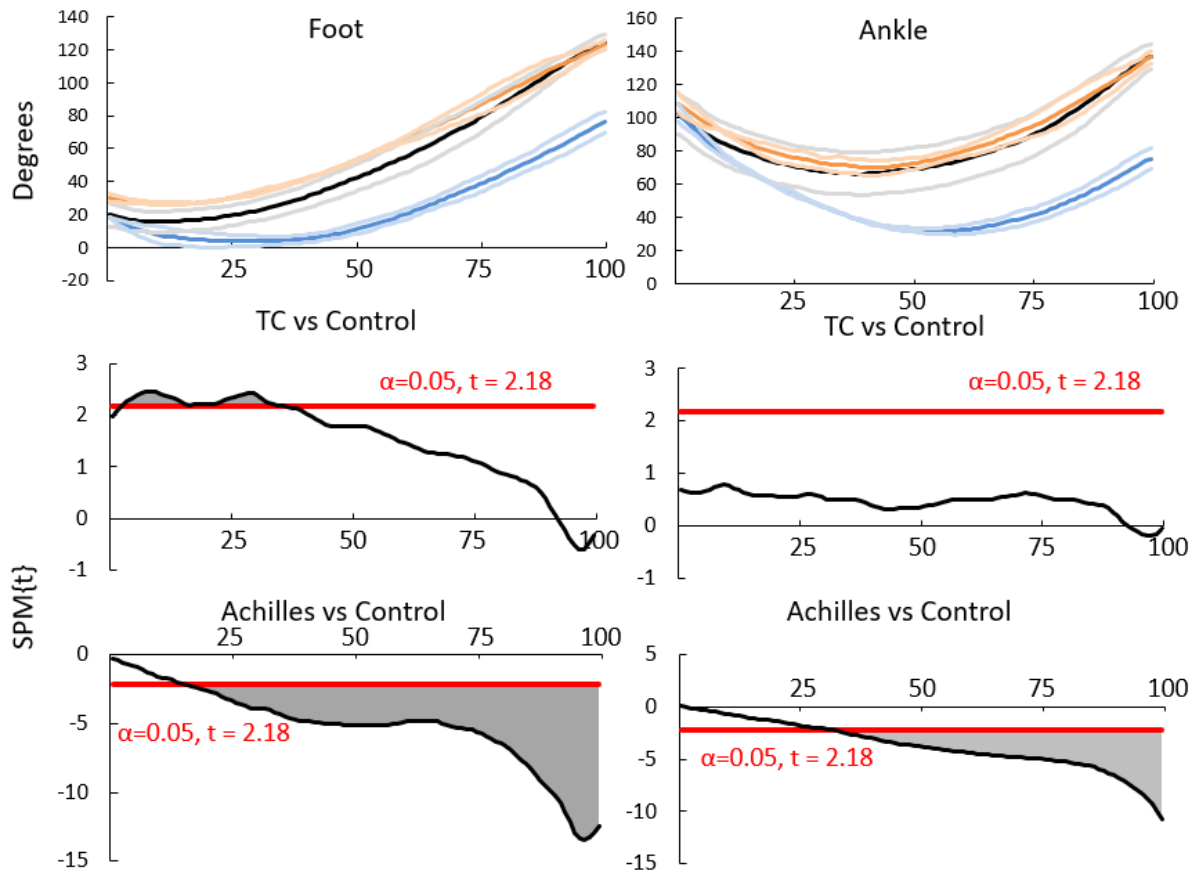


Figure 7.2. SPM comparison of pressure mat data throughout stance phase between surgical groups and healthy control at S5. (Left) TC rabbits showed statistically similar foot angles to a healthy control group during the last 70% of stance. Achilles rabbits showed significantly lower foot angles than controls during the final 80% of stance phase. **(Right)** TC rabbits showed statistically similar ankle angles to controls throughout the entirety of stance. Achilles rabbits showed significantly lower ankle angles than controls during the final 75% of stance phase.

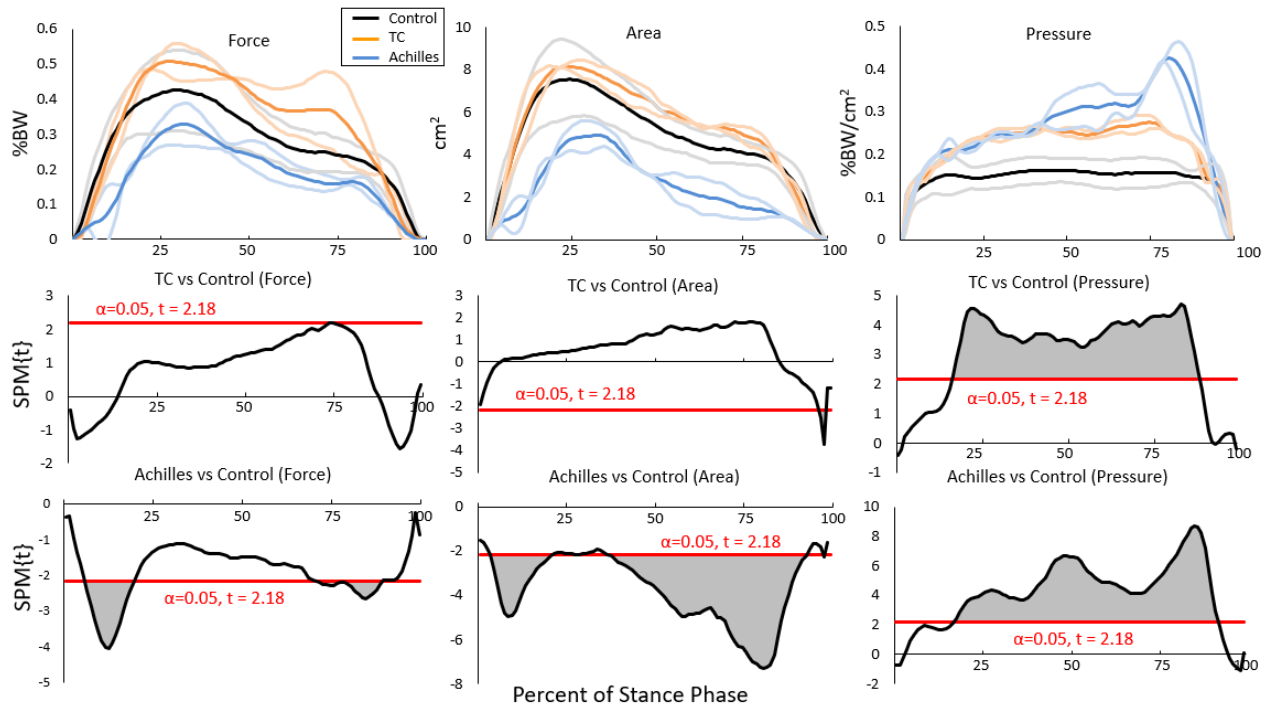


Figure 7.3. SPM comparison of pressure mat data throughout stance phase between surgical groups and healthy control at S5. (Left) TC rabbits showed statistically similar vGRF to a healthy control group throughout the entirety of stance. Achilles rabbits showed significantly lower vGRF than controls during 10-20% and 70-85% of stance. **(Middle)** TC rabbits showed statistically similar contact area to controls throughout the entirety of stance. Achilles rabbits showed statistically lower contact area throughout most of stance phase. **(Right)** Both TC and Achilles rabbits showed statistically higher foot-ground pressure than controls between 20-90% of stance.

During stance phase, rabbits with TC replacement and the control group had similar normalized kinematics at S5 (Fig. 7.4). At foot strike, the foot angle was higher in the TC group than in the control group, resulting in a knee joint center position difference of 0.4 NLUs between TC and control groups. As the rabbits progressed through stance phase, the hindlimb kinematics became more similar to the control group, resulting in a distance of 0.05 NLUs between TC and control knee position at toe off. Both groups displayed similar knee trajectories of forward and downward movement, with the TC rabbits knee position moving 5.13 NLUs forward and 1.55 NLUs downward, while the control group moved 5.46 NLUs forward and 1.25 NLUs downward during stance phase.

Achilles Group

At S5, rabbits with Achilles replacement had significantly different foot and ankle angles starting at 15% and 31% of stance phase, respectively, compared to the control group (Fig 7.2). The minimum ankle angle was 34.4° lower and occurred later in stance (57%), in the Achilles group than in the control group. The Achilles group showed significantly different (qualitatively lower) vGRF during 7-20% and 72-89% of stance (Fig. 7.3) and significantly different (qualitatively lower) contact area during 6-22% and 39-94% of stance. However, the lower contact area resulted in significantly higher pressure during 19-92% of stance phase, specifically during forward propulsion when the pressure was 3 times higher than in the control group.

Rabbits with Achilles replacement showed qualitatively different kinematics compared to healthy controls (Fig. 7.4). Though kinematics at foot strike were similar between Achilles and control groups, the Achilles group was more flat-footed during loading response, resulting in different knee trajectories throughout stance. Specifically, the vertical knee position of the Achilles group decreased by 2.23 NLUs before increasing by 0.56 NLUs (1.67 NLUs downward from start to end), and only moved 4.11 NLUs forward, compared to the control group that continuously moved in the same direction with a distance of 5.46 NLUs forward and 1.25 NLUs downward.

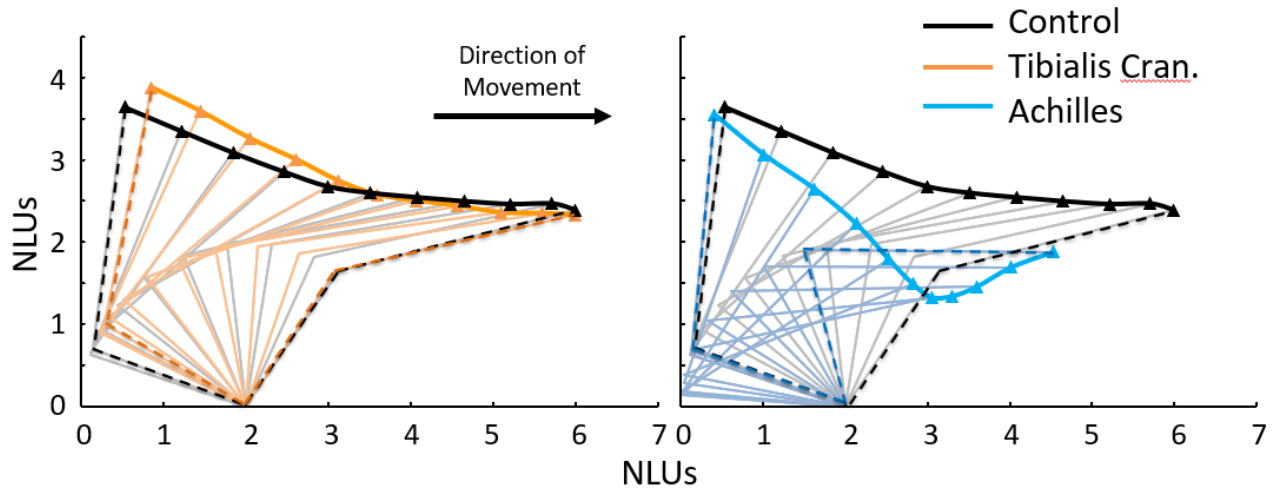


Figure 7.4. Comparison of normalized hindlimb kinematics between surgical and control groups at S5. (Left) Comparison of TC rabbits to a group of healthy control rabbits. The only qualitative difference between the kinematics of TC and control rabbits is a higher starting foot angle in the surgical group. (Right) Comparison of Achilles rabbits to a group of healthy control rabbits. Achilles rabbits start stance phase with similar kinematics to control rabbits. However, both the foot and ankle angles of the Achilles rabbits are significantly smaller than the control rabbits by toe off. Additionally, when mapping the knee trajectory, Achilles rabbits have a “dip” in movement not seen in the other two groups.

Post-surgical Functional Recovery based on Summary Outcome Measures

TC Group

Rabbits with TC replacement had similar foot and ankle range of motion (ROM) across all timepoints (Fig. 7.5). The foot angle at foot strike increased from 11.5 at S0 to 28.8 degrees at S1 and maintained at least this level of extension at foot strike throughout the remainder of testing (Fig. 7.6). However, the ankle angle at foot strike and the foot and ankle angles at toe off were similar across all post-surgery timepoints (S1-S5) to pre-surgery measurements (S0). The vGRF and contact area, averaged across stance, decreased at S1 by 6 %BW and 1.22 cm², respectively, but returned to pre-surgical levels by S3 (Fig. 7.7). Additionally, the average pressure showed similar values at every timepoint.

Achilles Group

At S1, rabbits with Achilles replacement had lower foot and ankle angle ROM by 51.3 and 39.2 degrees, respectively, compared to S0 (Fig. 7.5). The foot ROM never noticeably increased throughout post-surgical testing. However, ankle ROM increase back to pre-surgical levels by S5. The increase in ankle ROM between S1 and S5 was primarily due to an increase in the maximum ankle angle (S1: 73.5 degrees; S5: 102.9 degrees), rather than a decrease in the minimum ankle angle (S1: 36.4 degrees; S5: 31.3degrees). At foot strike, both the foot and ankle angles were similar across timepoints (Fig. 7.6). However, the foot and ankle angles at toe off decreased by 58.3 and 69.6 degrees, respectively, after surgery and never returned to pre-surgical levels. The average vGRF and contact area throughout stance decreased by 14.5 %BW and 3.13 cm², respectfully, initially post-surgery (Fig. 7.7). Despite never returning to pre-surgical levels, both average vGRF and contact area increased by 6.6 %BW and 0.96 cm², respectively, toward pre-surgical values by S5. The average pressure throughout stance increased from S0 to S1, but at S3 began decreasing back towards pre-surgical levels.

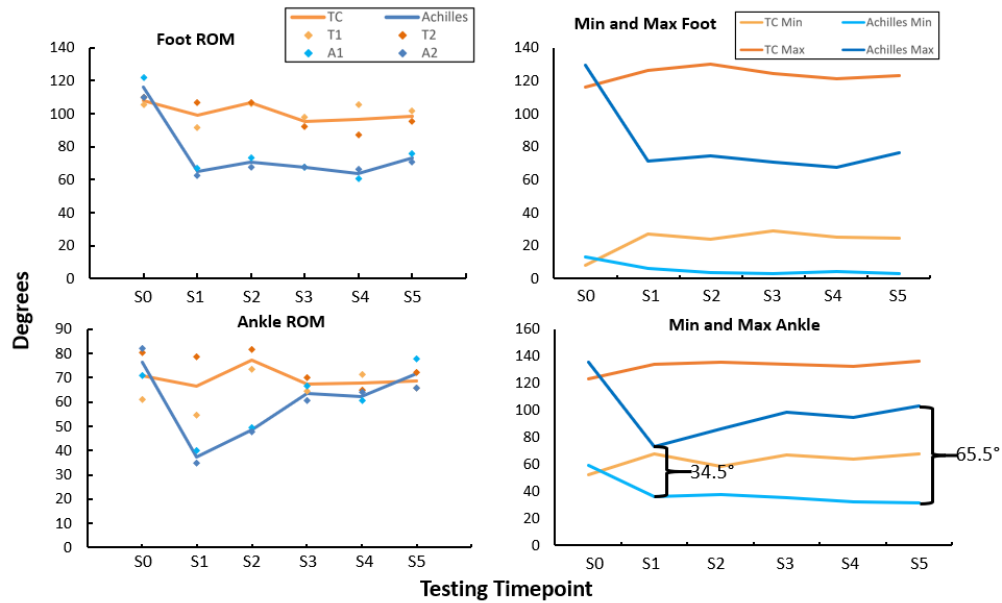


Figure 7.5. ROM measured across all testing timepoints. Orange line represents the average between T1 and T2. Blue line represents the average between A1 and A2. **(Left)** TC rabbits showed similar ROM to pre-surgical testing across all testing timepoints. Achilles rabbits showed decrease in the ROM of the foot angle following surgery that never recovered. However, despite an initial decrease in ankle ROM following surgery, Achilles rabbits returned to pre-surgical ROM by S5. **(Bottom Right)** Increases in ankle ROM in achilles rabbits is attributed to an increase in the maximum ankle angle rather than a decrease in the minimum ankle angle.

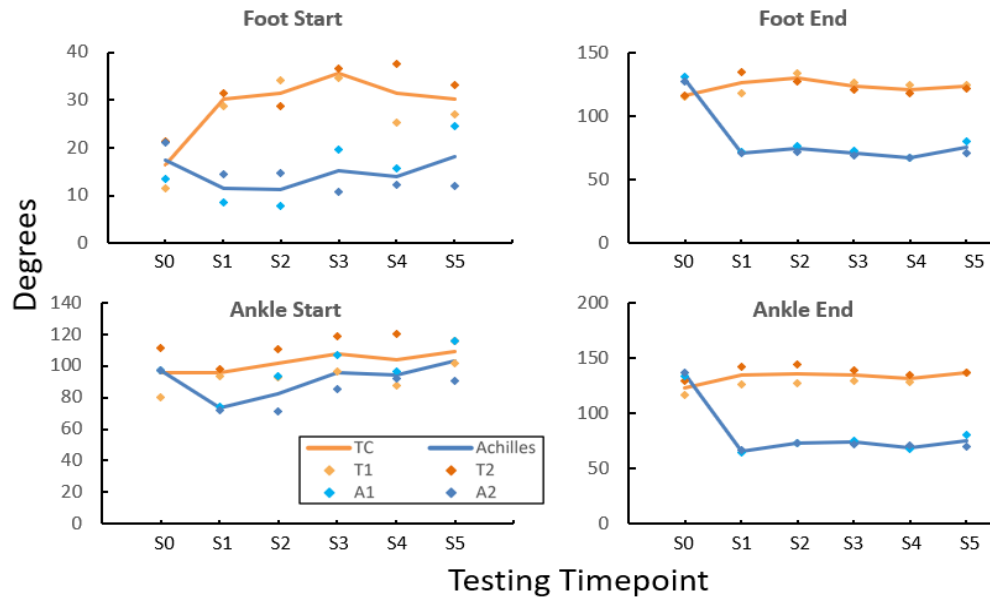


Figure 7.6. Start and end angles measured across all testing timepoints. Orange line represents the average between T1 and T2. Blue line represents the average between A1 and A2. **(Left)** TC rabbits showed similar ankle starting angles throughout all testing timepoints but showed a significantly higher foot starting angle following surgery that never recovered. Achilles rabbits showed a slight decrease in starting angles for both the foot and ankle throughout all testing timepoints but returned to pre-surgical levels by S3. **(Right)** TC rabbits showed similar endpoint joint angles to pre-surgical testing across all testing timepoints. Achilles rabbits showed a decrease in the end starting angle after surgery that never significantly increased throughout post-surgical testing.

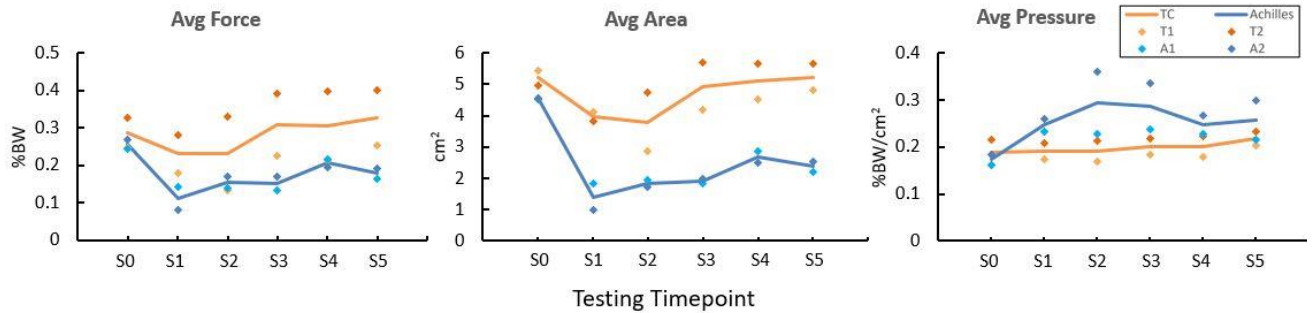


Figure 7.7. Pressure mat data measured across all testing timepoints. Orange line represents the average between T1 and T2. Blue line represents the average between A1 and A2. **(Left)** TC rabbits showed a decrease in average vGRF immediately after surgery but recover to presurgical levels by S3. Achilles rabbits had lower average vGRF after surgery but showed recovery despite never returning to pre surgical levels. **(Middle)** TC rabbits showed a decrease in average contact area immediately after surgery but recover to presurgical levels by S3. Achilles rabbits had lower average contact area after surgery but showed recovery despite never returning to pre surgical levels. **(Right)** TC rabbits showed similar average pressure across all testing timepoints. Achilles rabbits showed an increase in pressure in the first two week followed by a decrease back towards pre surgical levels starting in S3.

DISCUSSION

In this study we showed that, in support of our hypothesis, rabbits were able to recover to pre-surgical levels of function with TC replacement and partial levels of function with Achilles replacement. There was a smaller functional decline within the TC group from S0 to S1, so there was a smaller “distance” to full recovery compared to the Achilles group. The Achilles group experienced a greater functional decline likely due to higher biomechanical demand on the triceps surae (Achilles) muscles than the TC muscle during locomotion.

For most summary outcome measures, rabbits with TC replacement returned to pre-surgical values by S5. The only difference in hindlimb kinematics following TC replacement was for higher foot angle during the first 35% of stance phase. The difference was similar to the “drop foot” condition in humans caused by strain or tear of the Tibialis Anterior tendon [28, 276]. The similarity suggests that there is laxity in the tendon unit, potentially caused by the *in-situ* length of the implanted artificial tendon. This laxity causes an inability for the artificial tendon to maintain proper tension, resulting in a slight failure to maintain dorsiflexion at the end of swing phase. Having a wider array of tendon sizes available during surgery might allow for a tighter implantation and minimize this drop foot affect.

Similar to TC rabbits, the functional deficit in kinematics is possibly from improper *in situ* length and stiffness of the tendon unit. Proper tensile force in the tendon is essential for proper locomotion [277, 278]. Therefore, if the artificial tendon is too long *in situ* compared to the biological tendon there could be laxity resulting in inefficient force transmission. With this laxity, the rabbit could have difficulty efficiently performing plantar flexion movements. The Achilles rabbits showed statistically similar kinematics to the control group at foot strike, but as stance phase progress, the increasing deviated from control kinematics. The pressure mat data for Achilles rabbits showed significantly lower force and area throughout stance. The SPM of both vGRF and contact area showed a bimodal pattern, consistent with the two phases of stance, with

the greatest SPM T-value magnitude occurring at peak levels of both loading response and forward propulsion. This is to be expected that the differences in the pressure data would be greatest when the hindlimb is at the most extreme periods of stance when the tendon is put under the most extreme period of loading during stance.

The decrease in contact area for Achilles rabbits is mostly attributed to flexion in the MTP joint throughout stance. The Achilles rabbits had a qualitatively unnatural level of flexion in the toes that maintained throughout stance. This led to the rabbits midfoot never contacting the ground (Fig. 9). Upon *ex vivo* dissection of A2 we noticed collagenous tissue fusing the artificial tendon to the flexor digitorum insertion tendon before it crossed over the ankle (Fig. 10). Pulling either the triceps surae (Achilles) muscle group or flexor digitorum muscle group individually caused plantar flexion. This showed that this tissue connection likely influenced the deficits in locomotor function. However, for a muscle driven endoprosthesis with a single joint, both the flexor digitorum and Achilles muscle could be joined to both contribute to plantar flexion.

Severe traumatic injury, such as amputation, may result in partial or complete loss of the tendon. It has been shown that not only can muscle in the residual limb still activate in coordinated patterns to replicate movement [119] without the tendon connecting it to bone, but also that surgically reengaging a residual muscles ability change length, in coordination with other muscles, can restore a sense of proprioception in the residual limb of an amputee [131, 147, 182]. Therefore, reconnecting the muscle and bone through artificial tendon linkages has the potential to restore sensorimotor function through biomimetic joint reconstruction. An endoprosthesis underneath the skin allows for direct artificial tendon connection between the residual muscle and the implanted device. The results from this study show that the artificial tendon has the potential to produce functional movement when attached to an endoprosthesis.

This study had several limitations. First, during surgery, we did not have a way to ensure that the muscle-tendon unit was in proper levels of tension. This could have caused the laxity that

we suspect contributed to the functional limitations of the intervention. In surgery, we have multiple tendon sizes for the surgeon to pick from to attempt to replicate biomimetic levels of tension in the tendon. Having additional tendon sizes available for the surgeon during surgery could allow the surgeon to more accurately implant the device under more appropriate tensile loads. Second, our sample size was small, with only 2 rabbits per experimental group. This limited our statistical power. However, both rabbits in each group showed similar trends that supported our hypothesis. Repeat testing on more rabbits would increase the statistical power and could help verify the results seen in this study. Third, during post-surgical recovery, the rabbits did not complete a formal physical therapy program. We gave enrichment and pen time as a form of informal, unstructured physical therapy. However, implementing a targeted physical therapy program to focus on lessening joint stiffness and encouraging mobility could allow for a greater or quicker recovery. Fourth, we had a relatively short post-surgical testing period. This proved sufficient for TC rabbit recovery. However, Achilles rabbits could have recovered more with more time. Fifth, our testing setup limited our ability to measure hindlimb biomechanics. Our testing setup only allowed for measurement of stance phase. During healthy gait, rabbits dorsiflex the ankle during swing phase, which should put the TC tendon under a greater loading demand than during stance phase. Therefore, it is possible that the TC group would show functional changes during swing phase that we were unable to measure with our testing set up. Additionally, the width of our pressure mat only allows for unilateral measurement of locomotion, limiting our ability to compare changes within each rabbit to their healthy contralateral hindlimb.

We based our artificial tendon design on one reported by Melvin, *et al.* [172]; In their *in vivo* goat study, they performed histology analysis and tensile testing of the muscle-artificial tendon unit. In a future study we plan to perform histology analysis on the muscle-tissue interface and compare our findings with those previously reported by Melvin, *et al.* This will allow us to measure how well the artificial tendons used in this study integrated into the muscle.

Many potential clinical applications for tendon replacement, specifically amputation, would require implantation of multiple tendons for musculoskeletal reconstruction of the damaged joint due to the large loss of tissue under traumatic circumstances. In future studies we plan to replace both the Achilles and TC insertion tendons simultaneously in a rabbit's hindlimb to analyze the locomotor function of the ankle joint primarily actuated through artificial tendons in two different directions. Additionally, future clinical applications of artificial tendons for joint reconstruction would likely be performed in muscle that is previously damaged or negatively affected. In order to analyze the efficacy of the locomotor restorative capabilities artificial tendons in impaired muscle, we plan to implant artificial tendons in rabbits who have undergone tenotomy of the biological tendon 1 month prior to implantation. This will allow the muscle to atrophy prior to implantation, so that we can analyze the effect of function restoration on a limb with impaired muscle.

In conclusion, we showed that artificial tendon replacement can at least partly maintain locomotor function in the rabbit hindlimb. Rabbits recovered towards pre-surgical levels of function, with the TC rabbits having similar biomechanics to a control group throughout most of the stance phase after 6-weeks post-surgery. These results show the promise of restoring musculoskeletal function with artificial tendons.

CHAPTER 8. CONCLUSION

CONTRIBUTIONS

The main contributions of this dissertation are:

- A biomechanical analysis of the shoulder neuromuscular response to a continuous overhead passive force that assists in shoulder elevation, which simulates the conditions of a passive exoskeleton.
- A feasibility study of a novel endoprosthesis concept in a rabbit model of hindlimb amputation. We tested the feasibility of implanting a limb prosthesis completely underneath the skin at the distal end of a limb.
- A quantitative analysis of the skin overlaying a stem endoprosthesis in rabbits to better understand the skin-device interaction.
- A report of hindlimb biomechanics in healthy rabbits based on noninvasive motion capture techniques. The biomechanics data, which included sagittal plane kinematics, vertical ground reaction forces, contact area, and pressure, can be used as control or reference data to compare with rabbits undergoing some study intervention.
- A biomechanical analysis of the effect of artificial tendon replacement across the rabbit ankle on hindlimb biomechanics. We reported differences in kinematics, vertical ground reaction forces, contact area, and pressure between rabbits with artificial tendon replacement and healthy rabbits.

APPLICATIONS

The following are a few possible applications of the work proposed in this dissertation:

The work presented in chapter 3 looking at the effect of passive overhead force sheds light on the application of passive exoskeletons. Passive shoulder exoskeletons have the potential to be used in both clinical and industrial applications. In a clinical setting, passive exoskeletons can assist patients recovering from shoulder impairment with rehabilitation. When

used according to physician guidelines they have the potential to offset the activation requirements of the damaged muscle while maintaining the user's ability to perform ADLs. In an industrial setting, passive shoulder exoskeletons can act as preventative devices to minimize the risk of shoulder injury. Overhead cyclic shoulder movement that is common in the factory settings often leads to shoulder impairment. The use of passive exoskeletons can offset the muscle requirements for this type of overhead loading and help prevent injury.

Our analysis of a fully implanted endoprosthesis underneath the skin opens the door for future MDE technologies. As discussed throughout this dissertation, MDE technologies have the potential to provide greater levels of sensorimotor function over external prostheses. Showing that it is feasible to implant an orthopedic device at the distal end of a residual limb allows future research into expanding the limb for full limb reconstruction applications. In addition to total limb reconstruction, MDE allows for reconstruction of major musculoskeletal defects. For example, a treatment for osteosarcoma called rotationplasty requires removal of the femur. Currently, there is no way to replace the bone and muscle connections for as large of a defect. However, an MDE would be able to not only replace the malignant bone but reattach the muscles back to the implant.

The rabbit biomechanics analysis presented in this dissertation can be applied to the rabbit model across a wide variety of orthopedic research. The rabbit model is a commonly used model for orthopedic research. However, it is rarely used to test interventions that may affect locomotion, such as stints, nerve technologies, and orthopedic devices. Part of this may be due to the limited information of rabbit kinematics. The rabbit data presented in chapter 6 provide a set of reference data for rabbit hindlimb biomechanics that can be used in future studies as a healthy control. This will further the use of the rabbit model in applications that affect locomotor function.

The artificial tendon analyzed in chapter 7 has potential applications in both limb reconstruction and major tendon repair. The artificial tendon test in chapter 7 showed potential to restore locomotor function. If the efficacy of this tendon device can be further tested and proved, then it has the potential to be used in a wide variety of surgical applications. As outlined in chapter 7, there are several conditions that cause irreparable impairment to biological tendon. Similar to how artificial heart valves circumvent the need to find a replacement valve or use a pig valve, an artificial tendon could prevent the need to graft tendon from a different part of the body. This could allow for repair of the damaged tendon without the need to compromise a healthy tendon.

FUTURE WORK

There are many possible future directions for the work presented in this dissertation, some of which are presented below. These and other research endeavors would begin the translation of our conceptual assistive devices towards clinical application and utility.

Exoskeleton Testing

The work presented in chapter 3 has helped inform the design of a passive exoskeleton that uses a cam wheel to gear passive force to overcome the shoulder gravitational moment. However, this shoulder exoskeleton has not been tested to see if it assists in shoulder elevation. Future studies should use the testing paradigm outlined in chapter 3 to assess the potential for the exoskeleton to decrease muscular activation in muscles that cross the shoulder. Additionally, more moves can be tested that more appropriately mirror ADLs.

Expanded Endoprosthesis Devices

In chapters 4 and 5 I analyzed a simple stem endoprosthesis. The positive results presented in this dissertation inform future testing of larger, more complex endoprosthetic devices. Future surgeries should analyze the extent to which healthy distal skin can be preserved and be healthy enough for the incision closure to fully heal around an implanted device. Analyzing the vasculature and temperature of the skin during surgery would allow prediction of the risk of

skin ischemia during the recovery process. Once it is determined how much skin can safely be used to enclose an endoprosthesis, future studies should perform the same feasibility approach outlined in chapter 4 to test larger endoprostheses with a rigid ankle and foot segment.

Additionally, for the stem endoprosthesis tested in chapter 4, the tendon was tied down to a rigid loop. However, in a functional endoprosthesis, the muscle tendon unit would be attached across a mobile ankle joint to allow for plantar and dorsiflexion. Before an MDE is tested with artificial tendon attached across a mobile ankle joint, studies should analyze the locomotor function of an MDE device that has healthy tendon attached across the ankle. This would allow for a negative control comparison for the final MDE prototype that uses artificial tendon. Using a mobile MDE with healthy tendon would allow for troubleshooting in the design of the mobile device. Implanted the MDE device with the artificial tendon would mask whether impairments in locomotion were caused the design of the MDE device or an interaction between the muscle, artificial tendon, and MDE connections.

The studies performed in this dissertation toward the advancement of the MDE application focused on implanting devices in and within healthy tissue. However, amputees, who would be the eventual recipients of clinical MDEs, have damaged or disused tissue. Therefore, future studies need to analyze the practical application of how these devices would work in previously amputated limbs. Below are two examples of future work toward this direction of research.

Strengthening Residual Muscles after Atrophy

During amputation surgery, muscles are spared in the residual limb, but are either left to retract or are grounded through anchors or a bone bridge [87-90]. These muscles, despite their ability to still be activated, produce less mechanical output due to their inability to change length or tensile force. This can lead to noticeable muscle atrophy in the residual limb. These muscular conditions in the residual limb can be considered a variation of disuse because the amputated muscle is no longer experiencing the same tension and excursion (i.e., length changes) as an

intact muscle. When disused, not only does the maximum force generation produced through muscular contraction decrease, but the muscle also shortens and can no longer extend to the same length.

A conceptual prototype for an MDE assumes that the residual muscle will have the ability to produce healthy levels of force and excursion. However, residual muscle has never previously been tested to see its ability to hypertrophy and return to healthy levels of function. Future work with MDEs should focus on the ability of residual muscles to rehabilitate following atrophy and shortening. Further research could inform interventions needed to stretch and strengthen the residual muscle prior to implantation of an MDE, similar to show skin expanders stretch and strengthen healthy skin before implantation of various devices.

Skin Expansion and Grafting Techniques

In the research presented in chapters 4 and 5 we showed the feasibility of implanting a device underneath skin. However, amputation and implantation occurred during the same surgery and the surgeon closed the incision with the rabbits' native healthy skin. This allowed the surgeon to create a pocket within the skin in which the endoprosthesis would fit. In a clinical setting, the amputation procedure would occur before the implantation of an MDE. The remaining skin in a residual limb would not allow the surgeon to create a large enough pocket within the skin to fully cover an implanted device. Prior to clinical application, future work needs to investigate strategies in skin expansion and skin grafting to create a larger area underneath the skin to allow for implantation of a larger MDE device. Skin expanders have previously shown the ability to not just expand the skin, but also strengthen the vascular network in the expanded area. This technique could not only allow for a larger residual skin pocket, but also strengthen the skin and promote a healthier recovery following implantation.

REFERENCES

- [1] CDC. "Disability Impacts All of Us." <https://www.cdc.gov/ncbddd/disabilityandhealth/infographic-disability-impacts-all.html#:~:text=61%20million%20adults%20in%20the,is%20highest%20in%20the%20South.> (accessed).
- [2] R. A. MCCABE, S. J. NICHOLAS, K. D. MONTGOMERY, J. J. FINNERAN, and M. P. MCHUGH, "The effect of rotator cuff tear size on shoulder strength and range of motion," *The Journal of orthopaedic and sports physical therapy*, vol. 35, no. 3, pp. 130-135, 2005.
- [3] A. Ferretti, E. Monaco, and A. Vadala, "Rotatory instability of the knee after ACL tear and reconstruction," *Journal of Orthopaedics and Traumatology*, vol. 15, no. 2, pp. 75-79, 2014.
- [4] T. J. Noonan and W. E. Garrett Jr, "Muscle strain injury: diagnosis and treatment," *JAAOS-Journal of the American Academy of Orthopaedic Surgeons*, vol. 7, no. 4, pp. 262-269, 1999.
- [5] F. G. Miskelly, "Assistive technology in elderly care," *Age and ageing*, vol. 30, no. 6, pp. 455-458, 2001.
- [6] A. Sunderland, D. Tinson, L. Bradley, and R. L. Hewer, "Arm function after stroke. An evaluation of grip strength as a measure of recovery and a prognostic indicator," *Journal of Neurology, Neurosurgery & Psychiatry*, 10.1136/jnnp.52.11.1267 vol. 52, no. 11, p. 1267, 1989. [Online]. Available: <http://jnnp.bmj.com/content/52/11/1267.abstract>.
- [7] S. E. Folstein, B. Jensen, R. J. Leigh, and M. F. Folstein, "The measurement of abnormal movement: methods developed for Huntington's disease," *Neurobehavioral Toxicology & Teratology*, 1983.
- [8] A. Van Gemmert, H.-L. Teulings, J. L. Contreras-Vidal, and G. Stelmach, "Parkinsons disease and the control of size and speed in handwriting," *Neuropsychologia*, vol. 37, no. 6, pp. 685-694, 1999.
- [9] D. D. Dunlop, S. L. Hughes, and L. M. Manheim, "Disability in activities of daily living: patterns of change and a hierarchy of disability," *American journal of public health*, vol. 87, no. 3, pp. 378-383, 1997.
- [10] J. C. Millán-Calenti *et al.*, "Prevalence of functional disability in activities of daily living (ADL), instrumental activities of daily living (IADL) and associated factors, as predictors of morbidity and mortality," *Archives of gerontology and geriatrics*, vol. 50, no. 3, pp. 306-310, 2010.
- [11] M. E. Vidt *et al.*, "The effects of a rotator cuff tear on activities of daily living in older adults: a kinematic analysis," *Journal of biomechanics*, vol. 49, no. 4, pp. 611-617, 2016.
- [12] R. Gopura, D. Bandara, K. Kiguchi, and G. K. Mann, "Developments in hardware systems of active upper-limb exoskeleton robots: A review," *Robotics and Autonomous Systems*, vol. 75, pp. 203-220, 2016.
- [13] J. E. Pratt, B. T. Krupp, C. J. Morse, and S. H. Collins, "The RoboKnee: an exoskeleton for enhancing strength and endurance during walking," in *Robotics and Automation, 2004. Proceedings. ICRA'04. 2004 IEEE International Conference on*, 2004, vol. 3: IEEE, pp. 2430-2435.
- [14] T. Rahman, W. Sample, S. Jayakumar, and M. M. King, "Passive exoskeletons for assisting limb movement," *Journal of rehabilitation research and development*, vol. 43, no. 5, p. 583, 2006.
- [15] S. M. Cain, K. E. Gordon, and D. P. Ferris, "Locomotor adaptation to a powered ankle-foot orthosis depends on control method," *Journal of NeuroEngineering and Rehabilitation*, vol. 4, no. 1, p. 48, 2007/12/21 2007, doi: 10.1186/1743-0003-4-48.
- [16] H. Herr, G. P. Whiteley, and D. S. Childress, "Cyborg Technology - Biomimetic Prosthetic and Orthotic Technology," in *Biologically Inspired Intelligent Robots*, Y. Bar-Cohen and C. L. Breazeal Eds. Bellingham, WA, USA: SPIE Press, 2003, pp. 104-144.

- [17] L. Resnik, S. L. Klinger, and K. Etter, "The DEKA Arm: Its features, functionality, and evolution during the Veterans Affairs Study to optimize the DEKA Arm," *Prosthetics and orthotics international*, vol. 38, no. 6, pp. 492-504, 2014.
- [18] J. T. McConville, C. E. Clauser, T. D. Churchill, J. Cuzzi, and I. Kaleps, "Anthropometric relationships of body and body segment moments of inertia," ANTHROPOLOGY RESEARCH PROJECT INC YELLOW SPRINGS OH, 1980.
- [19] N. C. Heglund, "A simple design for a force-plate to measure ground reaction forces," *Journal of Experimental Biology*, vol. 93, no. 1, pp. 333-338, 1981.
- [20] A. Karlsson and G. Frykberg, "Correlations between force plate measures for assessment of balance," *Clinical Biomechanics*, vol. 15, no. 5, pp. 365-369, 2000.
- [21] Z. Su *et al.*, "Force estimation and slip detection/classification for grip control using a biomimetic tactile sensor," in *2015 IEEE-RAS 15th International Conference on Humanoid Robots (Humanoids)*, 2015: IEEE, pp. 297-303.
- [22] R. L. Lieber and J. Fridén, "Clinical significance of skeletal muscle architecture," *Clinical orthopaedics and related research*, vol. 383, pp. 140-151, 2001.
- [23] A. Cappozzo, "Gait analysis methodology," *Human movement science*, vol. 3, no. 1-2, pp. 27-50, 1984.
- [24] S. Ounpuu, "The biomechanics of walking and running," *Clinics in sports medicine*, vol. 13, no. 4, pp. 843-863, 1994.
- [25] C. Yam, M. S. Nixon, and J. N. Carter, "Gait recognition by walking and running: a model-based approach," 2002.
- [26] S. J. Abbass and G. Abdulrahman, "Kinematic analysis of human gait cycle," *Al-Nahrain Journal for Engineering Sciences*, vol. 16, no. 2, pp. 208-222, 2013.
- [27] A. Kharb, V. Saini, Y. Jain, and S. Dhiman, "A review of gait cycle and its parameters," *IJCEM International Journal of Computational Engineering & Management*, vol. 13, pp. 78-83, 2011.
- [28] J. Perry and J. R. Davids, "Gait analysis: normal and pathological function," *Journal of Pediatric Orthopaedics*, vol. 12, no. 6, p. 815, 1992.
- [29] S. Winiarski and A. Rutkowska-Kucharska, "Estimated ground reaction force in normal and pathological gait," *Acta of Bioengineering & Biomechanics*, vol. 11, no. 1, 2009.
- [30] M. Karadsheh. "Gait Cycle." <https://www.orthobullets.com/foot-and-ankle/7001/gait-cycle>
- [31] R. Grasso, L. Bianchi, and F. Lacquaniti, "Motor patterns for human gait: backward versus forward locomotion," *Journal of neurophysiology*, vol. 80, no. 4, pp. 1868-1885, 1998.
- [32] M. D. K. Breteler, C. W. Spoor, and F. C. Van der Helm, "Measuring muscle and joint geometry parameters of a shoulder for modeling purposes," *Journal of biomechanics*, vol. 32, no. 11, pp. 1191-1197, 1999.
- [33] B. Sanchez. "What a Pain in the Shoulder!" <https://www.bodyinmotionrehab.com/blogs/december-08th-2016>
- [34] L. U. Bigliani, R. Kelkar, E. L. Flatow, R. G. Pollock, and V. C. Mow, "Glenohumeral Stability: Biomechanical Properties of Passive and Active Stabilizers," *Clinical Orthopaedics and Related Research (1976-2007)*, vol. 330, pp. 13-30, 1996.
- [35] J. B. Wickham and J. Brown, "The function of neuromuscular compartments in human shoulder muscles," *Journal of neurophysiology*, vol. 107, no. 1, pp. 336-345, 2012.
- [36] G. R. Tobin, "Pectoralis major segmental anatomy and segmentally split pectoralis major flaps," *Plastic and reconstructive surgery*, vol. 75, no. 6, pp. 814-824, 1985.
- [37] J. D. Borstad and P. M. Ludewig, "Comparison of scapular kinematics between elevation and lowering of the arm in the scapular plane," *Clinical Biomechanics*, vol. 17, no. 9-10, pp. 650-659, 2002.

- [38] S. Dayanidhi, M. Orlin, S. Kozin, S. Duff, and A. Karduna, "Scapular kinematics during humeral elevation in adults and children," *Clinical Biomechanics*, vol. 20, no. 6, pp. 600-606, 2005.
- [39] A. R. Karduna, P. W. McClure, and L. A. Michener, "Scapular kinematics: effects of altering the Euler angle sequence of rotations," *Journal of Biomechanics*, vol. 33, no. 9, pp. 1063-1068, 2000/09/01/ 2000, doi: [https://doi.org/10.1016/S0021-9290\(00\)00078-6](https://doi.org/10.1016/S0021-9290(00)00078-6).
- [40] A. R. Karduna, P. W. McClure, L. A. Michener, and B. Sennett, "Dynamic measurements of three-dimensional scapular kinematics: a validation study," *J. Biomech. Eng.*, vol. 123, no. 2, pp. 184-190, 2001.
- [41] P. M. Ludewig and T. M. Cook, "Alterations in Shoulder Kinematics and Associated Muscle Activity in People With Symptoms of Shoulder Impingement," *Physical Therapy*, vol. 80, no. 3, pp. 276-291, 2000, doi: 10.1093/ptj/80.3.276.
- [42] P. M. Ludewig and J. F. Reynolds, "The association of scapular kinematics and glenohumeral joint pathologies," *journal of orthopaedic & sports physical therapy*, vol. 39, no. 2, pp. 90-104, 2009.
- [43] M. K. Timmons, C. A. Thigpen, A. L. Seitz, A. R. Karduna, B. L. Arnold, and L. A. Michener, "Scapular kinematics and subacromial-impingement syndrome: a meta-analysis," *Journal of sport rehabilitation*, vol. 21, no. 4, pp. 354-370, 2012.
- [44] G. Wu *et al.*, "ISB recommendation on definitions of joint coordinate systems of various joints for the reporting of human joint motion—Part II: shoulder, elbow, wrist and hand," *Journal of Biomechanics*, vol. 38, no. 5, pp. 981-992, 2005/05/01/ 2005, doi: <https://doi.org/10.1016/j.jbiomech.2004.05.042>.
- [45] M. A. Zacchilli and B. D. Owens, "Epidemiology of shoulder dislocations presenting to emergency departments in the United States," (in eng), *The Journal of bone and joint surgery. American volume*, vol. 92, no. 3, pp. 542-549, 2010/03// 2010, doi: 10.2106/jbjs.i.00450.
- [46] C. R. Rowe, "Prognosis in Dislocations of the Shoulder," *JBJS*, vol. 38, no. 5, 1956. [Online]. Available: https://journals.lww.com/jbjsjournal/Fulltext/1956/38050/Prognosis_in_Dislocations_of_the_Shoulder.1.aspx.
- [47] A. Yamamoto *et al.*, "Prevalence and risk factors of a rotator cuff tear in the general population," *Journal of Shoulder and Elbow Surgery*, vol. 19, no. 1, pp. 116-120, 2010/01/01/ 2010, doi: <https://doi.org/10.1016/j.jse.2009.04.006>.
- [48] C. Gerber, A. G. Schneeberger, M. Beck, and U. Schlegel, "Mechanical strength of repairs of the rotator cuff," *Journal of Bone & Joint Surgery, British Volume*, vol. 76-B, no. 3, p. 371, 1994. [Online]. Available: <http://www.bjj.boneandjoint.org.uk/content/76-B/3/371.abstract>.
- [49] F. Pegreffi, P. Paladini, F. Campi, and G. Porcellini, "Conservative management of rotator cuff tear," (in eng), *Sports Med Arthrosc Rev*, vol. 19, no. 4, pp. 348-353, 2011/12// 2011, doi: 10.1097/jsa.0b013e3182148dc6.
- [50] D. L. Crouch, A. C. Santago II, J. F. Plate, Z. Li, and K. R. Saul, "Relationship between maximum isometric joint moment and functional task performance in patients with brachial plexus injury: a pilot study," *Gait & posture*, vol. 44, pp. 238-244, 2016.
- [51] B. Ovbiagele and M. N. Nguyen-Huynh, "Stroke epidemiology: advancing our understanding of disease mechanism and therapy," *Neurotherapeutics*, vol. 8, no. 3, pp. 319-329, 2011.
- [52] D. O'Neill, F. Horgan, A. Hickey, and H. McGee, "Long term outcome of stroke: Stroke is a chronic disease with acute events," (in eng), *BMJ*, vol. 336, no. 7642, pp. 461-461, 2008, doi: 10.1136/bmj.39500.434086.1F.
- [53] L. M. Galatz, C. M. Ball, S. A. Teefey, W. D. Middleton, and K. Yamaguchi, "The outcome and repair integrity of completely arthroscopically repaired large and massive rotator cuff tears," *JBJS*, vol. 86, no. 2, pp. 219-224, 2004.

- [54] P. Maciejasz, J. Eschweiler, K. Gerlach-Hahn, A. Jansen-Troy, and S. Leonhardt, "A survey on robotic devices for upper limb rehabilitation," (in eng), *Journal of neuroengineering and rehabilitation*, vol. 11, pp. 3-3, 2014, doi: 10.1186/1743-0003-11-3.
- [55] H. S. Lo and S. Q. Xie, "Exoskeleton robots for upper-limb rehabilitation: state of the art and future prospects," (in eng), *Med Eng Phys*, vol. 34, no. 3, pp. 261-268, 2012/04// 2012, doi: 10.1016/j.medengphy.2011.10.004.
- [56] K. H. Low, "Robot-assisted gait rehabilitation: From exoskeletons to gait systems," in *2011 Defense Science Research Conference and Expo (DSR)*, 3-5 Aug. 2011 2011, pp. 1-10, doi: 10.1109/DSR.2011.6026886.
- [57] J. Brackenridge, L. Bradnam, S. Lennon, J. Costi, and D. Hobbs, "A Review of Rehabilitation Devices to Promote Upper Limb Function Following Stroke," *Neuroscience and Biomedical Engineering*, vol. 04, pp. 1-1, 03/03 2016, doi: 10.2174/2213385204666160303220102.
- [58] L. Marchal-Crespo and D. J. Reinkensmeyer, "Review of control strategies for robotic movement training after neurologic injury," *Journal of neuroengineering and rehabilitation*, vol. 6, no. 1, p. 20, 2009.
- [59] S. Kim, M. A. Nussbaum, M. I. M. Esfahani, M. M. Alemi, S. Alabdulkarim, and E. Rashedi, "Assessing the influence of a passive, upper extremity exoskeletal vest for tasks requiring arm elevation: Part I—"Expected" effects on discomfort, shoulder muscle activity, and work task performance," *Applied ergonomics*, vol. 70, pp. 315-322, 2018.
- [60] W. V. Dijk, H. V. d. Kooij, and E. Hekman, "A passive exoskeleton with artificial tendons: Design and experimental evaluation," in *2011 IEEE International Conference on Rehabilitation Robotics*, 29 June-1 July 2011 2011, pp. 1-6, doi: 10.1109/ICORR.2011.5975470.
- [61] K. Huysamen, T. Bosch, M. de Looze, K. S. Stadler, E. Graf, and L. W. O'Sullivan, "Evaluation of a passive exoskeleton for static upper limb activities," *Applied ergonomics*, vol. 70, pp. 148-155, 2018.
- [62] E. Pirondini *et al.*, "Evaluation of the effects of the Arm Light Exoskeleton on movement execution and muscle activities: a pilot study on healthy subjects," *Journal of neuroengineering and rehabilitation*, vol. 13, no. 1, p. 9, 2016.
- [63] J. C. Perry, J. Rosen, and S. Burns, "Upper-limb powered exoskeleton design," *IEEE/ASME transactions on mechatronics*, vol. 12, no. 4, pp. 408-417, 2007.
- [64] E. Papadopoulos and G. Patsianis, "Design of an exoskeleton mechanism for the shoulder joint," in *12th IFToMM World Congress*, 2007 2007: Citeseer, 2007, pp. 18-21.
- [65] H.-C. Hsieh, D.-F. Chen, L. Chien, and C.-C. Lan, "Design of a parallel actuated exoskeleton for adaptive and safe robotic shoulder rehabilitation," *IEEE/ASME Transactions on Mechatronics*, vol. 22, no. 5, pp. 2034-2045, 2017.
- [66] S. Christensen and S. Bai, "Kinematic analysis and design of a novel shoulder exoskeleton using a double parallelogram linkage," *Journal of Mechanisms and Robotics*, vol. 10, no. 4, p. 041008, 2018.
- [67] M. B. Wiggin, G. S. Sawicki, and S. H. Collins, "An exoskeleton using controlled energy storage and release to aid ankle propulsion," in *2011 IEEE International Conference on Rehabilitation Robotics*, 2011: IEEE, pp. 1-5.
- [68] T. Bosch, J. van Eck, K. Knitel, and M. de Looze, "The effects of a passive exoskeleton on muscle activity, discomfort and endurance time in forward bending work," *Applied ergonomics*, vol. 54, pp. 212-217, 2016.
- [69] R. Altenburger, D. Scherly, and K. S. Stadler, "Design of a passive, iso-elastic upper limb exoskeleton for gravity compensation," *Robomech Journal*, vol. 3, no. 1, p. 12, 2016.

- [70] S. J. Housman, V. Le, T. Rahman, R. J. Sanchez, and D. J. Reinkensmeyer, "Arm-training with T-WREX after chronic stroke: preliminary results of a randomized controlled trial," in *2007 IEEE 10th International Conference on Rehabilitation Robotics*, 2007: IEEE, pp. 562-568.
- [71] J. Chen and P. S. Lum, "Pilot testing of the spring operated wearable enhancer for arm rehabilitation (SpringWear)," (in eng), *Journal of neuroengineering and rehabilitation*, vol. 15, no. 1, pp. 13-13, 2018, doi: 10.1186/s12984-018-0352-4.
- [72] A. Bjelle, M. Hagberg, and G. Michaelson, "Occupational and individual factors in acute shoulder-neck disorders among industrial workers," *Occupational and Environmental Medicine*, vol. 38, no. 4, pp. 356-363, 1981.
- [73] M. Hagberg and D. Wegman, "Prevalence rates and odds ratios of shoulder-neck diseases in different occupational groups," *Occupational and environmental medicine*, vol. 44, no. 9, pp. 602-610, 1987.
- [74] J. C. Gillette and M. L. Stephenson, "EMG Assessment of a Shoulder Support Exoskeleton During On-Site Job Tasks," in *American Society of Biomechanics Boulder, CO*, 2017.
- [75] L. Van Engelhoven, N. Poon, H. Kazerooni, A. Barr, D. Rempel, and C. Harris-Adamson, "Evaluation of an adjustable support shoulder exoskeleton on static and dynamic overhead tasks," in *Proceedings of the Human Factors and Ergonomics Society Annual Meeting*, 2018, vol. 62, no. 1: SAGE Publications Sage CA: Los Angeles, CA, pp. 804-808.
- [76] M. P. De Looze, T. Bosch, F. Krause, K. S. Stadler, and L. W. O'Sullivan, "Exoskeletons for industrial application and their potential effects on physical work load," *Ergonomics*, vol. 59, no. 5, pp. 671-681, 2016.
- [77] D. Magermans, E. Chadwick, H. Veeger, and F. Van Der Helm, "Requirements for upper extremity motions during activities of daily living," *Clinical biomechanics*, vol. 20, no. 6, pp. 591-599, 2005.
- [78] L. Zhou, S. Bai, M. S. Andersen, and J. Rasmussen, "Modeling and design of a spring-loaded, cable-driven, wearable exoskeleton for the upper extremity," *Modeling, Identification, and Control*, vol. 36, 3, pp. 167-177. 2015.
- [79] J. S. Schroeder and J. C. Perry, "Development of a series wrapping cam mechanism for energy transfer in wearable arm support applications," in *2017 International Conference on Rehabilitation Robotics (ICORR)*, 17-20 July 2017 2017, pp. 585-590, doi: 10.1109/ICORR.2017.8009311.
- [80] A. Nelson, P. T. Hall, and D. L. Crouch, "Effect of Mechanically-Passive, Wearable Shoulder Exoskeletons on Muscle Output During Dynamic Upper Extremity Movements: A Computational Simulation Study," *Journal of Applied Biomechanics*, vol. Accepted, 2020.
- [81] D. K. Kuechle, S. R. Newman, E. Itoi, B. F. Morrey, and K.-N. An, "Shoulder muscle moment arms during horizontal flexion and elevation," *J Shoulder Elbow Surg*, vol. 6, no. 5, pp. 429-439, 1997.
- [82] K. Ziegler-Graham, E. J. MacKenzie, P. L. Ephraim, T. G. Travison, and R. Brookmeyer, "Estimating the prevalence of limb loss in the United States: 2005 to 2050," *Archives of physical medicine and rehabilitation*, vol. 89, no. 3, pp. 422-429, 2008.
- [83] T. R. Dillingham, L. E. Pezzin, and E. J. MacKenzie, "Limb amputation and limb deficiency: epidemiology and recent trends in the United States," *Southern medical journal*, vol. 95, no. 8, pp. 875-883, 2002.
- [84] R. T. Gregory *et al.*, "The mangled extremity syndrome (M.E.S.): a severity grading system for multisystem injury of the extremity," (in eng), *The Journal of trauma*, vol. 25, no. 12, pp. 1147-1150, 1985/12// 1985. [Online]. Available: <http://europepmc.org/abstract/MED/3934398>.

- [85] M. S. Roessler, D. H. Wisner, and J. W. Holcroft, "The mangled extremity: When to amputate?," *Archives of Surgery*, vol. 126, no. 10, pp. 1243-1249, 1991, doi: 10.1001/archsurg.1991.01410340085012.
- [86] K. Johansen, M. Daines, T. Howey, D. Helfet, and J. S. Hansen, "Objective criteria accurately predict amputation following lower extremity trauma," *The Journal of trauma*, vol. 30, no. 5, pp. 568-72; discussion 572-3, 1990.
- [87] H. E. Loon, "Below-knee amputation surgery," *Artif. Limbs*, vol. 6, no. 1, pp. 86-99, 1962.
- [88] M. Pinto and W. Harris, "Fibular segment bone bridging in trans-tibial amputation," *Prosthetics and orthotics international*, vol. 28, no. 3, pp. 220-224, 2004.
- [89] M. S. Pinzur, J. Beck, R. Himes, and J. Callaci, "Distal tibiofibular bone-bridging in transtibial amputation," *The Journal of bone and joint surgery. American volume*, vol. 90, no. 12, p. 2682, 2008.
- [90] R. Dederich, "Plastic treatment of the muscles and bone in amputation surgery," *The Journal of Bone and Joint Surgery. British volume*, vol. 45, no. 1, pp. 60-66, 1963.
- [91] B. F. Kavanagh, D. M. Ilstrup, and J. R. Fitzgerald, "Revision total hip arthroplasty," *The Journal of bone and joint surgery. American volume*, vol. 67, no. 4, pp. 517-526, 1985.
- [92] J. N. Insall, R. Binazzi, M. Soudry, and L. A. Mestriner, "Total knee arthroplasty," *Clinical orthopaedics and related research*, no. 192, pp. 13-22, 1985.
- [93] B. H. Fruhstorfer, E. L. Hodgson, and C. M. Malata, "Early experience with an anatomical soft cohesive silicone gel prosthesis in cosmetic and reconstructive breast implant surgery," *Annals of plastic surgery*, vol. 53, no. 6, pp. 536-542, 2004.
- [94] K. Chin, C. B. Margolin, and P. T. Finger, "Early ocular prosthesis insertion improves quality of life after enucleation," *Optometry-Journal of the American Optometric Association*, vol. 77, no. 2, pp. 71-75, 2006.
- [95] K. Raizada and D. Rani, "Ocular prosthesis," *Contact Lens and Anterior Eye*, vol. 30, no. 3, pp. 152-162, 2007.
- [96] R. H. Brey, G. W. Facer, M. B. Trine, S. G. Lynn, A. M. Peterson, and V. J. Suman, "Vestibular effects associated with implantation of a multiple channel cochlear prosthesis," *The American journal of otology*, vol. 16, no. 4, pp. 424-430, 1995.
- [97] G. Loeb *et al.*, "Design and fabrication of an experimental cochlear prosthesis," *Medical and Biological Engineering and Computing*, vol. 21, no. 3, pp. 241-254, 1983.
- [98] A. Radosh, W. Kuczko, R. Wichniarek, and F. Górski, "Prototyping of cosmetic prosthesis of upper limb using additive manufacturing technologies," *Advances in Science and Technology Research Journal*, vol. 11, 2017.
- [99] W. Gaine, C. Smart, and M. Bransby-Zachary, "Upper limb traumatic amputees: Review of prosthetic use," *Journal of Hand Surgery*, vol. 22, no. 1, pp. 73-76, 1997.
- [100] B. Brackx, M. Van Damme, A. Matthys, B. Vanderborght, and D. Lefeber, "Passive ankle-foot prosthesis prototype with extended push-off," *International journal of advanced robotic systems*, vol. 10, no. 2, p. 101, 2013.
- [101] R. Unal, R. Carloni, S. M. Behrens, E. E. Hekman, S. Stramigioli, and H. F. Koopman, "Towards a fully passive transfemoral prosthesis for normal walking," in *2012 4th IEEE RAS & EMBS International Conference on Biomedical Robotics and Biomechatronics (BioRob)*, 2012: IEEE, pp. 1949-1954.
- [102] C. Mancinelli *et al.*, "Comparing a passive-elastic and a powered prosthesis in transtibial amputees," in *2011 Annual International Conference of the IEEE Engineering in Medicine and Biology Society*, 2011: IEEE, pp. 8255-8258.

- [103] B. T. Dyer, P. Sewell, and S. Noroozi, "How should we assess the mechanical properties of lower-limb prosthesis technology used in elite sport?: An initial investigation," *Journal of Biomedical Science and Engineering*, vol. 6, no. 2, pp. 116-123, 2013.
- [104] A. Saikia, S. Mazumdar, N. Sahai, and S. Paul, "Below Elbow Prosthetic: A Path to Independent Era," *International Journal of Advanced Information Science and Technology*, vol. 34, pp. 9-14, 02/01 2015.
- [105] R. Weir *et al.*, "New multifunctional prosthetic arm and hand systems," in *2007 29th Annual International Conference of the IEEE Engineering in Medicine and Biology Society*, 2007: IEEE, pp. 4359-4360.
- [106] P. J. Kyberd and P. H. Chappell, "The Southampton Hand: an intelligent myoelectric prosthesis," *Journal of rehabilitation Research and Development*, vol. 31, no. 4, pp. 326-334, 1994.
- [107] P. J. Kyberd, C. Light, P. H. Chappell, J. M. Nightingale, D. Whatley, and M. Evans, "The design of anthropomorphic prosthetic hands: A study of the Southampton Hand," *Robotica*, vol. 19, no. 6, pp. 593-600, 2001.
- [108] H. M. Herr and A. M. Grabowski, "Bionic ankle-foot prosthesis normalizes walking gait for persons with leg amputation," *Proceedings of the Royal Society B: Biological Sciences*, vol. 279, no. 1728, pp. 457-464, 2011.
- [109] S. Au, M. Berniker, and H. Herr, "Powered ankle-foot prosthesis to assist level-ground and stair-descent gaits," *Neural Networks*, vol. 21, no. 4, pp. 654-666, 2008.
- [110] M. C. Carrozza, G. Cappiello, S. Micera, B. B. Edin, L. Beccai, and C. Cipriani, "Design of a cybernetic hand for perception and action," *Biological cybernetics*, vol. 95, no. 6, p. 629, 2006.
- [111] M. C. Carrozza *et al.*, "The SPRING hand: development of a self-adaptive prosthesis for restoring natural grasping," *Autonomous Robots*, vol. 16, no. 2, pp. 125-141, 2004.
- [112] L. Zollo, S. Roccella, E. Guglielmelli, M. C. Carrozza, and P. Dario, "Biomechatronic design and control of an anthropomorphic artificial hand for prosthetic and robotic applications," *IEEE/ASME Transactions On Mechatronics*, vol. 12, no. 4, pp. 418-429, 2007.
- [113] K. Horch, S. Meek, T. G. Taylor, and D. T. Hutchinson, "Object discrimination with an artificial hand using electrical stimulation of peripheral tactile and proprioceptive pathways with intrafascicular electrodes," *IEEE Transactions on Neural Systems and Rehabilitation Engineering*, vol. 19, no. 5, pp. 483-489, 2011.
- [114] S. Wendelken *et al.*, "Restoration of motor control and proprioceptive and cutaneous sensation in humans with prior upper-limb amputation via multiple Utah Slanted Electrode Arrays (USEAs) implanted in residual peripheral arm nerves," *Journal of neuroengineering and rehabilitation*, vol. 14, no. 1, p. 121, 2017.
- [115] M. C. Carrozza *et al.*, "Experimental analysis of an innovative prosthetic hand with proprioceptive sensors," in *2003 IEEE International Conference on Robotics and Automation (Cat. No. 03CH37422)*, 2003, vol. 2: IEEE, pp. 2230-2235.
- [116] C. Antfolk, M. D'alonzo, B. Rosén, G. Lundborg, F. Sebelius, and C. Cipriani, "Sensory feedback in upper limb prosthetics," *Expert review of medical devices*, vol. 10, no. 1, pp. 45-54, 2013.
- [117] J. Pons *et al.*, "The MANUS-HAND dextrous robotics upper limb prosthesis: mechanical and manipulation aspects," *Autonomous Robots*, vol. 16, no. 2, pp. 143-163, 2004.
- [118] B. E. Lawson, J. Mitchell, D. Truex, A. Shultz, E. Ledoux, and M. Goldfarb, "A robotic leg prosthesis: Design, control, and implementation," *IEEE Robotics & Automation Magazine*, vol. 21, no. 4, pp. 70-81, 2014.
- [119] D. L. Crouch and H. H. J. J. o. n. e. Huang, "Musculoskeletal model-based control interface mimics physiologic hand dynamics during path tracing task," vol. 14, no. 3, p. 036008, 2017.
- [120] M. Kawato, "Internal models for motor control and trajectory planning," *Current opinion in neurobiology*, vol. 9, no. 6, pp. 718-727, 1999.

- [121] D. L. Crouch and H. J. J. o. b. Huang, "Lumped-parameter electromyogram-driven musculoskeletal hand model: A potential platform for real-time prosthesis control," vol. 49, no. 16, pp. 3901-3907, 2016.
- [122] E. Chadwick *et al.*, "Continuous neuronal ensemble control of simulated arm reaching by a human with tetraplegia," *Journal of neural engineering*, vol. 8, no. 3, p. 034003, 2011.
- [123] H. Huang, T. A. Kuiken, and R. D. Lipschutz, "A strategy for identifying locomotion modes using surface electromyography," *IEEE Transactions on Biomedical Engineering*, vol. 56, no. 1, pp. 65-73, 2009.
- [124] J. L. Collinger *et al.*, "High-performance neuroprosthetic control by an individual with tetraplegia," *The Lancet*, vol. 381, no. 9866, pp. 557-564, 2013.
- [125] B. Wodlinger, J. Downey, E. Tyler-Kabara, A. Schwartz, M. Boninger, and J. Collinger, "Ten-dimensional anthropomorphic arm control in a human brain-machine interface: difficulties, solutions, and limitations," *Journal of neural engineering*, vol. 12, no. 1, p. 016011, 2014.
- [126] A. Ameri, E. N. Kamavuako, E. J. Scheme, K. B. Englehart, and P. A. Parker, "Support vector regression for improved real-time, simultaneous myoelectric control," *IEEE Transactions on Neural Systems and Rehabilitation Engineering*, vol. 22, no. 6, pp. 1198-1209, 2014.
- [127] D. Yatsenko, D. McDonnall, and K. S. Guillory, "Simultaneous, proportional, multi-axis prosthesis control using multichannel surface EMG," in *2007 29th Annual International Conference of the IEEE Engineering in Medicine and Biology Society*, 2007: IEEE, pp. 6133-6136.
- [128] A. J. Young, L. H. Smith, E. J. Rouse, and L. J. Hargrove, "Classification of simultaneous movements using surface EMG pattern recognition," *IEEE Transactions on Biomedical Engineering*, vol. 60, no. 5, pp. 1250-1258, 2013.
- [129] N. Jiang, K. B. Englehart, and P. A. Parker, "Extracting simultaneous and proportional neural control information for multiple-DOF prostheses from the surface electromyographic signal," *IEEE Transactions on Biomedical Engineering*, vol. 56, no. 4, pp. 1070-1080, 2009.
- [130] A. Fougner, Ø. Stavadahl, P. J. Kyberd, Y. G. Losier, and P. A. Parker, "Control of upper limb prostheses: Terminology and proportional myoelectric control—A review," *IEEE Transactions on neural systems and rehabilitation engineering*, vol. 20, no. 5, pp. 663-677, 2012.
- [131] S. Srinivasan *et al.*, "On prosthetic control: A regenerative agonist-antagonist myoneural interface," *Science Robotics*, vol. 2, no. 6, p. eaan2971, 2017.
- [132] G. Guo, J. Zhang, and W. Gruver, "Optimal design of a six-bar linkage with one degree of freedom for an anthropomorphic three-jointed finger mechanism," *Proceedings of the Institution of Mechanical Engineers, Part H: Journal of Engineering in Medicine*, vol. 207, no. 3, pp. 185-190, 1993.
- [133] P. Chappell, J. Nightingale, P. Kyberd, and M. Barkhordar, "Control of a single degree of freedom artificial hand," *Journal of biomedical engineering*, vol. 9, no. 3, pp. 273-277, 1987.
- [134] J. A. Doeringer and N. Hogan, "Performance of above elbow body-powered prostheses in visually guided unconstrained motion tasks," *IEEE Transactions on Biomedical Engineering*, vol. 42, no. 6, pp. 621-631, 1995.
- [135] M. E. Cupo and S. J. Sheredos, "Clinical evaluation of a new, above-elbow, body-powered prosthetic arm: A final report," *Journal of rehabilitation research and development*, vol. 35, no. 4, p. 431, 1998.
- [136] A. L. Muilenburg and M. A. LeBlanc, "Body-powered upper-limb components," in *Comprehensive management of the upper-limb amputee*: Springer, 1989, pp. 28-38.
- [137] L. H. Huinink, H. Bouwsema, D. H. Plettenburg, C. K. Van der Sluis, and R. M. Bongers, "Learning to use a body-powered prosthesis: changes in functionality and kinematics," *Journal of neuroengineering and rehabilitation*, vol. 13, no. 1, pp. 1-12, 2016.

- [138] E. Biddiss and T. Chau, "Upper-limb prosthetics: critical factors in device abandonment," *American journal of physical medicine & rehabilitation*, vol. 86, no. 12, pp. 977-987, 2007.
- [139] U. Proske, "Kinesthesia: the role of muscle receptors," *Muscle & Nerve: Official Journal of the American Association of Electrodiagnostic Medicine*, vol. 34, no. 5, pp. 545-558, 2006.
- [140] U. Proske, "The Golgi tendon organ. Properties of the receptor and reflex action of impulses arising from tendon organs," *International review of physiology*, vol. 25, pp. 127-171, 1981.
- [141] R. C. Miall and D. M. Wolpert, "Forward models for physiological motor control," *Neural networks*, vol. 9, no. 8, pp. 1265-1279, 1996.
- [142] H. Van de Meent, M. T. Hopman, and J. P. Frölke, "Walking Ability and Quality of Life in Subjects With Transfemoral Amputation: A Comparison of Osseointegration With Socket Prostheses," *Archives of Physical Medicine and Rehabilitation*, vol. 94, no. 11, pp. 2174-2178, 2013, doi: 10.1016/j.apmr.2013.05.020.
- [143] J. P. M. Frölke, R. A. Leijendekkers, and H. van de Meent, "Osseointegrated prosthesis for patients with an amputation : Multidisciplinary team approach in the Netherlands Osseointegrierte Prothese für Patienten nach Amputation : Multidisziplinärer Behandlungsansatz in den Niederlanden," *Der Unfallchirurg*, vol. 120, no. 4, pp. 293-299, 2017, doi: 10.1007/s00113-016-0302-1.
- [144] K. Hagberg, E. Häggström, S. Jönsson, B. Rydevik, and R. Brånemark, "Osseoperception and osseointegrated prosthetic limbs," in *Psychoprosthetics*: Springer, 2008, pp. 131-140.
- [145] M. E. Farrugia *et al.*, "Concentric and single fiber needle electrodes yield comparable jitter results in myasthenia gravis," vol. 39, no. 5, pp. 579-585, 2009.
- [146] D. S. Childress, "Control strategy for upper-limb prostheses," in *Proceedings of the 20th Annual International Conference of the IEEE Engineering in Medicine and Biology Society. Vol. 20 Biomedical Engineering Towards the Year 2000 and Beyond (Cat. No. 98CH36286)*, 1998, vol. 5: IEEE, pp. 2273-2275.
- [147] T. R. Clites *et al.*, "Proprioception from a neurally controlled lower-extremity prosthesis," vol. 10, no. 443, p. eaap8373, 2018.
- [148] N. Jiang, J. L. Vest-Nielsen, S. Muceli, and D. Farina, "EMG-based simultaneous and proportional estimation of wrist/hand kinematics in uni-lateral trans-radial amputees," *Journal of neuroengineering and rehabilitation*, vol. 9, no. 1, p. 42, 2012.
- [149] C. Cipriani *et al.*, "Online myoelectric control of a dexterous hand prosthesis by transradial amputees," *IEEE Transactions on Neural Systems and Rehabilitation Engineering*, vol. 19, no. 3, pp. 260-270, 2011.
- [150] A. C. Blaschke, H. Jampol, and C. L. Taylor, "Biomechanical Consideration in Cineplasty," *Journal of applied physiology*, vol. 5, no. 5, pp. 195-206, 1952.
- [151] R. Beasley, "The tendon exteriorization cineplasty, a preliminary report," *Inter-clinic Information Bulletin. Committee on Prosthetics Research and Development*, vol. 5, no. 8, pp. 6-8, 1966.
- [152] R. Weir, C. Heckathorne, and D. Childress, "Cineplasty as a control input for externally powered prosthetic components," *Journal of rehabilitation research and development*, vol. 38, no. 4, p. 357, 2001.
- [153] S. Nambu, M. Ikebuchi, M. Taniguchi, C. S. Park, and T. Kitagawa, "Advantages of externally powered prosthesis with feedback system using pseudo-cineplasty," *Journal of rehabilitation research and development*, vol. 51, no. 7, p. 1095, 2014.
- [154] R. F. Weir, C. W. Heckathorne, and D. S. Childress, "Cineplasty as a control input for externally powered prosthetic components," *J Rehabil Res Dev*, vol. 38, no. 4, pp. 357-63, Jul-Aug 2001. [Online]. Available: <https://www.ncbi.nlm.nih.gov/pubmed/11563487>.
- [155] J. A. Thomson, *Outlines of zoology*. J. Pentland, 1899.

- [156] R. L. Lieber and F. T. Blevins, "Skeletal muscle architecture of the rabbit hindlimb: functional implications of muscle design," *Journal of morphology*, vol. 199, no. 1, pp. 93-101, 1989.
- [157] P. R. Klokkevold, R. D. Nishimura, M. Adachi, and A. Caputo, "Osseointegration enhanced by chemical etching of the titanium surface. A torque removal study in the rabbit," *Clinical oral implants research*, vol. 8, no. 6, pp. 442-447, 1997.
- [158] J. Steigenga, K. Al-Shammari, C. Misch, F. H. Nociti Jr, and H. L. Wang, "Effects of implant thread geometry on percentage of osseointegration and resistance to reverse torque in the tibia of rabbits," *Journal of periodontology*, vol. 75, no. 9, pp. 1233-1241, 2004.
- [159] A. Yıldız, E. Esen, M. Kürkcü, İ. Damlar, K. Dağlıoğlu, and T. Akova, "Effect of zoledronic acid on osseointegration of titanium implants: an experimental study in an ovariectomized rabbit model," *Journal of Oral and Maxillofacial Surgery*, vol. 68, no. 3, pp. 515-523, 2010.
- [160] C. de Carvalho Lopes and B. K. Júnior, "Histological findings of bone remodeling around smooth dental titanium implants inserted in rabbit's tibias," *Annals of Anatomy-Anatomischer Anzeiger*, vol. 184, no. 4, pp. 359-362, 2002.
- [161] K. R. Blickenstaff, W. A. Grana, and D. Egle, "Analysis of a semitendinosus autograft in a rabbit model," *The American journal of sports medicine*, vol. 25, no. 4, pp. 554-559, 1997.
- [162] D. Laurent, J. Wasvary, E. O'Byrne, and M. Rudin, "In vivo qualitative assessments of articular cartilage in the rabbit knee with high-resolution MRI at 3 T," *Magnetic Resonance in Medicine: An Official Journal of the International Society for Magnetic Resonance in Medicine*, vol. 50, no. 3, pp. 541-549, 2003.
- [163] D. Amiel, T. Toyoguchi, K. Kobayashi, K. Bowden, M. Amiel, and R. Healey, "Long-term effect of sodium hyaluronate (Hyalgan®) on osteoarthritis progression in a rabbit model," *Osteoarthritis and cartilage*, vol. 11, no. 9, pp. 636-643, 2003.
- [164] F. Bonnel, E. Peruchon, P. Baldet, A. Dimeglio, and P. Rabischong, "Effects of compression on growth plates in the rabbit," *Acta orthopaedica Scandinavica*, vol. 54, no. 5, pp. 730-733, 1983.
- [165] C. Colombo *et al.*, "A new model of osteoarthritis in rabbits," *Arthritis & Rheumatism: Official Journal of the American College of Rheumatology*, vol. 26, no. 7, pp. 875-886, 1983.
- [166] T. Holmström, P. Paavolainen, P. Slätis, and E. Karaharju, "Effect of compression on fracture healing: plate fixation studied in rabbits," *Acta Orthopaedica Scandinavica*, vol. 57, no. 4, pp. 368-372, 1986.
- [167] H. Barbeau and S. Rossignol, "Recovery of locomotion after chronic spinalization in the adult cat," *Brain research*, vol. 412, no. 1, pp. 84-95, 1987.
- [168] P. D. Polly, "Limbs in mammalian evolution," *Fins into limbs: evolution, development and transformation*, pp. 245-268, 2007.
- [169] P. Myers, R. Espinosa, C. S. Parr, T. Jones, G. S. Hammond, and T. A. Dewey, "The Animal Diversity Web," 2021. [Online]. Available: https://animaldiversity.org/accounts/Sciuridae/specimens/collections/contributors/anatomical_images/feet_and_legs/posture/?start=15.
- [170] D. L. Gushue, J. Houck, and A. L. Lerner, "Rabbit knee joint biomechanics: Motion analysis and modeling of forces during hopping," *Journal of Orthopaedic Research*, vol. 23, no. 4, pp. 735-742, 2005, doi: 10.1016/j.orthres.2005.01.005.
- [171] T. M. Griffin, R. P. Main, and C. T. Farley, "Biomechanics of quadrupedal walking: how do four-legged animals achieve inverted pendulum-like movements?," *Journal of Experimental Biology*, vol. 207, no. 20, pp. 3545-3558, 2004, doi: 10.1242/jeb.01177.
- [172] A. Melvin, A. Litsky, J. Mayerson, D. Witte, D. Melvin, and N. Juncosa-Melvin, "An artificial tendon with durable muscle interface," *Journal of orthopaedic research*, vol. 28, no. 2, pp. 218-224, 2010.

- [173] A. Melvin, A. Litsky, J. Mayerson, K. Stringer, D. Melvin, and N. Juncosa-Melvin, "An artificial tendon to connect the quadriceps muscle to the Tibia," *Journal of Orthopaedic Research*, vol. 29, no. 11, pp. 1775-1782, 2011.
- [174] S. Namdari *et al.*, "Defining functional shoulder range of motion for activities of daily living," *Journal of shoulder and elbow surgery*, vol. 21, no. 9, pp. 1177-1183, 2012.
- [175] T. C. Pataky, "Generalized n-dimensional biomechanical field analysis using statistical parametric mapping," *Journal of Biomechanics*, vol. 43, no. 10, pp. 1976-1982, 2010.
- [176] V. Novakovic and V. Sanguineti, "Adaptation to constant-magnitude assistive forces: kinematic and neural correlates," *Experimental Brain Research*, journal article vol. 209, no. 3, pp. 425-436, March 01 2011, doi: 10.1007/s00221-011-2573-7.
- [177] B. Bigland-Ritchie, E. Cafarelli, and N. Vollestad, "Fatigue of submaximal static contractions," *Acta Physiol Scand Suppl*, vol. 556, pp. 137-148, 1986.
- [178] J. B. Ogston and P. M. Ludewig, "Differences in 3-dimensional shoulder kinematics between persons with multidirectional instability and asymptomatic controls," *The American journal of sports medicine*, vol. 35, no. 8, pp. 1361-1370, 2007.
- [179] L. Van Engelhoven, N. Poon, H. Kazerooni, D. Rempel, A. Barr, and C. Harris-Adamson, "Experimental Evaluation of a Shoulder-Support Exoskeleton for Overhead Work: Influences of Peak Torque Amplitude, Task, and Tool Mass," *IIEE Trans Occupl Ergon Human Factors*, 2019.
- [180] L. Resnik *et al.*, "Advanced upper limb prosthetic devices: implications for upper limb prosthetic rehabilitation," *Archives of physical medicine and rehabilitation*, vol. 93, no. 4, pp. 710-717, 2012.
- [181] P. J. Kyberd *et al.*, "Two-degree-of-freedom powered prosthetic wrist," *Journal of Rehabilitation Research & Development*, vol. 48, no. 6, 2011.
- [182] S. S. Srinivasan, M. Diaz, M. Carty, and H. M. Herr, "Towards functional restoration for persons with limb amputation: A dual-stage implementation of regenerative agonist-antagonist myoneural interfaces," *Scientific Reports*, vol. 9, no. 1, p. 1981, 2019/02/13 2019, doi: 10.1038/s41598-018-38096-z.
- [183] A. Hulth and S. Olerud, "Studies on amputation stumps in rabbits," *The Journal of bone and joint surgery. British volume*, vol. 44, no. 2, pp. 431-435, 1962.
- [184] M. Sanna, C. Sanna, F. Caputo, G. Piu, and M. Salvi, "Surgical approaches in total knee arthroplasty," *Joints*, vol. 1, no. 2, pp. 34-44, 2013.
- [185] D. R. Shanklin and D. L. Smalley, "Dynamics of wound healing after silicone device implantation," *Exp Mol Pathol*, vol. 67, no. 1, pp. 26-39, Sep 1999, doi: 10.1006/exmp.1999.2269.
- [186] P. F. Millington and R. Wilkinson, *Skin* (Biological structure and function, no. 9). Cambridge Cambridgeshire ; New York: Cambridge University Press, 1983, pp. xii, 224 p.
- [187] N. Langrana, H. Alexander, I. Strauchler, A. Mehta, and J. Ricci, "Effect of mechanical load in wound healing," *Annals of plastic surgery*, vol. 10, no. 3, pp. 200-208, 1983.
- [188] E. J. F. Timmenga, T. T. Andreassen, H. J. Houthoff, and P. J. Kloppe, "The effect of mechanical stress on healing skin wounds: an experimental study in rabbits using tissue expansion," *British Journal of Plastic Surgery*, vol. 44, no. 7, pp. 514-519, 1991/01/01/ 1991, doi: [https://doi.org/10.1016/0007-1226\(91\)90008-8](https://doi.org/10.1016/0007-1226(91)90008-8).
- [189] M. A. Erlich and A. Parhiscar, "Nasal dorsal augmentation with silicone implants," *Facial plastic surgery*, vol. 19, no. 04, pp. 325-330, 2003.
- [190] T. Sato, M. Araki, N. Nakajima, K. Omori, and T. Nakamura, "Biodegradable polymer coating promotes the epithelization of tissue-engineered airway prostheses," *The Journal of thoracic and cardiovascular surgery*, vol. 139, no. 1, pp. 26-31, 2010.

- [191] S. Jönsson, K. Caine-Winterberger, and R. Brånemark, "Osseointegration amputation prostheses on the upper limbs: methods, prosthetics and rehabilitation," *Prosthetics and orthotics international*, vol. 35, no. 2, pp. 190-200, 2011.
- [192] W. Lu, J. J. Li, B. Bosley, and M. Muderis, *The Osseointegrated Prosthetic Limb (OPL) for the reconstruction of lower limb amputees*. 2016.
- [193] A. Mavrogenis, R. Dimitriou, J. Parvizi, and G. Babis, "Biology of implant osseointegration," *J Musculoskelet Neuronal Interact*, vol. 9, no. 2, pp. 61-71, 2009.
- [194] D. E. Anderson *et al.*, "Improved osseointegration of calcium phosphate-coated external fixation pins. Studies in calves," *Acta Orthop Scand*, vol. 68, no. 6, pp. 571-6, Dec 1997, doi: 10.3109/17453679708999029.
- [195] E. A. Lewallen *et al.*, "Biological strategies for improved osseointegration and osteoinduction of porous metal orthopedic implants," *Tissue Engineering Part B: Reviews*, vol. 21, no. 2, pp. 218-230, 2014.
- [196] C. A. Engh, P. Massin, and K. E. Suthers, "Roentgenographic assessment of the biologic fixation of porous-surfaced femoral components," *Clinical orthopaedics and related research*, no. 257, pp. 107-128, 1990.
- [197] P. T. Hall *et al.*, "Fully Implanted Prostheses for Musculoskeletal Limb Reconstruction After Amputation: An In Vivo Feasibility Study," *Annals of Biomedical Engineering*, 2020/10/09 2020, doi: 10.1007/s10439-020-02645-3.
- [198] T. Albrektsson and C. Johansson, "Osteoinduction, osteoconduction and osseointegration," *European Spine Journal*, journal article vol. 10, no. 2, pp. S96-S101, October 01 2001, doi: 10.1007/s005860100282.
- [199] R. Brånemark, P. Brånemark, B. Rydevik, and R. R. Myers, "Osseointegration in skeletal reconstruction and rehabilitation: a review," *Journal of rehabilitation research and development*, vol. 38, no. 2, pp. 175-182, 2001.
- [200] D. R. Carter, "Mechanical loading histories and cortical bone remodeling," *Calcified tissue international*, vol. 36, no. 1, pp. S19-S24, 1984.
- [201] J. L. Schriefer, S. J. Warden, L. K. Saxon, A. G. Robling, and C. H. Turner, "Cellular accommodation and the response of bone to mechanical loading," *Journal of biomechanics*, vol. 38, no. 9, pp. 1838-1845, 2005.
- [202] P.-I. Brånemark and T. Albrektsson, "Titanium implants permanently penetrating human skin," *Scandinavian journal of plastic and reconstructive surgery*, vol. 16, no. 1, pp. 17-21, 1982.
- [203] G. D. Winter, "Transcutaneous implants: Reactions of the skin-implant interface," *Journal of biomedical materials research*, vol. 8, no. 3, pp. 99-113, 1974.
- [204] A. Wahlsten *et al.*, "Mechanical stimulation induces rapid fibroblast proliferation and accelerates the early maturation of human skin substitutes," *Biomaterials*, vol. 273, p. 120779, 2021.
- [205] J. E. Sanders, B. S. Goldstein, and D. F. Leotta, "Skin response to mechanical stress: adaptation rather than breakdown-a review of the literature," *Journal of rehabilitation research and development*, vol. 32, pp. 214-214, 1995.
- [206] Y. H. An and R. J. Friedman, "Animal models of orthopedic implant infection," *Journal of Investigative Surgery*, vol. 11, no. 2, pp. 139-146, 1998.
- [207] W. Chen *et al.*, "Surface functionalization of titanium implants with chitosan-catechol conjugate for suppression of ROS-induced cells damage and improvement of osteogenesis," *Biomaterials*, vol. 114, pp. 82-96, 2017.
- [208] J. P. Charles, O. Cappellari, A. J. Spence, J. R. Hutchinson, and D. J. Wells, "Musculoskeletal geometry, muscle architecture and functional specialisations of the mouse hindlimb," *PLoS One*, vol. 11, no. 4, 2016.

- [209] K. Springett, "The influence of forces generated during gait on the clinical appearance and physical properties of skin callus," University of Brighton, 1993.
- [210] E. Koc, M. Tunca, A. Akar, A. H. Erbil, B. Demiralp, and E. Arca, "Skin problems in amputees: a descriptive study," *International journal of dermatology*, vol. 47, no. 5, pp. 463-466, 2008.
- [211] J. DesGroseilliers, J. DesJardins, J. Germain, and A. Krol, "Dermatologic problems in amputees," *Canadian Medical Association Journal*, vol. 118, no. 5, p. 535, 1978.
- [212] K. Omori *et al.*, "Regenerative medicine of the trachea: the first human case," *Annals of Otology, Rhinology & Laryngology*, vol. 114, no. 6, pp. 429-433, 2005.
- [213] R. E. Jones, D. S. Foster, M. S. Hu, and M. T. Longaker, "Wound healing and fibrosis: current stem cell therapies," *Transfusion*, vol. 59, no. S1, pp. 884-892, 2019.
- [214] F. Mirrashed and J. C. Sharp, "In vivo morphological characterisation of skin by MRI micro-imaging methods," *Skin research and technology*, vol. 10, no. 3, pp. 149-160, 2004.
- [215] H. Tran, F. Charleux, M. Rachik, A. Ehrlacher, and M. Ho Ba Tho, "In vivo characterization of the mechanical properties of human skin derived from MRI and indentation techniques," *Computer methods in biomechanics and biomedical engineering*, vol. 10, no. 6, pp. 401-407, 2007.
- [216] G. Karakurum, M. Karakok, M. Tarakcioglu, N. E. Kocer, R. Kocabas, and C. Bagci, "Comparative effect of intra-articular administration of hyaluronan and/or cortisone with evaluation of malondialdehyde on degenerative osteoarthritis of the rabbit's knee," *The Tohoku journal of experimental medicine*, vol. 199, no. 3, pp. 127-134, 2003.
- [217] M. P. H. Le Graverand, J. Eggerer, E. Vignon, I. G. Otterness, L. Barclay, and D. A. Hart, "Assessment of specific mRNA levels in cartilage regions in a lapine model of osteoarthritis," *Journal of orthopaedic research*, vol. 20, no. 3, pp. 535-544, 2002.
- [218] J. M. Mansour, F. A. Wentorf, and K. M. DeGoede, "In vivo kinematics of the rabbit knee in unstable models of osteoarthritis," *Annals of biomedical engineering*, vol. 26, no. 3, pp. 353-360, 1998.
- [219] K. Messner, A. Fahlgren, I. Ross, and B. Andersson, "Simultaneous changes in bone mineral density and articular cartilage in a rabbit meniscectomy model of knee osteoarthritis," *Osteoarthritis and cartilage*, vol. 8, no. 3, pp. 197-206, 2000.
- [220] K. Messner, A. Fahlgren, J. Persliden, and B.-M. Andersson, "Radiographic joint space narrowing and histologic changes in a rabbit meniscectomy model of early knee osteoarthritis," *The American journal of sports medicine*, vol. 29, no. 2, pp. 151-160, 2001.
- [221] R. Moskowitz and V. Goldberg, "Studies of osteophyte pathogenesis in experimentally induced osteoarthritis," *The Journal of rheumatology*, vol. 14, no. 2, p. 311, 1987.
- [222] R. W. Moskowitz *et al.*, "Experimentally induced degenerative joint lesions following partial meniscectomy in the rabbit," *Arthritis & Rheumatism: Official Journal of the American College of Rheumatology*, vol. 16, no. 3, pp. 397-405, 1973.
- [223] J. P. Pelletier *et al.*, "In vivo selective inhibition of mitogen-activated protein kinase kinase 1/2 in rabbit experimental osteoarthritis is associated with a reduction in the development of structural changes," *Arthritis & Rheumatism: Official Journal of the American College of Rheumatology*, vol. 48, no. 6, pp. 1582-1593, 2003.
- [224] R. L. Sah *et al.*, "Physical properties of rabbit articular cartilage after transection of the anterior cruciate ligament," *Journal of Orthopaedic Research*, vol. 15, no. 2, pp. 197-203, 1997.
- [225] E. Vignon *et al.*, "Histological cartilage changes in a rabbit model of osteoarthritis," *The Journal of rheumatology*, vol. 14, pp. 104-106, 1987.
- [226] L. Wachsmuth, R. Keiffer, H.-P. Juretschke, R. X. Raiss, N. Kimmig, and E. Lindhorst, "In vivo contrast-enhanced micro MR-imaging of experimental osteoarthritis in the rabbit knee joint at 7.1 T," *Osteoarthritis and cartilage*, vol. 11, no. 12, pp. 891-902, 2003.

- [227] G. Lovász *et al.*, "Effects of valgus tibial angulation on cartilage degeneration in the rabbit knee," *Journal of orthopaedic research*, vol. 13, no. 6, pp. 846-853, 1995.
- [228] I. Reimann, "Experimental osteoarthritis of the knee in rabbits induced by alteration of the load-bearing," *Acta Orthopaedica Scandinavica*, vol. 44, no. 4-5, pp. 496-504, 1973.
- [229] D. Wu, D. Burr, R. Boyd, and E. Radin, "Bone and cartilage changes following experimental varus or valgus tibial angulation," *Journal of Orthopaedic Research*, vol. 8, no. 4, pp. 572-585, 1990.
- [230] R. L. Lieber and J. Fridén, "Functional and clinical significance of skeletal muscle architecture," *Muscle & Nerve: Official Journal of the American Association of Electrodiagnostic Medicine*, vol. 23, no. 11, pp. 1647-1666, 2000.
- [231] R. L. Lieber, M. C. Schmitz, D. K. Mishra, and J. Fridén, "Contractile and cellular remodeling in rabbit skeletal muscle after cyclic eccentric contractions," *Journal of Applied Physiology*, vol. 77, no. 4, pp. 1926-1934, 1994.
- [232] D. Longino, C. Frank, T. Leonard, M. A. Vaz, and W. Herzog, "Proposed model of botulinum toxin-induced muscle weakness in the rabbit," *Journal of orthopaedic research*, vol. 23, no. 6, pp. 1411-1418, 2005.
- [233] V. Vasilev, H. Merker, and N. Vidinov, "Ultrastructural changes in the synovial membrane in experimentally-induced osteoarthritis of rabbit knee joint," *Histology and histopathology*, vol. 7, no. 1, p. 119, 1992.
- [234] A. Anastasiou and L. Hall, "A novel RF coil configuration for in-vivo and ex-vivo imaging of arthritic rabbit knee joints," *Magnetic resonance imaging*, vol. 21, no. 1, pp. 61-68, 2003.
- [235] I. N. Beloozerova, P. V. Zelenin, L. B. Popova, G. N. Orlovsky, S. Grillner, and T. G. Deliagina, "Postural control in the rabbit maintaining balance on the tilting platform," *Journal of neurophysiology*, vol. 90, no. 6, pp. 3783-3793, 2003.
- [236] A. Wennerberg, R. Jimbo, S. Stübinger, M. Obrecht, M. Dard, and S. Berner, "Nanostructures and hydrophilicity influence osseointegration: a biomechanical study in the rabbit tibia," *Clinical oral implants research*, vol. 25, no. 9, pp. 1041-1050, 2014.
- [237] J. Prat *et al.*, "Load transmission through the callus site with external fixation systems: theoretical and experimental analysis," *Journal of biomechanics*, vol. 27, no. 4, pp. 469-478, 1994.
- [238] R. Fiker, L. H. Kim, L. A. Molina, T. Chomiak, and P. J. Whelan, "Visual Deep Lab Cut: A user-friendly approach to gait analysis," *Journal of Neuroscience Methods*, p. 108775, 2020.
- [239] S. Tinga *et al.*, "Femorotibial kinematics in dogs with cranial cruciate ligament insufficiency: a three-dimensional in-vivo fluoroscopic analysis during walking," *BMC veterinary research*, vol. 14, no. 1, pp. 1-9, 2018.
- [240] T. J. Koh and W. Herzog, "Excursion is important in regulating sarcomere number in the growing rabbit tibialis anterior," *The Journal of physiology*, vol. 508, no. 1, pp. 267-280, 1998.
- [241] J. R. Jarrell, B. J. Farrell, R. S. Kistenberg, J. F. Dalton IV, M. Pitkin, and B. I. Prilutsky, "Kinetics of individual limbs during level and slope walking with a unilateral transtibial bone-anchored prosthesis in the cat," *Journal of biomechanics*, vol. 76, pp. 74-83, 2018.
- [242] R. Steiner *et al.*, "Biometric Data Comparison Between Lewis and Sprague Dawley Rats," (in English), *Frontiers in Veterinary Science*, Original Research vol. 6, no. 469, 2019-December-20 2019, doi: 10.3389/fvets.2019.00469.
- [243] J. D. Sheldon, M. J. Adkesson, M. C. Allender, R. S. Bailey, J. N. Langan, and S. K. Chinnadurai, "Evaluation of a pressure sensitive walkway for objective gait analysis in normal and arthritic domestic ducks (*Cairina moschata domestica*)," *PloS one*, vol. 14, no. 7, p. e0220468, 2019.
- [244] V. C. de Carvalho, I. de Alencar Nääs, M. M. Neto, and S. R. L. de Souza, "Measurement of pig claw pressure distribution," *biosystems engineering*, vol. 103, no. 3, pp. 357-363, 2009.

- [245] Y. Li and E. Hsiao-Weckler, "Gait mode recognition and control for a portable-powered ankle-foot orthosis," *IEEE ... International Conference on Rehabilitation Robotics : [proceedings]*, vol. 2013, pp. 1-8, 06/01 2013, doi: 10.1109/ICORR.2013.6650373.
- [246] B. A. Bensley, *Practical anatomy of the rabbit*. The University Press, 1910.
- [247] Y. H. Chang *et al.*, "Progressive adaptation of whole-limb kinematics after peripheral nerve injury," *Biol Open*, vol. 7, no. 8, Aug 6 2018, doi: 10.1242/bio.028852.
- [248] J. Wannop, J. T. Worobets, and D. Stefanyshyn, "Normalization of ground reaction forces, joint moments, and free moments in human locomotion," *Journal of applied biomechanics*, vol. 28 6, pp. 665-76, 2012.
- [249] P. T. Hall *et al.*, "Fully Implanted Prostheses for Musculoskeletal Limb Reconstruction after Amputation: An *In Vivo* Feasibility Study," *bioRxiv*, p. 2020.07.02.184994, 2020, doi: 10.1101/2020.07.02.184994.
- [250] A. Mathis *et al.*, "Markerless tracking of user-defined features with deep learning," *arXiv preprint arXiv:1804.03142*, 2018.
- [251] A. Mathis *et al.*, "DeepLabCut: markerless pose estimation of user-defined body parts with deep learning," *Nature neuroscience*, vol. 21, no. 9, pp. 1281-1289, 2018.
- [252] L. Nistor, "Surgical and non-surgical treatment of Achilles Tendon rupture. A prospective randomized study," *The Journal of bone and joint surgery. American volume*, vol. 63, no. 3, pp. 394-399, 1981.
- [253] J. Leppilahti and S. Orava, "Total Achilles tendon rupture," *Sports medicine*, vol. 25, no. 2, pp. 79-100, 1998.
- [254] J. Leppilahti, J. Puranen, and S. Orava, "Incidence of Achilles tendon rupture," *Acta orthopaedica Scandinavica*, vol. 67, no. 3, pp. 277-279, 1996.
- [255] R. F. Zernicke, J. Garhammer, and F. Jobe, "Human patellar-tendon rupture," *JBJS*, vol. 59, no. 2, pp. 179-183, 1977.
- [256] D. I. Ilan, N. Tejwani, M. Keschner, and M. Leibman, "Quadriceps tendon rupture," *JAAOS- Journal of the American Academy of Orthopaedic Surgeons*, vol. 11, no. 3, pp. 192-200, 2003.
- [257] E. Bass, "Tendinopathy: why the difference between tendinitis and tendinosis matters," (in eng), *Int J Ther Massage Bodywork*, vol. 5, no. 1, pp. 14-17, 2012, doi: 10.3822/ijtmb.v5i1.153.
- [258] A. Mishra and T. Pavelko, "Treatment of chronic elbow tendinosis with buffered platelet-rich plasma," *The American journal of sports medicine*, vol. 34, no. 11, pp. 1774-1778, 2006.
- [259] R. P. Nirschl, "Elbow tendinosis/tennis elbow," *Clinics in sports medicine*, vol. 11, no. 4, pp. 851-870, 1992.
- [260] M. Ibrahim, J.-T. Kartus, S. E. Steigen, R. Olsen, and K. Meknas, "More tendon degeneration in patients with shoulder osteoarthritis," *Knee Surgery, Sports Traumatology, Arthroscopy*, vol. 27, no. 1, pp. 267-275, 2019.
- [261] G. Riley, R. Harrall, C. Constant, M. Chard, T. Cawston, and B. Hazleman, "Tendon degeneration and chronic shoulder pain: changes in the collagen composition of the human rotator cuff tendons in rotator cuff tendinitis," *Annals of the rheumatic diseases*, vol. 53, no. 6, pp. 359-366, 1994.
- [262] H. Alfredson and R. Lorentzon, "Chronic achilles tendinosis," *Critical Reviews™ in Physical and Rehabilitation Medicine*, vol. 12, no. 2, 2000.
- [263] J. Yuan, G. A. Murrell, A. Q. Wei, and M. X. Wang, "Apoptosis in rotator cuff tendonopathy," *Journal of orthopaedic research*, vol. 20, no. 6, pp. 1372-1379, 2002.
- [264] P. Davis, S. Huang, L. Ambrosio, D. Ronca, and L. Nicolais, "A biodegradable composite artificial tendon," *Journal of Materials Science: Materials in Medicine*, vol. 3, no. 5, pp. 359-364, 1992.

- [265] A. Moshiri, A. Oryan, and A. Meimandi-Parizi, "Role of tissue-engineered artificial tendon in healing of a large Achilles tendon defect model in rabbits," *Journal of the American College of Surgeons*, vol. 217, no. 3, pp. 421-441. e8, 2013.
- [266] S. Yunoki, H. Hatayama, M. Ebisawa, E. Kondo, and K. Yasuda, "A novel fabrication method to create a thick collagen bundle composed of uniaxially aligned fibrils: An essential technology for the development of artificial tendon/ligament matrices," *Journal of Biomedical Materials Research Part A*, vol. 103, no. 9, pp. 3054-3065, 2015.
- [267] D. Jenkins, I. Forster, B. McKibbin, and Z. Ralis, "Induction of tendon and ligament formation by carbon implants," *The Journal of bone and joint surgery. British volume*, vol. 59, no. 1, pp. 53-57, 1977.
- [268] D. De-Yao and S. Zhi-Yong, "Experimental permanent artificial tendon for the hand," *Journal of biomedical engineering*, vol. 10, no. 5, pp. 406-410, 1988.
- [269] D. Dong and C. Sheng, "Study of permanent artificial tendon," *Biomaterials, artificial cells and artificial organs*, vol. 16, no. 5, pp. 927-944, 1988.
- [270] J. Franklin, J. Marler, M. Byrne, A. Melvin, S. Clarson, and D. Melvin, "Fiber technology for reliable repair of skeletal muscle," *Journal of Biomedical Materials Research Part B: Applied Biomaterials*, vol. 90, no. 1, pp. 259-266, 2009.
- [271] D. B. Melvin *et al.*, "A durable load bearing muscle to prosthetic coupling," *Asaio Journal*, vol. 49, no. 3, pp. 314-319, 2003.
- [272] B. D. Robertson and G. S. Sawicki, "Exploiting elasticity: modeling the influence of neural control on mechanics and energetics of ankle muscle–tendons during human hopping," *Journal of theoretical biology*, vol. 353, pp. 121-132, 2014.
- [273] R. Don *et al.*, "Relationship between recovery of calf-muscle biomechanical properties and gait pattern following surgery for Achilles tendon rupture," *Clinical biomechanics*, vol. 22, no. 2, pp. 211-220, 2007.
- [274] I. Ogbonmwan, B. D. Kumar, and B. Paton, "New lower-limb gait biomechanical characteristics in individuals with Achilles tendinopathy: a systematic review update," *Gait & posture*, vol. 62, pp. 146-156, 2018.
- [275] P. T. Hall, C. Stubbs, D. E. Anderson, C. B. Greenacre, and D. L. Crouch, "Biomechanical Analysis of the Rabbit Hindlimb during the Stance Phase of Hopping Gait," *Journal of Biomechanics*, vol. In Review, 2021.
- [276] C. Lambrinudi, "New operation on drop-foot," *British Journal of Surgery*, vol. 15, no. 58, pp. 193-200, 1927.
- [277] A. E. Cronkite, "The tensile strength of human tendons," *The anatomical record*, vol. 64, no. 2, pp. 173-186, 1936.
- [278] J. V. Benedict, L. B. Walker, and E. H. Harris, "Stress-strain characteristics and tensile strength of unembalmed human tendon," *Journal of Biomechanics*, vol. 1, no. 1, pp. 53-63, 1968.

VITA

Patrick Timothy Hall was born June 2, 1995 in Nashville, Tennessee to Tim and Laurie Hall. He is the youngest of three children: Katherine and Stephen. Patrick attended Brentwood High School in Brentwood, Tennessee where he first developed an interest in engineering and medical practices. After graduating in 2013, he went on to study Biomedical Engineering at Baylor University. While studying at Baylor, Patrick served as the founding vice-president and later president of the Baylor chapter of the Biomedical Engineering Society. During the summer of 2016, Patrick worked as an intern for the Medical Engineering and Discovery Laboratory at Vanderbilt University developing continuum robots for exploratory operations. At Baylor he was awarded with the distinctions of “2017 Baylor Outstanding Student for the School of Engineering and Computer Science” and “Who’s Who in American Colleges and Universities”. He graduated from Baylor in 2017 with a Bachelor of Science in Engineering Degree. He then accepted a graduate research fellowship at the University of Tennessee in the department of Mechanical, Aerospace, and Biomedical Engineering. Patrick served as the first Ph.D. student in the Upper Limb Assist Lab, performing research alongside his advisor, Dr. Dustin Crouch. It was here he met his wife Christen Caradine. He was awarded a Ph.D. in Mechanical Engineering in June of 2021 and given the title “Outstanding Graduate Student for MABE Department”. Patrick is looking forward to pursuing a career involving research in the industrial setting, working in the field of assistive technologies.